

Design of biped robot walking based on non-linear periodical oscillations

Dissertation

zur Erlangung des akademischen Grades

**Doktoringenieur
(Dr.-Ing.)**

von M.Sc. Andriy Telesh

geb. am 27.03.1983 in Taganrog (Russische Föderation)

genehmigt durch die Fakultät für Elektrotechnik und Informationstechnik
der Otto-von-Guericke-Universität Magdeburg

Gutachter:

Univ.-Prof. Dr.-Ing. habil. Frank Palis

Prof. Alexander Formalskiy

Prof. Yannick Aoustin

Promotionskolloquium am 11. April 2012

Abstract

The main idea of this thesis is to consider walking of biped mechanisms as an oscillating process. The aim of this work is to design the effective methods of the control of oscillating underactuated system and to apply the principles gained to develop periodic and dynamic walking of a prototype of the robot ROTTO. The problem design of the control algorithms of oscillations of variable length pendulum, double pendulum and walking mechanical systems is considered. Different control methods are developed for variable length pendulum and double pendulum. The mathematical model of a two-legged mechanism including impact interaction between feet and support is studied. The method of synthesis of ballistic (natural) trajectories of movement of two-legged mechanical systems is considered for planar and 3D mathematical models. Special trajectories for a two link compass-like mechanism are developed analytically. The algorithms of dynamic walking of a two-legged robot separately in the frontal and sagittal plane and in 3D by maintaining the total energy are developed. The effectively and quality of the synthesized control systems of the mechanisms are simulated and proved experimentally.

Kurzfassung

Die Hauptidee der Dissertation ist die Betrachtung des Gehens von anthropomorphen Robotern als Schwingungsprozess. Das Ziel dieser Arbeit besteht in der Entwicklung von effektiven Methoden zur Regelung eines mechanischen Systems mit unvollständigen Steuergrößen und die Verwendung dieses Prinzips für die Synthese des dynamischen Gehens des zweibeinigen Roboters ROTTO. In der Arbeit wurde das Regelungssystem für die Schwingungsamplitude eines Pendels mit variabler Länge, eines Zwei-Massen-Pendels und eines Laufroboters betrachtet. Für das Pendel mit variabler Länge und das Zwei-Massen-Pendel wurden verschiedene Regelungsgesetze für die Schwingungsamplitude entwickelt. Es wurde das mathematische Modell eines zweibeinigen Laufmechanismus aufgestellt und seine Kontaktnahme mit dem Untergrund betrachtet. Hierfür wurde eine Methode zur Synthese der ballistischen Trajektorie für den 2D und 3D Mechanismus entwickelt. Für ein stark vereinfachtes Modell (Zirkelmodell) wurde eine spezielle Trajektorie analytisch abgeleitet. Für das dynamische Gehen eines zweibeinigen Roboters wurden die Algorithmen jeweils unabhängig voneinander in der frontalen und sagittalen Ebene und in 3D auf der Basis der Regelung der Gesamtenergie entwickelt. Effizienz und Qualität der entwickelten Regelungssysteme wurden durch Simulation und Experiment nachgewiesen.

Acknowledgements

This research work has been carried out within my Ph.D. student fellowship at the Institute of Electrical Power Systems Otto-von-Guericke University Magdeburg in cooperation with Fraunhofer Institute for Factory Operation and Automation IFF Magdeburg.

I owe special thanks to Univ.-Prof. Dr.-Ing. habil. Dr.h.c. Frank Palis for support and help rendered to me on this work task organization. He showed me invaluable scientific and interpersonal aspects of research work.

I would also like to extend my deepest gratitude to Prof. A.M. Formalskiy His invaluable guidance, criticism and inspiration have provided an invaluable experience that will help me in research work.

Also a note of thanks goes to Prof. Dr. sc. techn. Ulrich Schmucker and Dr.-Ing. habil. Anatoliy Schneider for excellent support during the research work .

My deep gratitude goes to Dr.-Ing. Yuriy Tsepkovskiy, Dr.-Ing. Yuriy Zavgorodniy, Dr.-Ing. Vadym Rusin, Dipl.Inf. Sergiy Dzhantimirov, M.Sc. Mykhaylo Konyev, M.Sc. Andriy Melnykov, M.Sc. Artem Rudskyy for an excellent teamwork and productive discussions that helped me to complete this work.

My appreciation and thanks to a group of qualified specialists of Institute of Electrical Power Systems and Fraunhofer Institute for Factory Operation and Automation IFF Magdeburg, for support and very good team work.

And finally I send my love and thanks to my wife Anja, son Volodymyr, daughter Katja and my parents, without whom this work and my studies were impossible.

Contents

List of symbols	8
Chapter 1. Introduction and problem formulation	9
1.1. Introduction.....	9
1.2. State of the Art	10
1.2.1. Mechanical Design of the Bipedal Robots	11
1.2.2. Design of Bipedal Robot “ROTT0”	13
1.3. Basic concepts of the Bipedal Walking Control.	14
1.3.1. “Stability” Applied to Bipedal Robotic	17
1.3.2. Orbital stability	18
1.4. Idea of this Thesis – Synthesis of the Periodic Motions of Dynamical Systems	19
Chapter 2. Control of variable length pendulum motions	21
2.1. Equations of motion.....	21
2.2. Increase of oscillation amplitude of the pendulum. Formulation of control problem.	23
2.3. Oscillation control of system of second order of general type.	26
2.3.1. Reachable sets and their limits.	27
2.3.2. Maximization and minimization of oscillation amplitude of pendulum.	28
2.3.3. Simulation of optimal swinging and pendulum damping.....	30
2.4. Synthesis of control system of periodic pendulum motions	31
2.4.1. Simulations	32
2.4.2. Experiments	36
Chapter 3. Oscillation control of double pendulum	42
3.1. Mathematical model.....	42
3.2. Synthesis of the pendulum oscillation control using the energy integral. ...	43
3.2.1. Speed gradient method in the oscillation control.	44
3.2.2. Simulation of the control system	46
3.3. Periodic motion synthesis via the combination of optimal laws of swinging and damping.....	48
3.3.1. Synthesis of the control system of the oscillation amplitude of the double pendulum.	50
3.3.2. Simulation results	51
3.4. Experiments	55

Chapter 4. Design of the movement of a two-legged mechanism in the frontal plane	62
4.1. Mathematical model of single support motion	62
4.2. Mathematical model of the perfectly inelastic impact for a two link mechanism	66
4.3. Synthesis of the oscillation control in the frontal plane on the basis of optimal laws of swinging and damping	75
4.4. Simulation of the system to control oscillations in the frontal plane.....	76
4.5. Intuitive approach to the synthesis of the oscillation control	79
4.6. Experimental results.....	81
Chapter 5. Design of dynamic walking of the biped robot ROTTO	85
5.1. Development of the dynamic model.....	85
5.2. Synthesis of the robot movement on the basis of ballistic trajectories	89
5.2.1. Basic of ballistic trajectories.....	89
5.2.2. Three-Dimensional Ballistic Walking of the Biped Model with many degrees of freedom.....	94
5.2.3. Ballistic Motion of Two Link Model.....	98
5.3. Walking control in sagittal plane	100
5.4. 3D walking synthesis. Experimental investigations	104
5.4.1. Swinging in frontal plane.....	105
5.4.2. 3D Walking on the horizontal surface	107
Conclusion.....	111
Zusammenfassung.....	113
References	115

List of symbols

T	kinetic energy
V	potential energy
H	total energy
Q_i	generalized nonconservative force
L	Lagrange function
D	reachable set
u	system input
$\dot{W}(t, x)$	full derivative of function
∇_u	denotes the derivative with respect to the parameter u
x	vector ($n \times 1$) of the object state
$G(x)$	non-linear function at the system input
$\frac{\partial H}{\partial x}$	partial derivatives of the function H
K	kinetic momentum
δW	Elementary work
R_1, R_2	reaction forces
δ	Dirac delta functions
$[\dot{x}], [\dot{y}]$	velocity steps
$\dot{z}(-0)$	vector of velocities before the impact
$\dot{z}(+0)$	vector of velocities before the impact

Chapter 1. Introduction and problem formulation

Equation Chapter 1 Section 1

If we can gain better insight into how humans walk, perhaps we could improve prosthetics for the gait-impaired, help correct neuro-muscular deficiencies, or build better two-legged walking robots.

Tad McGeer.

1.1. Introduction

At present there is a great variety of machines and vehicles mainly based on the application of a wheel which is considered to be one of the most outstanding inventions of people. However, all vehicles – cars, trains, ships or planes require highly-organized associated systems, namely airports, ports, roads, canals. Even today, it is difficult to reach some areas on the Earth. Apparatus which can move with the help of two limbs can change this situation and make it better.

Ability to walk is an outstanding and unique invention of nature. It is a universal and flexible process of locomotion and it is perfectly adapted to a natural habitat of living systems. Ability to walk enables living beings to reach every corner of the world. Walking, running, flying and swimming of animals and birds takes place within a person's sight and the fact that locomotion processes which living beings fulfill are extremely numerous and "ordinary" can create an impression that the secret of organization of these process are obvious. However, it is far from true...

Engineers have been investigating the process of walking for many years [5], [28], [36], [53], [55], [65], [73], [77], [82], [90]. A great number of two-legged locomotion machines having the ability to move on two legs have been created so far. Biped robots are electromechanical systems which morphologically imitate a human body structure and implement the main degrees of freedom (DOF) of a human body. Hence, it is very desirable for biped robots to move similar to a human being. Because of this, the analysis of person's motion (walking) has a significant meaning for the task how to find a goal-walking model. It is also necessary to remember the technical perfection of a mechanical structure, a mass distribution in a robot structure, dynamic properties of electromechanical actuators completely determine all physical parameters and dynamic properties of robots [6], [16], [58] [61], [68]. Hence, we can distinguish the following main tasks in the development of anthropomorphic robotic engineering:

- development of a mechanical structure,
- development of mechanical and physical properties of actuators,
- organization and control of robot locomotion.

Now let's consider in more details state of the art of biped robots and the main concepts how to plan and control walking of biped mechanisms.

1.2. State of the Art

It is not trivial at all to solve the task of motion synthesis. Many robots developed up to the present moment walk rather slow, in state conditions. At present, the majority of well-known algorithms for robot locomotion use only some part of dynamic robot capabilities. Despite the fact that the theory of automatic control is highly developed, the possibility to use many control algorithms is essentially bounded. The difficulties arising while developing the algorithms which can control biped locomotion are due to the fact that a biped mechanism represents an unstable underactuated mechanical system with a great number of DOF. Under underactuation is understanding that the number of actuated DOF of mechanical system is less than available.

One of the problems arising while controlling a biped robot is the coordination of robot joint movements. As a biped robot has a great number of degrees of freedom, the task to coordinate the movements in separate joints causes considerable difficulties. For example, at translational movement of center of mass (COM) of robot the required number of DOF is much less than is available. This kinematic problem has more than one solution. Hence, there appears the task to find the optimal solution of the problem. But in practice it is next to impossible to find the optimal solution for essentially non-linear system of the high order.

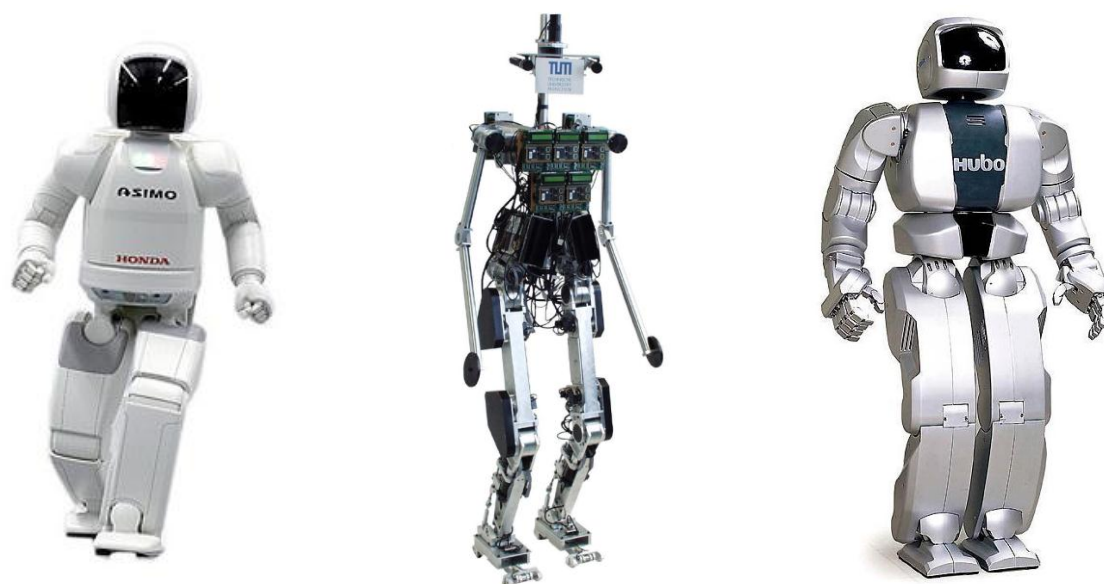
The second significant problem lies in highly non-linear hybrid dynamics of bipedal walking. Non-linear character of a mechanism dominates particularly when investigating the robot locomotion in 3D space. The interaction with the support surface plays a significant role during robot walking. To describe robot motions taking into account impact interactions with the support surface it is necessary to generate complex mathematical models. Such mathematical model comprises equations of motion and equations of impulsive interactions.

The next problem is that on in a large region of movement the biped robot is a multi-input multi-output (MIMO) underactuated mechanical system [30]. In comparison with industrial robots which are rigidly fixed to a foundation biped robots are mobile in space and the value of the torque applied in an ankle joint is limited by the feet size. Limitation of the torque applied results into the complexity of the control algorithms.

Strong interdependence between the task of planning the locomotions and the features of a mechanical structure makes it necessary to carry out the mathematical modeling even on the early stages of biped robot development. It is necessary to notice that the characteristics of movements received depend mainly on the dynamic capabilities of robots.

1.2.1. Mechanical Design of the Bipedal Robots

At present humanoids show some similitude, in other words, represent the reconstruction of a human body and they are electrical, hydraulic, pneumatic and mechanical systems. Perfection of a mechanical structure of a robot and the technologies applied is one of the most important constituents of the successful solution of the locomotion task and it determined the robot dynamic capabilities which can be achieved. Currently there are a lot of biped robots whose number of DOF is more than 30. The following robots are well-known all over the world: the robot named ASIMO developed by the company Honda [33], the robot Johnnie from TU München KHR-3 [86], KHR-3 HUBO from Korea Advanced Institute of Science and Technology [41] (s. Fig. 1.1).



a) ASIMO, Honda Motor Co. [33] b) Johnnie, TU München [86] c) KHR-3 HUBO, KAIST [41]

Figure 1.1 – Well-known robots

All these robots were developed according to a multi-link model of man: a head, a body, arms, legs and feet and they are 1,3m, 1,8m and 1,2m high respectively. The quickest of them is ASIMO: its walking speed is 2,7 km/h and running speed is 6,0 km/h. All three robots have similar mechanical concept: simple kinematics, high rigidity, self-contained system, relative high weight (>50 kg).

One of the most promising directions in the question of dynamic walking is the application of the Series Elastic Actuation technology. This type of an actuator has the following features: conservation of energy in the elastic element, position control with the desired impedance, implementation of the artificial spring with the desired value of stiffness.

The first works in this area of research belong to the robotics group from Massachusetts Institute of Technology [66], [67], [70], [71], [72]. The planar bipedal walking robot Spring Flamingo (s. Fig. 1.2 a) was created by this group as a pilot platform to test different locomotion algorithms. The robot has hip and ankle joints and knees. All robot motors are in the upper part of a body. Forces are transmitted via cable drives. Series Elastic

Actuation is employed at each degree of freedom, allowing for accurate application of torques and a high degree of shock tolerance [51]. The proposed algorithm Virtual Model Control (VMC) enabled to realize dynamic walking along the surface with different properties on the basis of the planar robot Spring Flamingo. The speed of walking 4,32 km/h was reached during the experimental research.

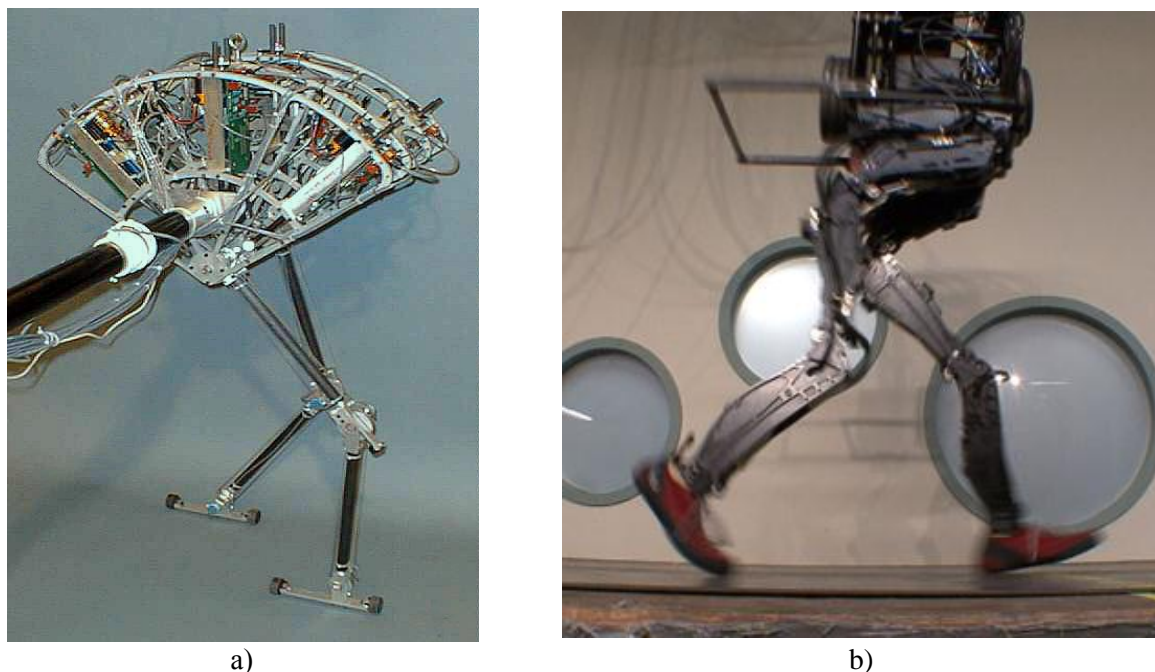


Figure 1.2 – a) Robot Spring Flamingo by MIT [51], b) Robot PETMAN by Boston Dynamics [6]

At present the fastest walking bipedal robot is the robot PETHMAN (s. Fig. 1.2 b) developed by an American military company Boston Dynamics. The speed of walking is 7,1 km/h and heel – toe walking is like human [6]. The peculiarity of the robot PETHMAN mechanical structure is the application of aeronautic hydraulics as power actuators and the application of series elastic actuation technology to provide the predetermined total impedance of the foot end points with supporting surface. The robot PETHMAN is designed to test military uniform clothing

When a person walks he moves some limbs of his body during definite stages of a step without any application of force in the joints [42]. That is why learning of passive/semi-passive dynamic walking robots are of great interest concerning the following tasks: analysis of natural walking, stable walking cycles, passive dynamics (by Tad McGeer), ballistic motion (Alexander M. Formalskiy in the 1970s), low energy cost [3], [21], [24], [25], [53], [55], [56]. The original model for passive dynamics is based on human and animal leg motions [53]. In robots like the Honda ASIMO the realization of legged movement is not optimal from the point of view of energy consumption as each joint has its own motor and it is controlled depending on its position separately from the whole system. Human walking is more perfect as the motion of many parts of a human body is similar to natural periodic oscillations. Only in some moments the muscles send additional impulse thus increasing the energy of the system to continue the periodic walking [8].

Energy efficiency in level-ground transport is quantified in terms of the dimensionless "specific cost of transport", which is the amount of energy required to carry a unit weight a unit distance [87]. Passive dynamic walkers such as the Cornell Efficient Biped [12] have the same specific cost of transport as humans, 0.20. Not incidentally, passive dynamic walkers have human-like gaits. By comparison, Honda's biped ASIMO, which does not utilize the passive dynamics of its own limbs, has a specific cost of transport of 3.23 [11]. The current distance record for walking robots, 65.17 km, is held by the passive dynamics based Cornell Ranger (s. Fig 1.3).



Figure 1.3 – Cornell Ranger [13] by Cornell University

1.2.2. Design of Bipedal Robot “ROTTTO”

The bipedal robot “ROTTTO” [40] was developed in Otto-von-Guericke University of Magdeburg during the period 2007-2010 (s. Fig. 1.4). This robot has a great number of different sensors, actuators and it is designed to do research in different area, such as investigations in gait generation and motion control, development of energy optimal gaits, investigation of robot ballistic motion, development of adaptive motion control using the feedback linearization methodology, development of force/impedance control inspection tasks in closed room, pipes, on complex terrain, especially in areas with harmful environmental conditions that are hazardous for human, development and optimization of various algorithms for motion, climbing and service operations and others [39], [40]. One of the most important tasks for the sake of which the robot ROTTO has been developed is the development of the algorithms to provide periodic and dynamic walking of a robot.

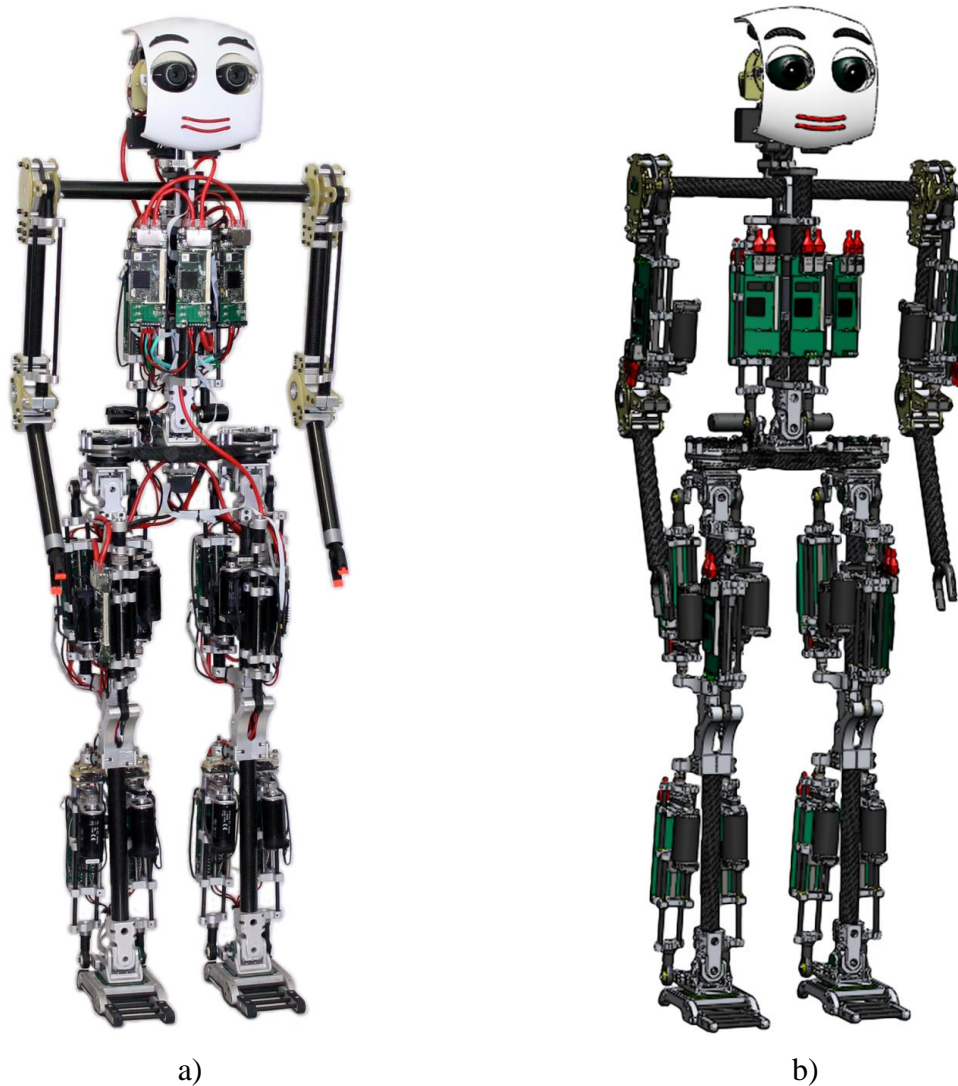


Figure 1.4 – Robot „ROTTO“
 a) Prototype,
 b) CAD Model

The detailed information about the robot ROTTO is given in chapter 5.

1.3. Basic concepts of the Bipedal Walking Control.

The robots analyzed in the previous item can be classified into two categories: open loop and closed loop control of the stable walking (s. Fig 1.5). Open loop systems include static, passive, quasi-passive walking. Closed loop systems include all the types of dynamic walking. Let's consider more detailed the methods how to plan and control bipedal walking.

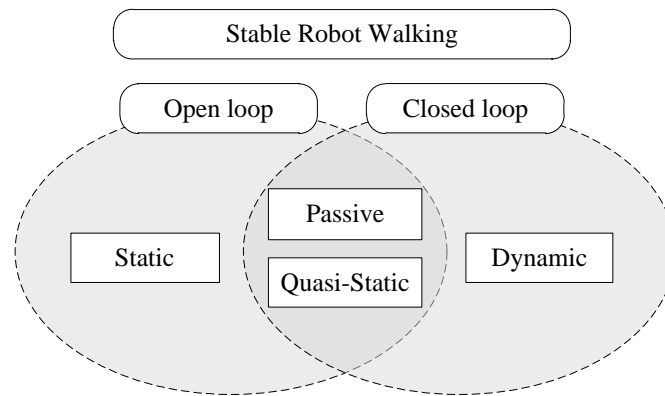


Figure 1.5 - Stable Walking of Robots

As a rule, a set of paths for definite robot movements is calculated offline and is stored in some data base. The robot selects online a suitable set of paths to fulfill this or that task, operation. Doing so [1], [48], [47], [79] locomotion is organized using the sequence of statically stable configurations in which the projection of the COM on the support surface is inside the supporting area. Such type of a gait synthesis is often used for small biped robots (s. Fig. 1.6).

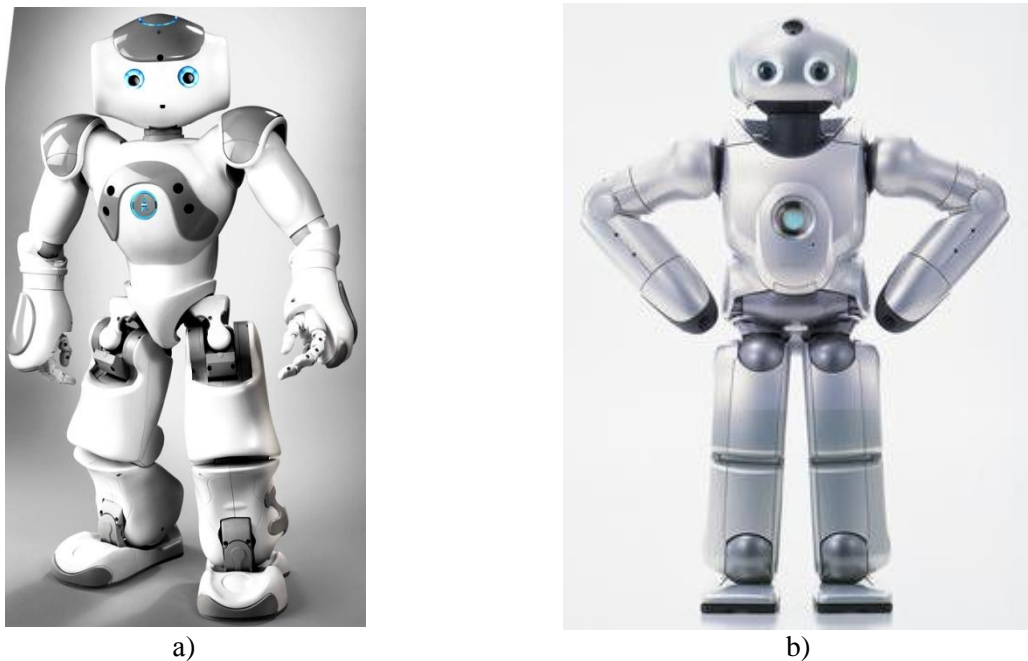


Figure 1.6 – a) Robot NAO [1], b) robot QRIO [20]

In the mode of static stability it is usually possible only to move slowly. This is due to the fact that robots are comparatively light and weigh only some kilograms and servomotor capabilities are insufficient to produce dynamic walking.

In some investigations walking is organized by setting and following the programmed trajectories. In papers [23], [31] the programmed trajectories are set in the form of time functions (polynomials). These programmed trajectories are followed by the drives installed in the joints. The polynomial coefficients change with each step depending on the behavior of double support phase. The authors are calling this algorithm an adaptive one. This algorithm

is implemented in dynamic walking of a planar bipedal robot with telescopic legs (s. Fig. 1.7 a) and in walking of a planar anthropomorphic robot (s. Fig 1.7 b).

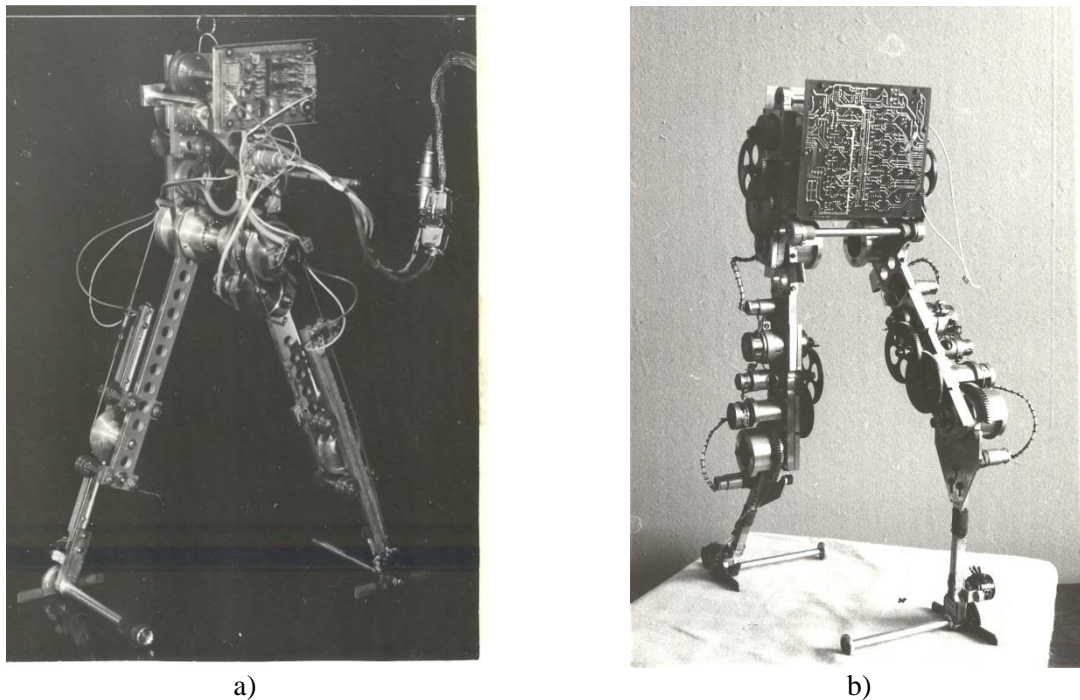


Figure 1.7 – Robots developed in Moscow State University
 a) Robot with telescopic legs [23]
 b) planar anthropomorphic biped robot [9]

Different postural criteria are used for synthesis and offline optimization of trajectories of quasi-static walking [29], [59], [69], [75], [89]. The design methods of quasi-static walking pattern (s. Fig. 1.8) are based on the concept of postural stability Zero Moment Point (ZMP) which was proposed by Miomir Vukobratovic in 1968. The criterion of ZMP [59] defines the point on the surface referring to which the moment of support reaction forces applied to the foot equals zero. Unlike static walking various ways of online correction of ground reference point positions are proposed in publications [18], [35]. The overwhelming majority of algorithms for locomotion of biped robots (Honda ASIMO [33], Johnnie TU München and others) are based on this conception.

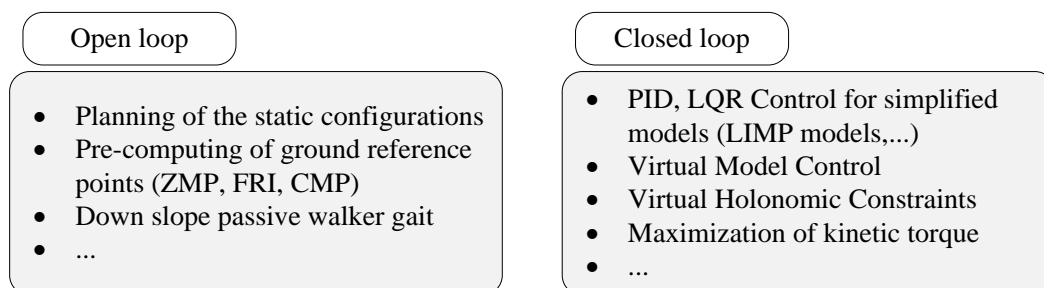


Figure 1.8 – Stable Walking Control Methods

Design of passive walking robots rests on the application of a sloping surface or, in some cases, of additional actuators to compensate the losses arising during impact interactions with support surface and the losses due to friction in joints.

All open-loop control systems have general disadvantages such as:

- it is not possible to compensate external disturbances ,
- dependence of gait stability on the surface characteristics.

While designing the closed-loop control system the algorithms based on the simplified models such as an inverse pendulum [43], spherical inverted pendulum [37], double inverted pendulum [93], inverted pendulum [80] and others are used more often to support the balance. Using such type of algorithms enables to produce stable walking. However, the simplified dynamic model of the anthropomorphic mechanism can be only used in the definite dynamic range.

Virtual model control is a motion control framework that uses simulations of virtual components to generate desired joint torques. These joint torques create the same effect that the virtual components would have created, had they existed, thereby creating the illusion that the simulated components are connected to the real robot [67]. This method was used to design the gait of the robot Flamingo Spring.

Virtual holonomic constraints approach [76], [78], is used to investigate the definite types of underactuated mechanical systems. The essential idea of this method is to find some movement of a mechanical system, this movement being the geometric function of the generalized coordinates. This method was applied to design the gait of the robot RABBIT [10] .

1.3.1. “Stability” Applied to Bipedal Robotic

Strictly speaking, there is only one way to keep a robot in balance, that is to apply the appropriate forces in the point of the support (a foot, feet) contact with the surface. Let’s consider such a set of robot movements when a robot doesn’t lose its balance and its support leg does not leave the support polygon. Support polygon is some kind of convex polygon which is formed by all the points of contact with the surface [91]. It is possible to formulate for such movements the criteria how to keep the balance with respect to the vertical line [60]:

- The normal projection of COM on the ground accounts for static gravitational forces. This criterion is not relevant for the movements which cause the dynamic forces acting on the mechanism.
- One of the commonly used criteria is ZMP. It is basically a renaming of the center of pressure (COP) defined as the point on the ground where the resultant of the ground reaction forces acts.

At present there is no strict conception how to keep a biped robot in balance. The term “in balance” more often implies the intuitive understanding “it does not overturn”. According to [91] the gait is considered to be stable in the following cases:

- *statically stable* if the normal projection of the robot’s COM does not leave the support polygon,
- *quasi-statically stable* if the COP of the stance foot remains strictly within the support polygon, and

- *dynamically stable* if the COP of the stance foot is on the boundary of the support polygon for at least part of the cycle and yet the biped does not overturn.

From the point of view of the control theory the main criterion of the control system stability is Lyapunov stability. Doing this it is necessary to check the system controllability, exponential convergence to the predetermined trajectory, asymptotical stability. Unfortunately, it is not possible to use the conception of asymptotical stability for such processes as walking because they occur in the finite intervals of time. In this particular case it is possible to speak about the stability for some number of step cycles using, for instance, the conceptions of motion repeatability, period walking and orbital stability.

1.3.2. Orbital stability

Orbital stability of solutions of the autonomous system of differential equations

$$\dot{\varphi} = f(\varphi), \quad \varphi \in G \subset R^n \quad (1.1)$$

is understood as the geometric proximity of disturbed and undisturbed motion in the phase space of the system (s. Fig. 1.9). Here, G is a restricted area in R^n .

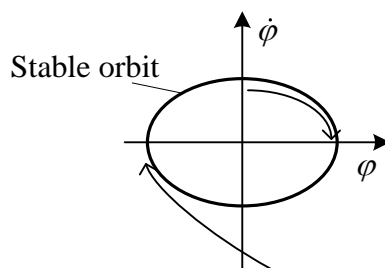


Figure 1.9 – Stable Orbit

At the present time some definitions of orbital stability are known. In the majority of definitions it is the orbital stability of periodic solution that is investigated. Two different approaches are used for defining the orbital stability. In the first approach the orbital stability of a trajectory is treated as the stability of the set in the phase space, and in the other one the orbital stability amounts in either way to Lyapunov stability after a special change of time in the system under the question (they are, for example, the definitions close to the definition of asymptotical phase) [44]. Both definitions coincide with each other for periodic solutions, however, in general case these approaches essentially differ.

Let's give the appropriate definitions of orbital stability [44]:

Definition 1: The solution $x = x(t, x_0)$, $t_0 \leq t < +\infty$, of the system (1.1) is called orbitally stable if for any $\varepsilon > 0$ there is $\delta = \delta(\varepsilon, t_0) > 0$ and $T > t_0$, so that for all $y_0 \in B_\delta(x_0)$ at any meaning of $t \geq T$ the following relation is true:

$$\rho(y(t, y_0), L^+(x_0)) < \varepsilon .$$

Here $L^+(x_0) = \{x(t, x_0) : t_0 \leq t < +\infty\}$ - is a positive half-orbit of the solution $x = x(t, x_0)$, $B_\delta(x_0)$ - is an open δ - sphere with the center in the point x_0 , $\rho(z, L)$ - is the distance between the point z and the set L , $\rho(z, L) = \inf \|z - y\|$; $\|\bullet\|$ - is the norm in R^n .

Definition 2: Orbitally stable solution $x = x(t, x_0)$ of the system (1.1) is called orbitally asymptotically stable if there is such meaning of $\delta_0 > 0$, so that for all $y_0 \in B_{\delta_0}(x_0)$ at $t \rightarrow +\infty$ the following relation is true:

$$\rho(y(t, y_0), L^+(x_0)) \rightarrow 0 .$$

This definition of orbital asymptotical stability with respect to orbital asymptotical stability of the closed trajectory can be explained in the following way. The orbital asymptotical stability of some closed trajectory in phase space means that the solution of a dynamic system at $t \rightarrow +\infty$ converges to this closed trajectory. At this the local stability in every point of the given phase trajectory is not guaranteed.

1.4. Idea of this Thesis – Synthesis of the Periodic Motions of Dynamical Systems

The main idea of this thesis is to consider walking of biped mechanisms like some oscillating process. Oscillations are the most common processes in nature and in engineering. Oscillations are the processes in which movements or states of the system periodically repeat in time. Oscillating processes are characterized by such physical values as a phase, period, frequency, amplitude. These values are also perfectly suitable to characterize human steps as well as steps of anthropomorphic mechanisms.

The consideration of the problem of dynamic walking synthesis in the context of oscillations allows us to have a new look at the tasks how to maintain balance, compensate external disturbances, form step cycles, it enables us to concentrate on maintaining the stability of a mechanical system, orbit stability and, as a consequence, periodic walking stability.

The aim of this work is to develop the effective methods of oscillating mechanical system control when there is not enough number of control actions and to apply the principles gained to develop periodic and dynamic walking of an experimental prototype of the anthropomorphic robot ROTTO.

The sequence of this work is the following (s. Fig. 1.10): a simple pendulum, double pendulum, two-legged mechanism in the frontal plane, two-legged mechanism in the sagittal plane, 3D realization of walking

				Two-legged mechanism in 3D
			Two-legged mechanism in the sagittal plane	Interrelation of plains
		Two-legged mechanism in the frontal plane	Virtual Constraints	
	Double pendulum	Impact interaction		
Pendulum	Non-linear dynamics			
Energy control				
Free trajectories of movement				
Underactuated mechanical system				

Figure 1.10 – “Stairs” (structure) of the Thesis

The second and the third chapters consider the examples of building up the systems controlling oscillations of simple underactuated mechanical systems. These mechanical systems which are considered to be classic in some way are: a simple variable length pendulum (swings) and double pendulum. Different control methods were developed for these two mechanical systems, the methods being based both on intuitive approach and on the application of Lyapunov functions. The experiments proving the efficiency of the methods applied were also carried out.

The fourth chapter represents the mathematical model of a two-legged mechanism including impact interaction between feet and support. On the basis of the methods developed in the previous chapters the systems exercising control by maintaining the energy of oscillations in the frontal plane were synthesized. The experiments showing the robustness and the mode of a system operation for different types of surfaces were also carried out.

The fifth chapter considers the method of synthesis of ballistic (natural) trajectories of movement of two-legged mechanical systems. Special trajectories, namely virtual holonomic constraints (VHC), for a two link compass-like mechanism were developed analytically. On the basis of the analysis the conclusions about some important characteristics of the obtained trajectories were made, these characteristics are step energy stability, independence of a step pitch from a step length and the possibility to scale the trajectory depending on a step length. The method how to synthesize the control of dynamic walking of a two-legged robot in the sagittal plane by maintaining the total energy of a system was developed and the simulation was carried out. This chapter also deals with the method of synthesis of 3D biped robot walking and the experiment was also carried out.

Chapter 2. Control of variable length pendulum motions

Equation Chapter 2 Section 2

In this chapter an example of control system construction for simple mechanical system's motions is considered. The Variable length pendulum can be considered as a model of swings with a human on them. For mechanical system one can synthesize an equation based on the *law of conservation of angular momentum*. The obtained equation allows to change the pendulum oscillations amplitude in desirable way. The experiments are also described which prove quality of constructed control systems.

2.1. Equations of motion

Let us consider a plane mathematical variable length pendulum (s. Fig. 2.1). The pendulum consists of a massless rod along which a single mass point m is moving. As generalized coordinates which define the system position we will take an angle φ and a distance l between single mass point and suspension point O . This distance l can change from l_{\min} till l_{\max} :

$$l_{\min} \leq l \leq l_{\max} \quad (2.1)$$

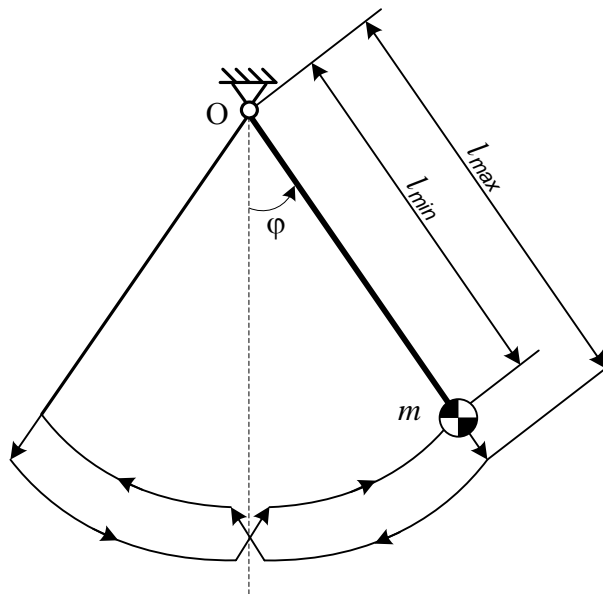


Figure 2.1 – Mathematical variable length pendulum

The system (s. Fig. 2.1) has two degrees of freedom. The equation of motion of the described system we set up using the Lagrange equation of second order [4], [49]

$$\frac{d}{dt} \left(\frac{\partial L}{\partial \dot{q}_i} \right) - \frac{\partial L}{\partial q_i} = Q_i \quad (i=1, \dots, n) \quad (2.2)$$

In the equations (2.2) q_i is a generalized coordinate, Q_i is generalized nonconservative force, $L=T-V$ is Lagrange function, T is kinetic energy, V is potential energy of the system. For the concerned here system $n=2$.

Expression for potential energy of the system has the following form:

$$V = mgl \cos \varphi. \quad (2.3)$$

Expression for kinetic energy of the system is:

$$T = \frac{1}{2} m \dot{l}^2 + \frac{1}{2} m l^2 \dot{\varphi}^2. \quad (2.4)$$

Using the equations (2.2), (2.3) and (2.4) we can set up the equations of motion of variable length pendulum:

$$\begin{cases} 2ml\dot{\varphi} + ml^2\ddot{\varphi} + mgl \sin \varphi = M \\ m\ddot{l} - ml\dot{\varphi}^2 - mg \cos \varphi = F \end{cases}. \quad (2.5)$$

In the equations (2.5) M is moment of external forces which affect the pendulum with respect to suspension point O , F is force that moves single mass point m along the massless rod.

In the work [50] for deducing of equation of mathematical pendulum motions the theorem about change of angular momentum is applied, according which a time derivative from the angular momentum is equal to the moment of external forces. The angular momentum of the pendulum with respect to suspension point O is equal to $ml^2\dot{\varphi}$, gravitation moment $M_s = -mgl \sin \varphi$. Equation of pendulum motions round the suspension point O when $M=0$ can be presented as:

$$\frac{d}{dt} (ml^2\dot{\varphi}) = 2ml\dot{\varphi} + ml^2\ddot{\varphi} = -mgl \sin \varphi. \quad (2.6)$$

Naturally the equation (2.6) coincides with the first equation (2.5). This equation can be simplified:

$$\ddot{\varphi} + \frac{2\dot{l}}{l} \dot{\varphi} + \frac{g}{l} \sin \varphi = 0. \quad (2.7)$$

2.2. Increase of oscillation amplitude of the pendulum. Formulation of control problem.

Mathematical pendulum, which length changes periodically, is a simplified model of swings with a human on them. As is generally known, swings are set in motion by rhythmical bending and straightening of body (or periodical bending and straightening of knees). As a result of it the center of gravity of the whole system comes up at the moment, when the pendulum (swings) passes the tough (fig. 2.1), and goes down at the moment, when the pendulum deviates from vertical at most. Such law of variation of the distance l can be presented by the following expression:

$$l = \begin{cases} l_{\min}, & \dot{\varphi} \cdot \varphi > 0 \\ l_{\max}, & \dot{\varphi} \cdot \varphi < 0 \end{cases} \quad (2.8)$$

As a result of such motions sequence, full energy of the system increases and vibration amplitude grows.

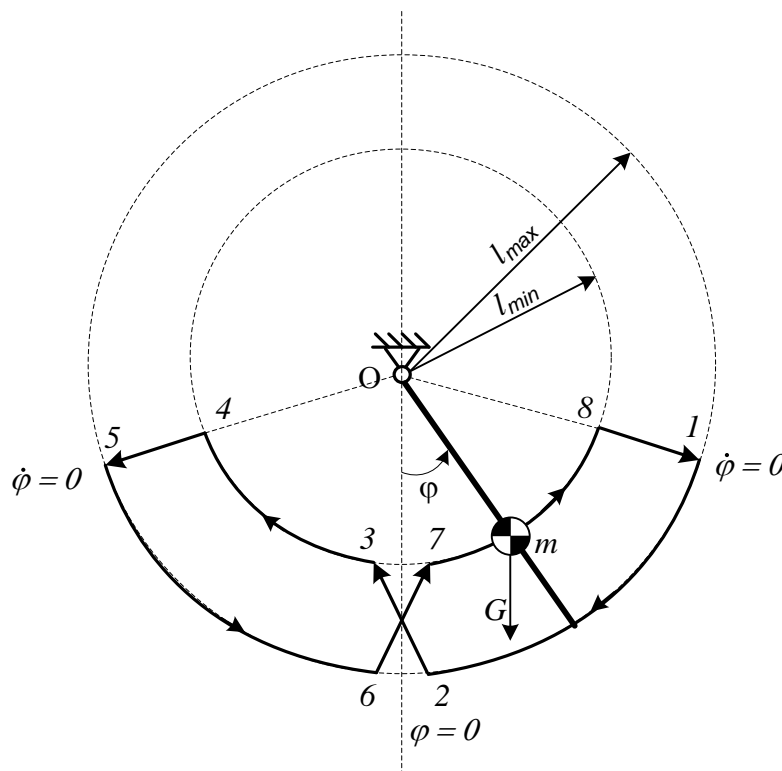


Figure 2.2 – Scheme of pendulum motions

Let us analyze the change of the full energy of pendulum while its vibration in concordance with the law (2.8) more detailed on section 1-2-3-4-5 (fig. 2.2).

In absence of nonconservative forces the energy-conservation equation can be written:

$$\frac{1}{2} ml^2 \dot{\varphi}^2 + mgl(1 - \cos \varphi) = mgl(1 - \cos \varphi_0). \quad (2.9)$$

Here φ_0 - angle of the pendulum derivation at the instant when $\dot{\varphi} = 0$

Angular speed in point 2 (fig. 2.2) is equal to

$$\dot{\varphi}_2^2 = \frac{2g}{l_{\max}}(1 - \cos \varphi_{01}), \quad (2.10)$$

here φ_{01} is initial deflection angle in position 1. A similar relation can be written also for speed in point 3:

$$\dot{\varphi}_3^2 = \frac{2g}{l_{\min}}(1 - \cos \varphi_{04}), \quad (2.11)$$

here φ_{04} is maximal deflection angle in position 4. While pendulum motion in section 2-3 momentary rise of center of mass of the system takes place. The forces causing it act along the rod and do not produce moment with respect to suspension point. Therefore the angular momentum in section 2-3 stays invariable

$$ml_{\max}^2 \dot{\varphi}_2 = ml_{\min}^2 \dot{\varphi}_3. \quad (2.12)$$

The relation between two speeds (2.12) enables to find connection between successive values of maximal deflections φ_{01} and φ_{04} . After squaring both parts of the relation (2.12) and after substitution of the result in (2.10) and (2.11), we can obtain the relation between maximal deflections of pendulum φ_{01} and φ_{04} :

$$l_{\max}^3 (1 - \cos \varphi_{01}) = l_{\min}^3 (1 - \cos \varphi_{04}). \quad (2.13)$$

It follows from this that

$$1 - \cos \varphi_{04} = \frac{l_{\max}^3}{l_{\min}^3} (1 - \cos \varphi_{01}) > 1 - \cos \varphi_{01} \quad (2.14)$$

i.e. $\cos \varphi_{04} < \cos \varphi_{01}$, and it means that $\varphi_{04} > \varphi_{01}$.

Change of system energy takes place only in those points, where the centre of gravity comes up or goes down momentary, and so for composing of energy balance equation we need to analyze only the processes that take place in points (2-3) and (4-5). According to [50] by momentary rise of mass point the system energy changes for value

$$H_{up} = mg(l_{\max} - l_{\min}) + \frac{1}{2} m(l_{\min}^2 \dot{\varphi}_3^2 - l_{\max}^2 \dot{\varphi}_2^2) \quad (2.15)$$

In this formula the first summand describes increment of potential energy, and the second one describes increment of kinetic one. Taking into consideration the relations (2.10),

(2.11) and (2.13) the expression (2.15) can be presented in form of function of initial amplitude φ_{01}

$$H_{up} = mg(l_{\max} - l_{\min}) + mgl_{\max}(1 - \cos \varphi_{01}) \left[\left(\frac{l_{\max}}{l_{\min}} \right)^2 - 1 \right]. \quad (2.16)$$

While rise of material point the potential energy decreases, and while its down movement there is increment of potential energy. In points of direction change we have

$$H_{down} = mg(l_{\min} - l_{\max}) \cos \varphi_{04} < 0. \quad (2.17)$$

Here φ_{04} is maximal deflection at the moment of the end of the increment phase. This consideration is given here for the case when $\varphi_{04} > -\frac{\pi}{2}$. If $\varphi_{04} < -\frac{\pi}{2}$, then $H_{down} > 0$

Thus, for one semi-oscillation, which includes rise and fall of a material point, we obtain total energy gain:

$$\Delta H = H_{up} + H_{down} \quad (2.18)$$

After substitution of the expressions (2.16) and (2.17) to the relation (2.18) we will obtain total energy gain for oscillation period

$$\Delta H = mg(l_{\max} - l_{\min})(1 - \cos \varphi_{04}) + \frac{1}{2} m l_{\max} (1 - \cos \varphi_{01}) \left[\left(\frac{l_{\max}}{l_{\min}} \right)^2 - 1 \right] \quad (2.19)$$

As is obvious from expressions (2.16) - (2.18), that for the oscillation period the system gains some energy ΔH . Characteristic property of increase of vibration amplitude is energy increase on sections 2-3 and 6-7 and its decrease on sections 4-5 and 8-1. Value of energy gain depends on the range of possible change of pendulum length $l_{\min} \leq l \leq l_{\max}$ and current vibration amplitude. If amplitude is small, energy gain is also "small". By small angles φ cosine is near to 1, and the quantity (2.19) is near to naught. By desired range (2.1) and «sufficiently» great dissipation there is some «limiting» oscillation amplitude of pendulum in the system.

By «return» motion of the material point (5-4-3-2-1),

$$l = \begin{cases} l_{\min}, & \dot{\varphi} \cdot \varphi < 0 \\ l_{\max}, & \dot{\varphi} \cdot \varphi > 0 \end{cases} \quad (2.20)$$

the pendulum energy – and its oscillation amplitude with is – will decrease.

Basing on above described properties of pendulum we will build a control system for swinging and oscillation support. Such control system is to solve the following tasks:

- Swinging of a pendulum,
- Pendulum damping,
- Support of oscillation amplitude with disturbances.

2.3. Oscillation control of system of second order of general type.

Differential equations of motion of a controlled mechanical system with one degree of freedom can be presented in the following form:

$$\begin{aligned}\dot{x} &= f_1(x, y, u) \\ \dot{y} &= f_2(x, y, u)\end{aligned}\tag{2.21}$$

In this case x is the positional coordinate and

$$f_1(x, y, u) = y\tag{2.22}$$

is linear or angular speed of the control object, and function $f_2(x, y, u)$ is generalized force divided by object mass or by moment of inertia.

Let for each piecewise continuous vector function $u(t)$ by desired initial conditions the system (2.21) possesses a unique solution $x(t)$, $y(t)$. Let thinking, that control parameter u belongs to given set $U(x, y)$. In other words, vector of the piecewise continuous function $u(t)$ is considered as permissible control, if

$$u(t) \in U(x(t), y(t))\tag{2.23}$$

In the equation (2.23) $x(t)$, $y(t)$ is solution of the equation (2.22) when $u = u(t)$. In the case, when the set $U(x, y)$ depends on state coordinate x , y , condition (2.23) can be verified only by finding solution for the system (2.21) with this equation.

Suppose, that function $f_1(x, y, u)$ do not turn into naught:

$$f_1(x, y, u) > 0\tag{2.24}$$

Then by meeting the conditions (2.24) the coordinate x will always increase. If the equations (2.21) are a mathematical model of mechanical system with one degree of freedom, then in this case the relation (2.22) is correct and the inequality (2.24) takes place in upper half of the phase plane (x, y) .

Let rewrite the system (2.21) in the form of a first-order equation

$$\frac{dy}{dx} = \frac{f_2(x, y, u)}{f_1(x, y, u)} = f(x, y, u)\tag{2.25}$$

and let coordinates

$$x(0) = x_0, y(0) = y_0 \quad (2.26)$$

initial conditions for the system (2.21) or for the equation (2.25). Suppose also, that $y_0 > 0$.

2.3.1. Reachable sets and their limits.

Suppose, that in phase plane (x, y) each trajectory $y(x)$, which begins in the point (2.26) and corresponds to the permissible control function $u(t)$, crosses the axis $Y = 0$ at some end point of time t by finite values of the coordinate x . Let consider the set of possible permissible control functions $u(t)$ and the set of appropriate trajectories $y(x)$, obtained while this control. More specifically, let consider only some of these trajectories, that begin from the point (2.26) and end on the abscissa $Y = 0$. The whole collection of these curves includes set of points of attainability domain [25] or so-called integral funnel [7], [81]. This set of attainability D is schematically shown in Figure 2.3

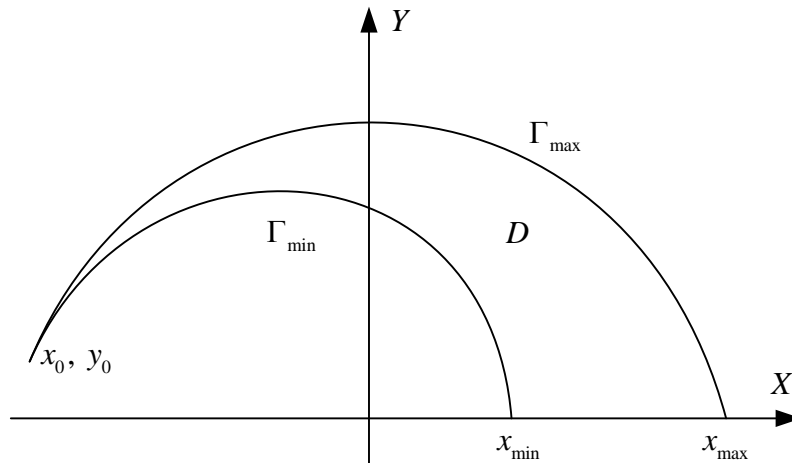


Figure 2.3 – Reachable set D

Let consider equation, that maximizes or minimizes the derivative dy/dx with help of variable u in point (x, y) . To create such equation one need to maximize or minimize the right part of the expression (2.25) with help of argument u , i.e.:

$$u = u_{\max}(x, y) = \arg \left[\max_{u \in U(x, y)} f(x, y, u) \right], \quad (2.27)$$

or correspondingly

$$u = u_{\min}(x, y) = \arg \left[\min_{u \in U(x, y)} f(x, y, u) \right]. \quad (2.28)$$

Support, that the function (2.25) and the set $U(x, y)$ are so, that for each point of phase space there is only one maximum in (2.27) and only one minimum (2.28), which are in the attainability domain D .

Also support, that solution of the system (2.21) by initial conditions (2.26) and control (2.27) or (2.28) is ensured by the piecewise continuous function $u(t)$. Let $y = y_{\max}(x)$ be solution of the equation

$$\frac{dy}{dx} = f[x, y, u_{\max}(x, y)], \quad (2.29)$$

and $y = y_{\min}(x)$ be solution of

$$\frac{dy}{dx} = f[x, y, u_{\min}(x, y)], \quad (2.30)$$

with initial conditions (2.26).

Let designate a part of the trajectory $y = y_{\max}(x)$ on interval $x_0 \leq x \leq x_{\max}$ with Γ_{\max} , where x_{\max} is value obtained by solution of $y_{\max}(x) = 0$. Let also designate a part of the trajectory $y = y_{\min}(x)$ on interval $x_0 \leq x \leq x_{\min}$ with Γ_{\min} , where x_{\min} is value obtained by solution of $y_{\min}(x) = 0$.

Now let show, that the curves Γ_{\max} and Γ_{\min} are the upper and the lower limits of the attainability domain D (fig. 2.3). For each function $u^*(x, y) \neq u_{\max}(x, y)$, by which the trajectory of the equation (2.25) starting from the point (2.26), is higher than point $(x, y) \in \Gamma_{\max}$, condition of unique solution $y = y_{\max}(x)$ and condition (2.27) are not fulfilled. Conclusions for the limit Γ_{\min} are similar

2.3.2. Maximization and minimization of oscillation amplitude of pendulum.

Task for maximization and minimization of derived function dy/dx for first-order mechanical system can be written in symbol form [26]

$$\max_{u \in U(x, y)}[x] \text{ if } y = 0 \quad (2.31)$$

$$\min_{u \in U(x, y)}[x] \text{ if } y = 0 \quad (2.32)$$

For concerned variable length pendulum (s. Fig 2.1) the equation (2.25) can be presented in such form:

$$\frac{d}{dt} \left[mu^2 \frac{dx}{dt} \right] = -mug \sin x - c \frac{dx}{dt}. \quad (2.33),$$

Taking into account the before agreed notations the equation (2.33) can be written as follows:

$$\frac{d}{dt} \left[ml^2 \frac{d\varphi}{dt} \right] = -mgl \sin \varphi - c \frac{d\varphi}{dt}. \quad (2.34)$$

here $c = \text{const}$ is viscous friction coefficient.

Let write the second-order equation (2.34) in form of first-order differential equations (2.21):

$$\begin{aligned} \dot{\varphi} &= \frac{y}{ml^2} \\ \dot{y} &= -mgl \sin \varphi - c \frac{y}{ml^2} \end{aligned} \quad (2.35)$$

here $y = ml^2 \dot{\varphi}$ is angular momentum.

Let also suppose, that pendulum has following initial conditions

$$\varphi(0) < 0, \quad y(0) = 0, \quad (2.36)$$

and distance l can change within the limits (2.1).

The task of control by maximization (minimization) of amplitude consists in finding the law of variation of distance l with account to inequality (2.1), by which values of angular deflection φ are maximal (minimal) in the state, when kinetic moment y turns into naught.

To creation the equation let write the system of equations (2.35) in the form of (2.25)

$$\frac{dy}{d\varphi} = -c - \frac{m^2 l^3 g \sin \varphi}{y} \quad (2.37)$$

According to the above given results, maximization of the right part of the equation (2.37) by argument l with account to limits (2.1) gives an *optimal* control law for swinging at semi-oscillation, for which $y > 0$

$$l = \begin{cases} l_{\max}, & \text{if } \varphi < 0 \\ l_{\min}, & \text{if } \varphi > 0 \end{cases} \quad (2.38)$$

For the next (second) semi-oscillation, for which $y < 0$, the control law can be found by analogy. Taking into consideration the fact, that by $y > 0$ the angular speed $\dot{\varphi}$ is positive, and by $y < 0$ negative, the control law for maximization of amplitude can be presented in form of a relation coinciding with (2.8).

$$l = \begin{cases} l_{\min}, & \dot{\varphi} \cdot \varphi > 0 \\ l_{\max}, & \dot{\varphi} \cdot \varphi < 0 \end{cases}. \quad (2.39)$$

While consideration of the task of amplitude *minimization* the following law of pendulum oscillation damping is obtained.

$$l = \begin{cases} l_{\min}, & \dot{\varphi} \cdot \varphi < 0 \\ l_{\max}, & \dot{\varphi} \cdot \varphi > 0 \end{cases} \quad (2.40)$$

2.3.3. Simulation of optimal swinging and pendulum damping

Let consider a pendulum with the following parameters:

$$m = 0.5 \text{ kg}, l_{\max} = 0,6 \text{ m}, l_{\min} = 0,5 \text{ m}, c = 0. \quad (2.41)$$

In Figure 2.4 there are graphics of angular change φ , angular speed $\dot{\varphi}$ and distance l as time function. These functions were obtained by solving the equations of motion (2.35) by the optimal control (2.39) and initial conditions $\varphi(0) = -0.1$, $y(0) = 0$. From the graphic is evident, that by control $l(\varphi, \dot{\varphi})$ the oscillation amplitude increases. Relay function of control $l(t)$ turns momentary from the value l_{\max} to the value l_{\min} by change of angle sign φ and returns to the value l_{\max} by change of speed sign $\dot{\varphi}$. Between the change points the value of $l = \text{const}$.

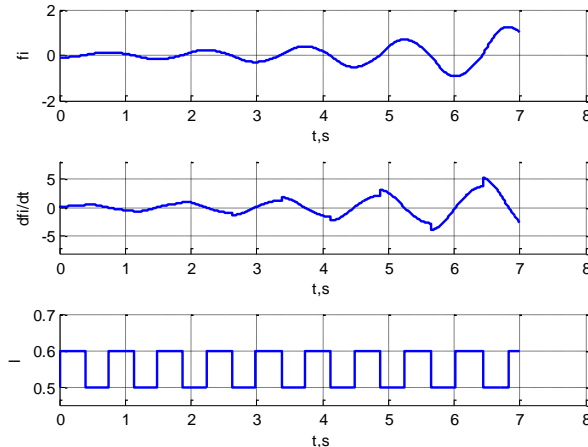


Figure 2.4 – Graphics of angular change $\varphi(t)$, angular speed $\dot{\varphi}(t)$ and length of pendulum $l(t)$ while swinging

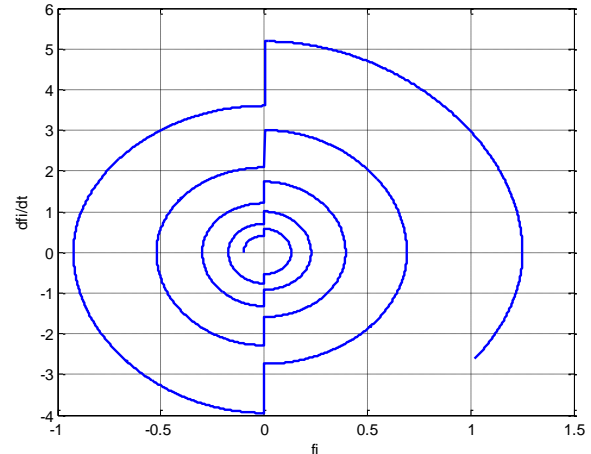


Figure 2.5 – Phase portrait in plane $(\varphi, \dot{\varphi})$ while swinging

In Figure 2.5 there is phase portrait of swinging of pendulum in plane $(\varphi, \dot{\varphi})$. In graphics 2.4 and 2.5 we can observe a jump of angular speed $\dot{\varphi}$ by switching of control $l(t)$ from the value l_{\max} to the value l_{\min} . This can be explained by the fact, that the moment of inertia of the mechanism decreases, and the angular speed increases according to the law of conservation of angular momentum.

In Figure 2.6 there are graphics of angular change φ , angular speed $\dot{\varphi}$ and control l as a time function. These functions were obtained by solving of equations of motion (2.35) by optimal control (2.40) and initial conditions $\varphi(0) = -\pi/2$, $y(0) = 0$. In Figure 2.6 it is obvious, that by control $l(\varphi, \dot{\varphi})$ the oscillation amplitude decreases. Relay function of control $l(t)$ turns momentary from the value l_{\min} to the value l_{\max} by change of angle sign φ and returns to the value l_{\min} by change of speed sign $\dot{\varphi}$. Between the change points the value of $l = \text{const}$.

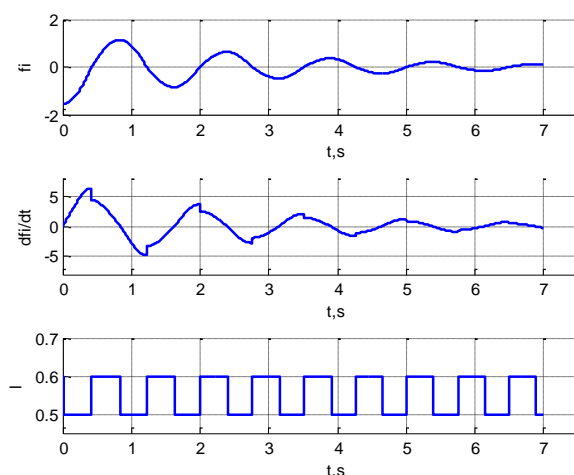


Figure 2.6 – Graphics of angular change $\varphi(t)$, angular speed $\dot{\varphi}(t)$ and length of pendulum $l(t)$ while oscillation damping

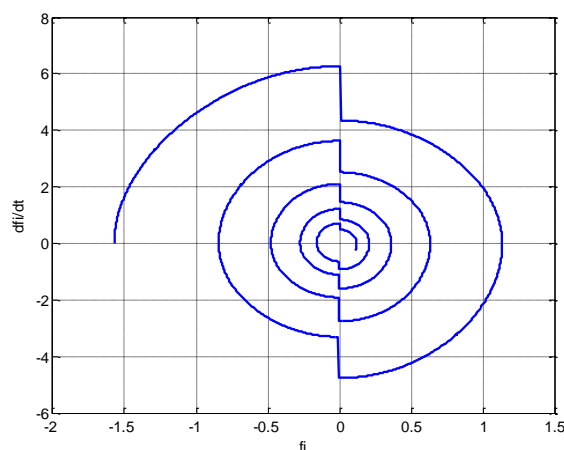


Figure 2.7 – Phase portrait in plane $(\varphi, \dot{\varphi})$

In Figure 2.7 there is phase portrait of damping of pendulum oscillation in plane $(\varphi, \dot{\varphi})$. In graphics 2.6 and 2.7 we can see a jump of angular speed $\dot{\varphi}$ by switching of control $l(t)$ from the value l_{\min} to the value l_{\max} . This can be explained by the fact that the moment of inertia of the mechanism increases and the angular speed decreases according to the law of conservation of angular momentum.

2.4. Synthesis of control system of periodic pendulum motions

Constant value of full energy unequivocally characterizes the current amplitude and pendulum oscillation frequency, corresponding to free motion of mechanical system. For ensuring of periodical motions of variable length pendulum we will take its full energy as controlled parameter.

$$H = \frac{1}{2}ml^2\dot{\varphi}^2 + mgl \cos \varphi \quad (2.42)$$

With help of maximization/minimization method of swinging amplitude by control (2.39) and (2.40) by the end of each semi-oscillation one can obtain some limited gain of system energy (2.19). For reaching of desired energy level by great measured error ($H_s - H$) between desired H_s and current energy level H , the mechanism must make several oscillations with using of the limits l_{\min} and l_{\max} . While going into the range

$$(H_s - H) < \Delta H \quad (2.43)$$

for exclusion of switching mode the change of pendulum length should be proportionate to $(H_s - H)$.

The expression of feedback control will take in this form:

$$u^* = l_0 + (H_s - H) \cdot \gamma \cdot \begin{cases} +\Delta l, & \dot{\varphi} \cdot \varphi > 0 \\ -\Delta l, & \dot{\varphi} \cdot \varphi < 0 \end{cases} \quad (2.44)$$

where γ is coefficient, that is chosen while simulation,

$$\begin{aligned} l_0 &= \frac{l_{\max} + l_{\min}}{2} \\ \Delta l &= \frac{l_{\max} - l_{\min}}{2} \end{aligned} \quad (2.45)$$

The expression (2.44) describes feedback for angle φ , angle speed $\dot{\varphi}$ and – on upper level – for deflection of the total energy value from its desirable value. For taking into account the limits (2.1) suppose, that

$$u = \begin{cases} l_{\max}, & u^* \geq l_{\max} \\ u^*, & l_{\min} < u^* < l_{\max} \\ l_{\min}, & u^* \leq l_{\min} \end{cases} \quad (2.46)$$

2.4.1. Simulations

Let consider simulations results of control system of variable length pendulum. Model of the mechanism under study (s. Fig. 2.8) was realized and researched with help of software package MATLAB-Simulink. The model has the following parameters: mass of material point $m = 0,5$ kg, minimal length $l_{\min} = 0,5$ m, maximal length $l_{\max} = 0,6$ m, viscous friction $c = 0.01$ N·m·s.

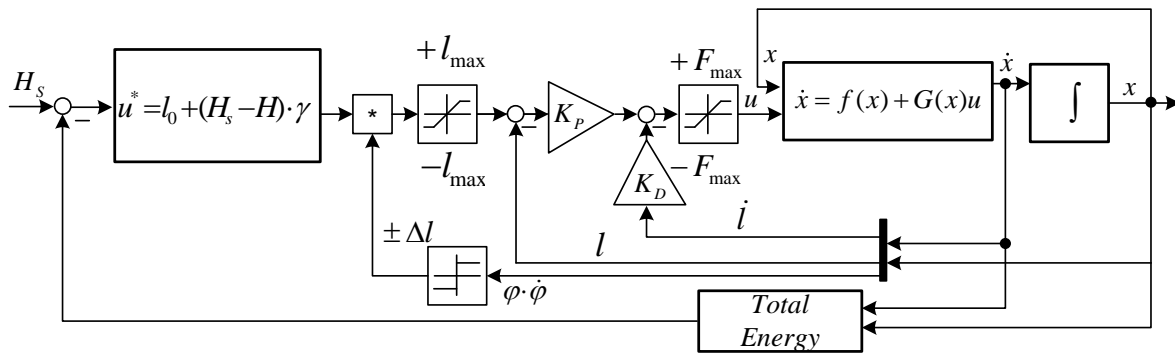


Figure 2.8 –Control system for a variable length pendulum

In Figure 2.9 there are transients while practicing of stepped task for control system of desirable energy level. These transients were obtained by modeling of control system with initial conditions $\varphi(0) = -0.1$ rad, $y(0) = 0$. In Figure 2.9 it is obvious, that by control $l(\varphi, \dot{\varphi})$ oscillation amplitude increases with increment of specified energy level. The function of control $l(t)$ turns from the value l_{\max} to the value l_{\min} by change of angle sign φ and returns to the value l_{\max} by change of speed sign $\dot{\varphi}$.

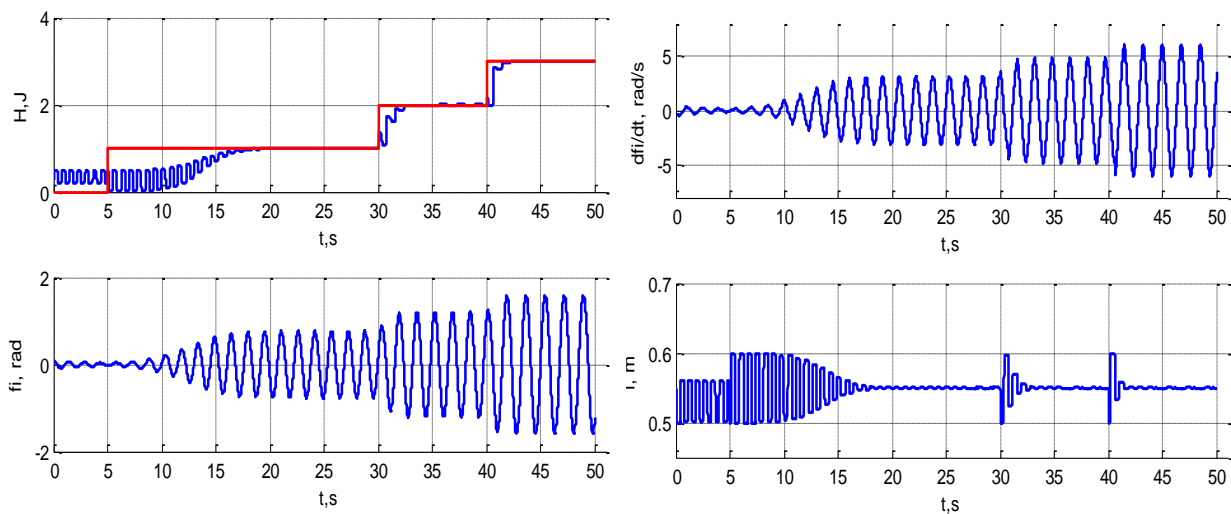


Figure 2.9 – Step responses of control system

In Figure 2.10 there is the phase portrait in plane $(\varphi, \dot{\varphi})$ by stepped increment of desired energy level on control system. On the phase portrait three closed orbits are visible – these are limit cycles, which correspond to three different energy levels. Passage from one trajectory into another one is fulfilled during several pendulum oscillations.

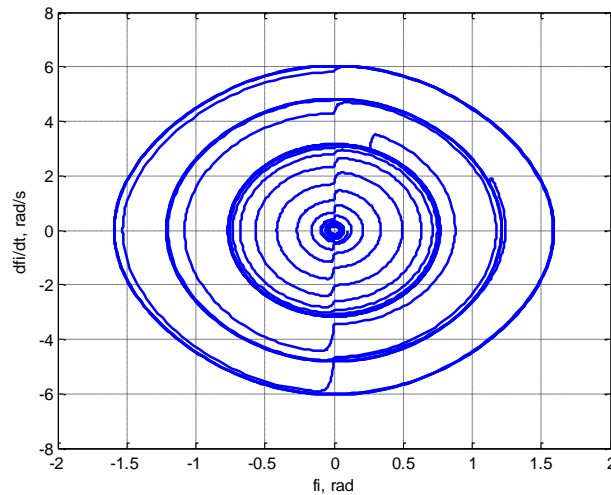


Figure 2.10 – Phase portrait in plane $(\varphi, \dot{\varphi})$

In Figure 2.11 there are transients while practicing of stepped decrement for control system of desirable energy level. From Figure 2.11 it is obvious, that while control (2.44) oscillation amplitude decreases with decrement of specified energy level. The function $l(t)$ turns from the value l_{\min} to the value l_{\max} by change of angle sign φ and returns to the value l_{\min} by change of speed sign $\dot{\varphi}$.

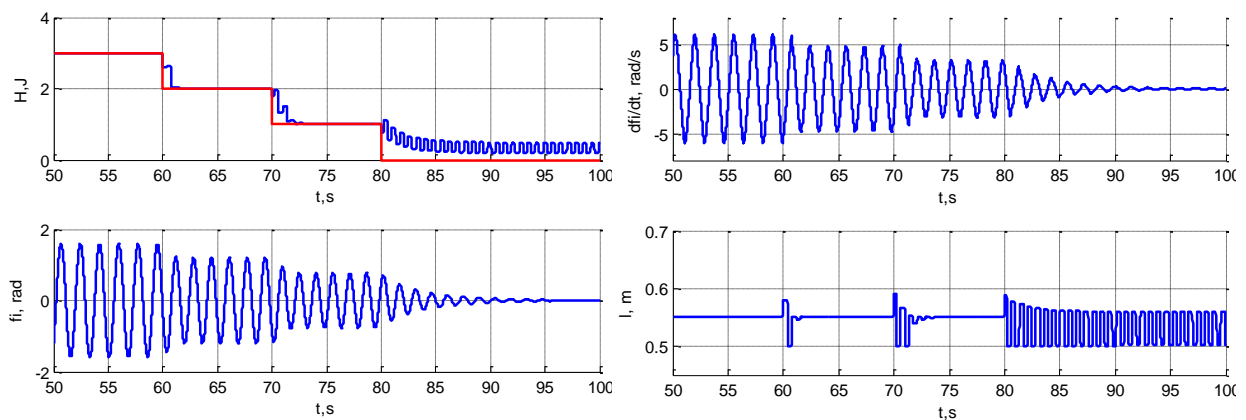


Figure 2.11 – Stepped decrement of desired energy

In Figure 2.12 there is the phase portrait in plane $(\varphi, \dot{\varphi})$ by stepped decrement of specified energy level on control system. On the phase portrait three closed trajectories are visible – these are limit cycles, which correspond to three different energy levels. Passage from one periodical mode into another one is fulfilled during several pendulum oscillations.

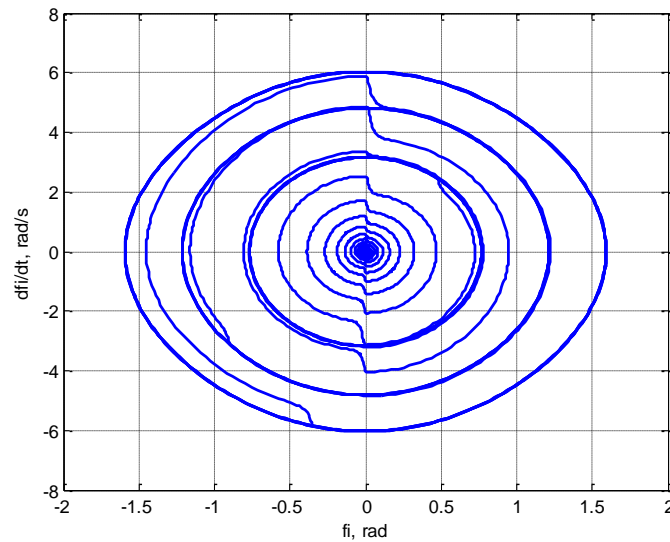


Figure 2.12 – Phase portrait of the system in plane $(\varphi, \dot{\varphi})$

In Figure 2.13 there are transients in the presence in the system of viscous friction with coefficient $c = 0.01 \text{ N} \cdot \text{m} \cdot \text{s}$. From Figure 2.13 it is visible, that with appearance of viscous friction (dissipation) in the system the oscillation amplitude reduces and energy level decreases. Total energy varies around some value. This can be explained by the fact, that loss compensation is fulfilled during a half of an oscillation period.

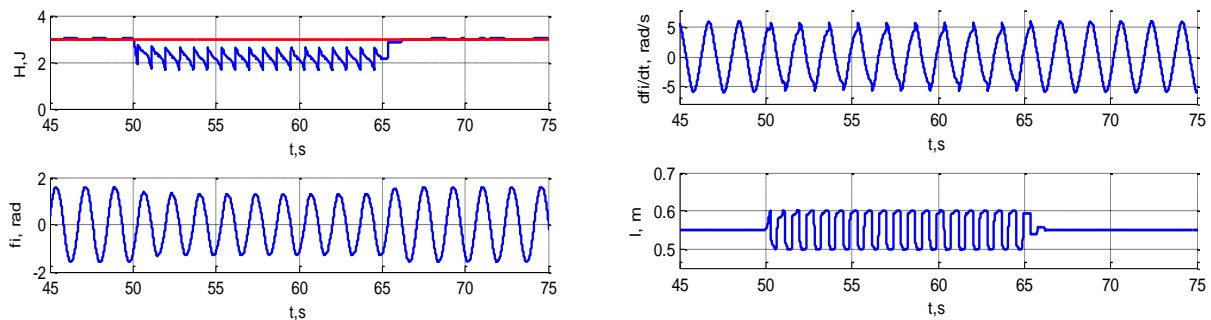


Figure 2.13 – Transients by $c = 0.01 \text{ N} \cdot \text{m} \cdot \text{s}$

In Figure 2.14 there is the phase portrait in plane $(\varphi, \dot{\varphi})$ in presence of dissipation with coefficient $c = 0.01 \text{ N} \cdot \text{m} \cdot \text{s}$. On the phase portrait two limit cycles are visible. Phase elliptically trajectory corresponds with free pendulum oscillations. The second closed trajectory corresponds to motions under dissipative forces. Curvature of phase trajectory has its explanation in presence of viscous friction, by which the speed $\dot{\varphi}$ noticeably decreases at each oscillation period. It is clearly visible, that at each semi-oscillation the control system tends to return the pendulum into the phase trajectory, which corresponds with free oscillations.

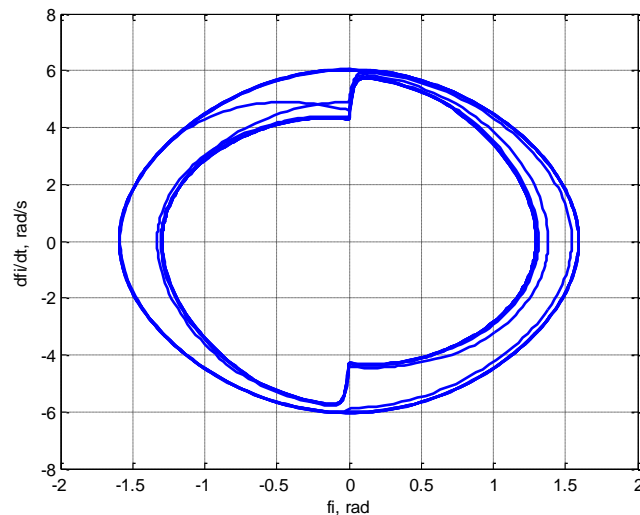


Figure 2.14 – Phase portrait with $c = 0.01 \text{ N} \cdot \text{m} \cdot \text{s}$

2.4.2. Experiments

Let consider experimental results of control system for variable length pendulum.

Control of experimental setup was realized with application of Matlab xPC-Target technology (fig. 2.15). On the basis of xPC-Target and with help of industrial communication network a group of drives of the experimental setup was connected to main (Master) computer.

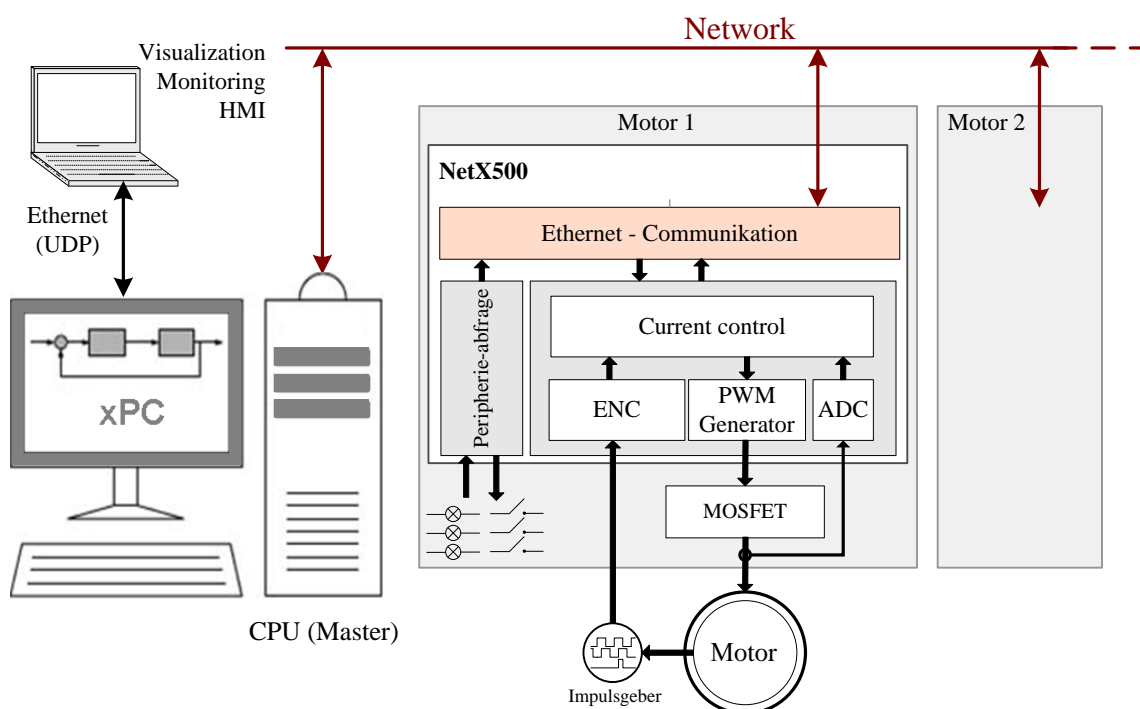


Figure 2.15 – Structure of experimental setup

In Figure 2.16 a photo and a schematic diagram of the experimental setup is presented. The experimental setup was constructed on the basis of power drive, detailed information

about which is presented in [39]. The pendulum consists of two masses m_1 and m_2 . The first mass is fastened by use of bearing in suspension point O (s. Fig. 2.16). The main difference between the experimental setup and above considered model is:

- Presence of two weighty links,
- Asymmetrical mass distribution.

State control counter for the moving mass has a «sufficiently» high operation speed.

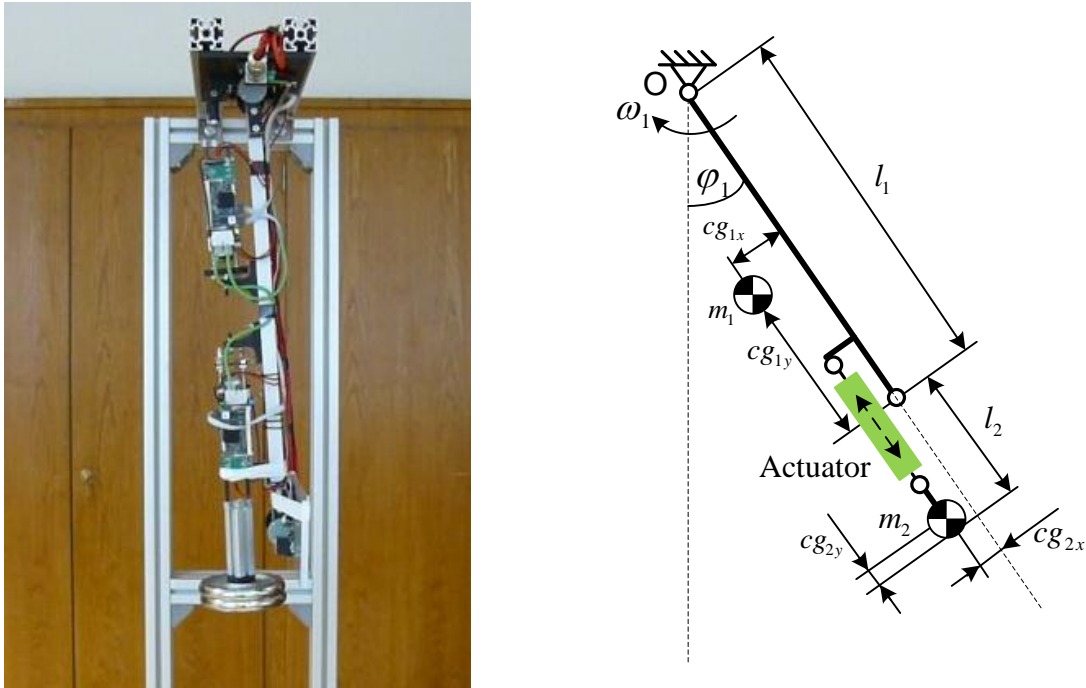


Figure 2.16 – Photo (left) and schematic diagram (right) of the experimental setup

The experimental setup has the following parameters:

$$\begin{aligned} cg_{1x} = 0,04 m, \quad cg_{1y} = -0,315 m, \quad l_1 = 0,63 m, \quad J_1 = 5,59 \cdot 10^{-2} \text{ kg} \cdot m^2, \quad m_1 = 0,63 m \\ cg_{2x} = 0,04 m, \quad cg_{2y} = -0,01 m, \quad l_2 = 0,2 m, \quad J_2 = 0,4 \cdot 10^{-2} \text{ kg} \cdot m^2, \quad m_2 = 2,2 m \end{aligned} \quad (2.47)$$

Here cg_{1x} , cg_{1y} , cg_{2x} , cg_{2y} are coordinates of links' centers of mass, l_1 , l_2 are links' lengths, m_1 , m_2 are their masses, J_1 , J_2 are moments of links' inertia with respect to their centers of mass.

Expression for potential energy of the system is of the following form:

$$E_p = E_0 + gmh = E_0 + g \cdot \begin{bmatrix} m_1 & m_2 \end{bmatrix} \cdot \begin{bmatrix} -(l_1 + cg_{1y}) \cos \varphi + cg_{1y} \sin \varphi \\ -(l_1 + l_2 + cg_{2y} - l) \cos \varphi + cg_{2y} \sin \varphi \end{bmatrix}, \quad (2.48)$$

where E_0 is displacement of the reference level of potential energy. Expression for kinetic energy of the system is:

$$E_K = \frac{1}{2} \cdot \begin{bmatrix} \omega^2 & v^2 \end{bmatrix} \cdot \begin{bmatrix} J_1 + m_1 R_1^2 + J_2 + m_2 R_2^2 \\ m_2 \end{bmatrix}. \quad (2.49)$$

Here $R_1^2 = \left((l_1 + cg_{1y})^2 + (cg_{1x})^2 \right)$, $R_2^2 = \left((l_1 + l_2 + cg_{2y} - l)^2 + (cg_{2x})^2 \right)$.

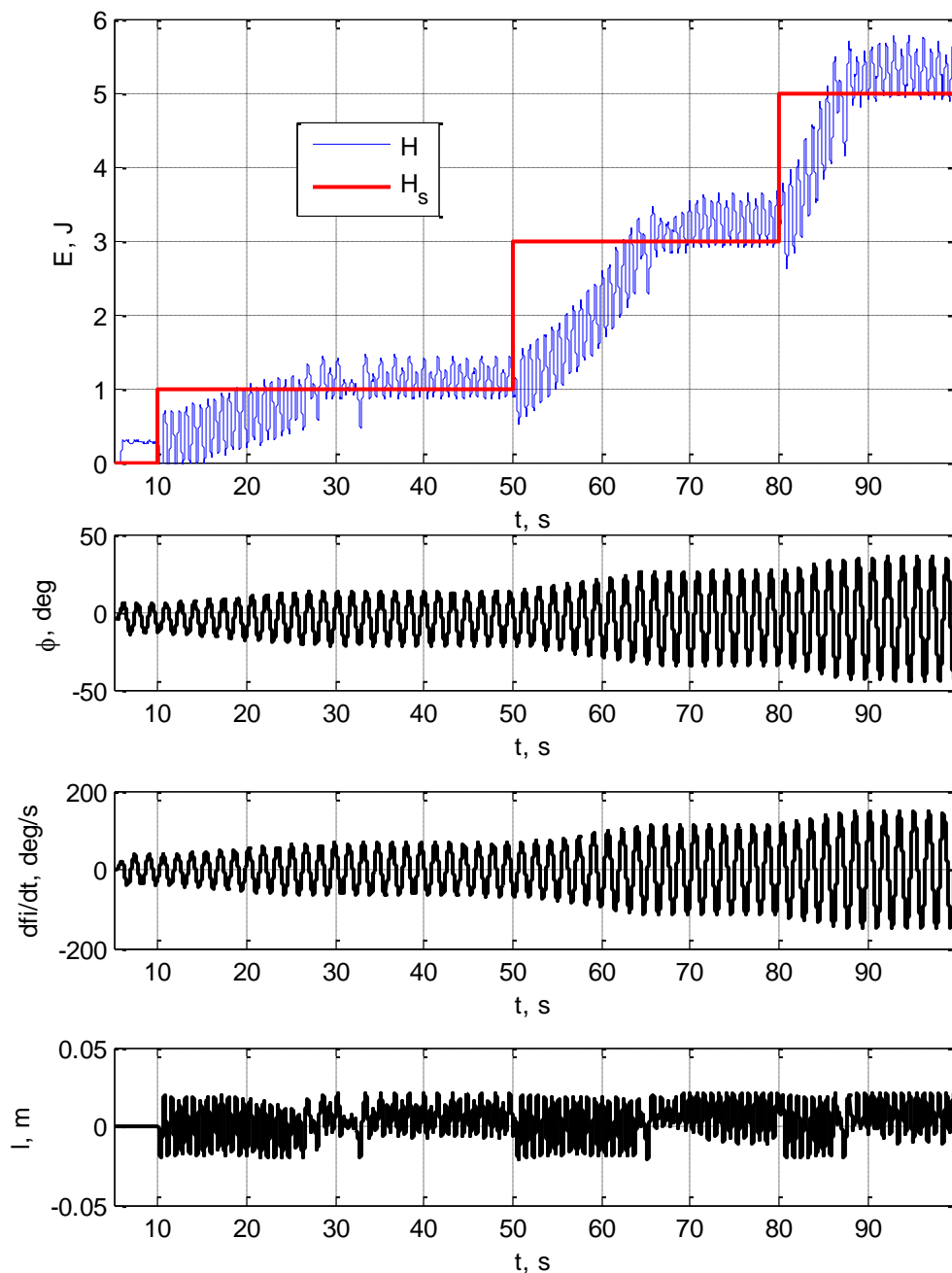


Figure 2.17 – Transients by stepped increment of specified energy level

In Figure 2.17 there are transients while practicing of stepped task for control system of desirable energy level. From the Figure 2.17 it is obvious, that by control $l(\varphi, \dot{\varphi})$ oscillation amplitude increases together with decrement of specified energy level. By change from 1 J to 3 J the experiment showed a period of the order of 14 s. A great duration of transients in comparison with simulation is connected with presence of dissipative forces in the experimental setup, which were not taken into account while mathematical modeling.

In Figure 2.18 there is the phase portrait in plane $(\varphi, \dot{\varphi})$ by stepped increment of specified energy level on control system. From the phase portrait three closed trajectories are visible, which correspond to three different energy levels. Passage from one trajectory into another one is fulfilled during several vibrations.

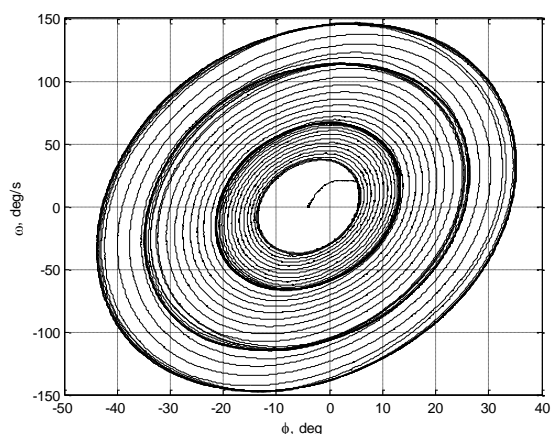


Figure 2.18 – Phase portrait in plane $(\varphi, \dot{\varphi})$ by increment of energy level

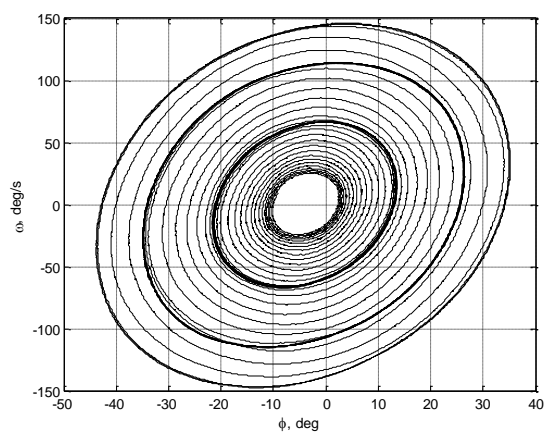


Figure 2.19 - Phase portrait in plane $(\varphi, \dot{\varphi})$ by decrement of energy level

In Figure 2.19 there is the phase portrait in plane $(\varphi, \dot{\varphi})$ by stepped decrement of specified energy level. From the phase portrait three closed trajectories are visible, which correspond to three different energy levels – the system tends to the desire orbits. Passage from one periodical mode into another one is fulfilled faster than by increment of specified energy level. This can be explained by the fact, that dissipative forces help to damp the mechanism.

In Figure 2.20 there are transients while practicing of stepped decrement of specified energy level. From Figure 2.20 it is obvious, that by control (2.44) the oscillation amplitude decreases with decrement of specified energy. By change from 3 J to 1 J the transient time amounts to approximately 8 s. Transients time by decrement of specified energy is less than by increment. This is connected with presence of dissipative forces in the experimental setup, which in case of damping affect the process positively.

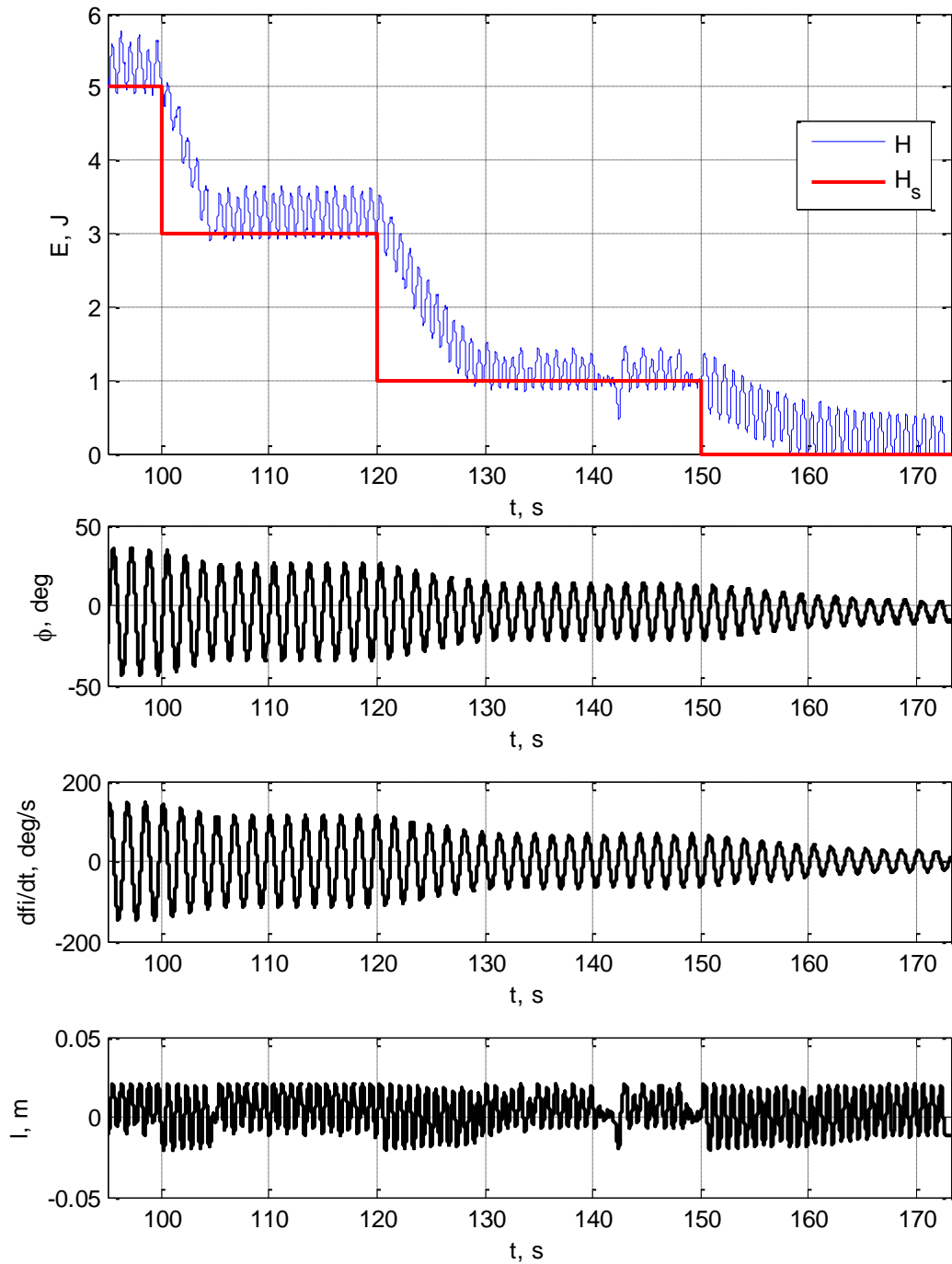


Figure 2.20 – Transients by stepped decrement of specified energy

Trajectory divergence from oscillation to oscillation is connected with energy loss, which can be inconstant, as well as with sensor noise and other factors. It is also to mention, that in the steady-state behavior the control system compensates the presence of dissipative forces in the experimental setup.

In Figure 2.21 the influence of coefficient γ (formula (2.44)) on speed of transients of the system is presented. Here the same properties are noticeable, that are inherit in P-regulator, and namely procrastination of transients and decrement of coefficient γ .

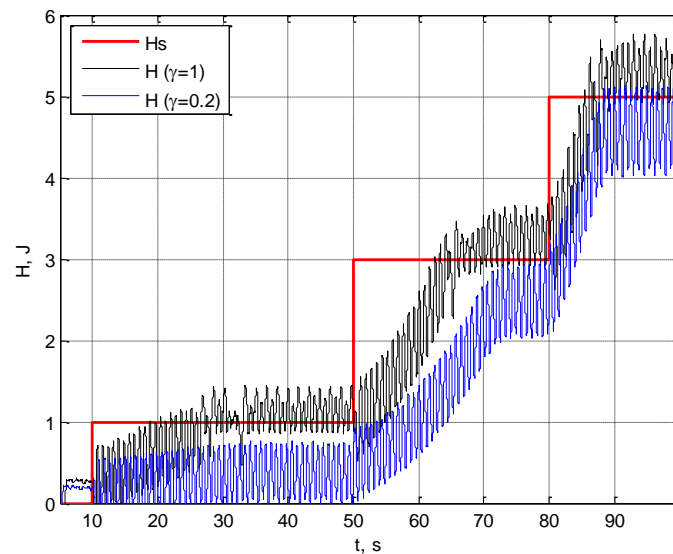


Figure 2.21 – Influence of coefficient γ on speed of transients

Thus, mathematical modeling and experiments demonstrate a possibility to support the systems oscillations at the specified amplitude by using feedback of signal about deflection of total energy value from its desired value.

In this chapter a relatively simple control object is considered – variable length pendulum. The control system was constructed, by which the pendulum oscillation amplitude increases. The control system was constructed as well, by which the pendulum oscillation amplitude decreases. Combining of these control laws allows to construct a control system by which a specified oscillation amplitude is supported. In this control law a feedback is used for deflection of a current energy value from the specified one. In the next chapter we consider the task of construction of periodical motions by a more complicated mechanism – double pendulum.

Chapter 3. Oscillation control of double pendulum

Equation Section (Next)

This chapter deals with the task to develop the control law of double pendulum oscillations. The system input is a torque in the interlink joint. For the mechanical system we developed some control laws based on the application of the speed gradient method and on the law of variation of angular momentum. Simulations were made as well as the experiments proving the efficiency of the control laws which were developed.

3.1. Mathematical model

The object of research is the pendulum consisting of two links. The first link of the pendulum OB and the second one BD are fixed with the help of joints in the points O and B (s. Fig. 3.1). In Figure 3.1 the letters m_1 and m_2 show the location of the centers of mass of the links. Torques M and M_c are applied in the joints O and B respectively. The given system is underactuated as only the torque M_c in the interlink joint is considered to be a controlling one. We are going to simulate different types of disturbing actions in the joint O of the double pendulum with the help of the torque M (constantly acting torque, viscous friction).

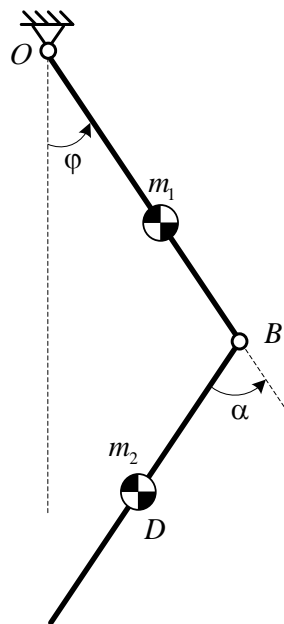


Figure 3.1 – Double pendulum

Let φ is the angle of deflection of the first link OB from the vertical, α is the angle of deflection of the second link BD with reference from the first link.

The expression of the potential energy of the system takes the following form:

$$V = b_1 \cos \varphi + b_2 \cos(\varphi + \alpha). \quad (3.1)$$

Here $b_1 = (m_1 r_1 + m_2 OB)g$, $b_2 = m_2 BDg$.

The expression of the kinetic energy of the system is

$$T = \frac{1}{2} \left[a_{11} \dot{\varphi}^2 + 2a_{12} \dot{\varphi}(\dot{\varphi} + \dot{\alpha}) \cos \alpha + a_{22} (\dot{\varphi} + \dot{\alpha})^2 \right], \quad (3.2)$$

where $a_{11} = I + m_2 OB^2$; $a_{12} = m_2 r_2 OB$; I is the inertia moment of the first link about point O ; m_1 , m_2 are the masses of the first and the second bodies; OB is the length of the first link, r_1 , r_2 are the distances from the points O and B to the centers of masses of the first and the second links; a_{22} is the inertia moment of the second link about point B ; g is the gravity acceleration.

Using the Lagrange equations (2.2), with the help of relations (3.1) and (3.2) it is possible to obtain the equations of motion for the double pendulum

$$\begin{aligned} j_1(\alpha) \ddot{\varphi} + j_2(\alpha) \ddot{\alpha} - 2a_{12} \dot{\varphi} \dot{\alpha} \sin \alpha - a_{12} \dot{\alpha}^2 \sin \alpha &= b_1 \sin \varphi + b_2 \sin(\varphi + \alpha) + M \\ j_2(\alpha) \ddot{\varphi} + a_{22} \ddot{\alpha} + a_{12} \dot{\varphi}^2 \sin \alpha &= b_2 \sin(\varphi + \alpha) + M_c \end{aligned} \quad (3.3)$$

Here the expression

$$j_1(\alpha) = a_{11} + a_{22} + 2a_{12} \cos \alpha \quad (3.4)$$

describes the inertia moment of the whole mechanism about point O and hence $j_1(\alpha) > 0$,

$$j_2(\alpha) = a_{22} + a_{12} \cos \alpha. \quad (3.5)$$

3.2. Synthesis of the pendulum oscillation control using the energy integral.

Let us consider the control method with the application of the speed gradient method for a system of the type

$$\dot{x} = f(x) + G(x)u \quad (3.6)$$

Here x is the vector ($n \times 1$) of the object state, u is the vector ($m \times 1$) of system input.

The key method [14] of Lyapunov functions construction when the task is to investigate the system stability is Chetayev method based on the usage of the information about the first integrals of the system. In paper [14] it is consider that the speed gradient method (SGM) should be used in combination with Lyapunov functions to synthesize the oscillation control.

According to the technique described in [27] the control should be chosen proportional to the gradient of the rate of decay of some goal function $W(t, x)$. The aim of control is to minimize or to maximize this function. The control law calculated using the speed gradient method is the following

$$u = -\gamma \cdot \nabla_u \dot{W}(t, x), \quad \gamma > 0 \quad (3.7)$$

where $\dot{W}(t, x)$ is the full derivative of function according to the system (3.6), and the sing ∇_u denotes the derivative with respect to the parameter u .

It is necessary to implement the ultimate equality

$$\lim_{t \rightarrow \infty} W(t, x(t)) = c, \quad (3.8)$$

where c is the desired value of the function $W(t, x)$.

We can write down the control algorithm using the speed gradient method in the following form:

$$u = -\gamma \cdot G^T(x)(W(t, x) - c) \frac{\partial W}{\partial x}, \quad \gamma > 0 \quad (3.9)$$

3.2.1. Speed gradient method in the oscillation control.

Let us use the total energy of the system as the goal function

$$W(\varphi, \dot{\varphi}, \alpha, \dot{\alpha}) = H(\varphi, \dot{\varphi}, \alpha, \dot{\alpha}). \quad (3.10)$$

where

$$H = T + V = \frac{1}{2} \left[a_{11} \dot{\varphi}^2 + 2a_{12} \dot{\varphi} (\dot{\varphi} + \dot{\alpha}) \cos \alpha + a_{22} (\dot{\varphi} + \dot{\alpha})^2 \right] + b_1 \cos \varphi + b_2 \cos(\varphi + \alpha) \quad (3.11)$$

Solving the equation (3.3) with respect to higher derivatives we obtain

$$\begin{aligned} \begin{bmatrix} \ddot{\varphi} \\ \ddot{\alpha} \end{bmatrix} &= \begin{bmatrix} j_1(\alpha) & j_2(\alpha) \\ j_2(\alpha) & a_{22} \end{bmatrix}^{-1} \cdot \begin{bmatrix} 2a_{12} \dot{\varphi} \dot{\alpha} \sin \alpha + a_{12} \dot{\alpha}^2 + b_1 \sin \varphi + b_2 \sin(\varphi + \alpha) \\ -a_{12} \dot{\varphi}^2 \sin \alpha + b_2 \sin(\varphi + \alpha) \end{bmatrix} + \\ &+ \begin{bmatrix} -j_2(\alpha) / (a_{22} j_1(\alpha) - j_2(\alpha)^2) \\ j_1(\alpha) / (a_{22} j_1(\alpha) - j_2(\alpha)^2) \end{bmatrix} u \end{aligned} \quad (3.12)$$

Here $u = M_C$ is the torque in the interlink joint. From equation (3.12) we can obtain the expression

$$G^T(x) = [0 \quad -j_2(\alpha) / (a_{22} j_1(\alpha) - j_2(\alpha)^2) \quad 0 \quad j_1(\alpha) / (a_{22} j_1(\alpha) - j_2(\alpha)^2)]. \quad (3.13)$$

Now we can find partial derivatives of the function (3.11)

$$\frac{\partial H}{\partial x} = \begin{bmatrix} \frac{\partial H}{\partial \varphi} \\ \frac{\partial H}{\partial \dot{\varphi}} \\ \frac{\partial H}{\partial \alpha} \\ \frac{\partial H}{\partial \dot{\alpha}} \end{bmatrix} = \begin{bmatrix} -b_2 \sin(\alpha + \varphi) - b_1 \sin \varphi \\ a_{11}\dot{\varphi} + a_{22}(\dot{\alpha} + \dot{\varphi}) + a_{12} \cos \alpha (\dot{\alpha} + \dot{\varphi}) + a_{12}\dot{\varphi} \cos \alpha \\ -b_2 \sin(\alpha + \varphi) - a_{12} \sin \alpha (\dot{\alpha} + \dot{\varphi})\dot{\varphi} \\ a_{22}(\dot{\alpha} + \dot{\varphi}) + a_{12}\dot{\varphi} \cos \alpha \end{bmatrix} \quad (3.14)$$

Substituting relations (3.13) and (3.14) into expression (3.9), we obtain the control law of the double pendulum

$$u = \gamma (H_s - H) \begin{bmatrix} 0 \\ \frac{j_2(\alpha)}{(a_{22}j_1(\alpha) - j_2(\alpha)^2)} \\ 0 \\ \frac{j_1(\alpha)}{(a_{22}j_1(\alpha) - j_2(\alpha)^2)} \end{bmatrix}^T \begin{bmatrix} -b_2 \sin(\alpha + \varphi) - b_1 \sin \varphi \\ a_{11}\dot{\varphi} + a_{22}(\dot{\alpha} + \dot{\varphi}) + a_{12} \cos \alpha (\dot{\alpha} + \dot{\varphi}) + a_{12}\dot{\varphi} \cos \alpha \\ -b_2 \sin(\alpha + \varphi) - a_{12} \sin \alpha (\dot{\alpha} + \dot{\varphi})\dot{\varphi} \\ a_{22}(\dot{\alpha} + \dot{\varphi}) + a_{12}\dot{\varphi} \cos \alpha \end{bmatrix}$$

or

$$u = \gamma (H_s - H) \frac{(j_1(\alpha) - j_2(\alpha))(a_{22}(\dot{\alpha} + \dot{\varphi}) + a_{12}\dot{\varphi} \cos \alpha) - j_2(\alpha)(a_{11}\dot{\varphi} + a_{12} \cos \alpha (\dot{\alpha} + \dot{\varphi}))}{a_{22}j_1(\alpha) - j_2(\alpha)^2} \quad (3.15)$$

Here H_s is the desired value of the goal function. Maximum possible value in the interlink joint is restricted $|u| \leq M_{MAX}$, that is:

$$u = \begin{cases} M_{MAX}, & u > M_{MAX} \\ u, & |u| \leq M_{MAX} \\ -M_{MAX}, & u < -M_{MAX} \end{cases}, \quad (3.16)$$

where M_{MAX} - maximal value of the torque in the interlink joint.

Below we can see a block-structure of the double pendulum model with a control system (see Picture 3.2).

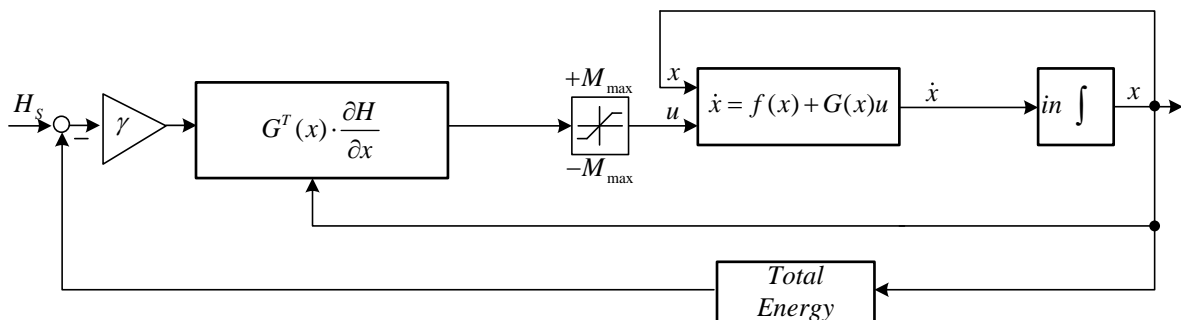


Figure 3.2 – Control system of pendulum

The model of the system consists of the following components: a model of pendulum dynamics, a model of torque (3.16), a model of calculation of the total energy, a model of a non-linear controller

3.2.2. Simulation of the control system

Let us consider the equation of the double pendulum motion with the following parameters:

$$\begin{aligned} m_1 = 2 \text{ kg}, m_2 = 2 \text{ kg}, l = 0,6 \text{ m}, g = -9.81 \text{ m/s}^2, \\ a_{22} = \frac{m_2 l^2}{3}, I = \frac{m_1 l^2}{3}, r_1 = \frac{l}{2}, r_2 = \frac{l}{2} \end{aligned} \quad (3.17)$$

Two different levels of the desired energy of a mechanism are applied discontinuously to the control system (s. Fig. 3.3). At first we suppose the desired energy level equals $H_s = 3,8 \text{ J}$, then the desired value of the energy level becomes 6 J and at last this value becomes equal to 8 J. The plots are obtained with the initial conditions $\varphi(0) = 0,2$, $\dot{\varphi}(0) = \alpha(0) = \dot{\alpha}(0) = 0$. Depending on the current value of the energy level the mechanism reaches the desired level of the energy within different time periods. When the energy changes from 3,8 J to 6 J it takes time 0,49 s to achieve steady-state oscillations. When the desired energy level changes from 6 J to 8 J the transients lasts for 0,25 s. Figure 3.3 shows two projections of a phase trajectory on the planes $(\varphi, \dot{\varphi})$ and $(\alpha, \dot{\alpha})$. Here we can see two closed phase trajectories and, consequently, two periodical oscillation modes.

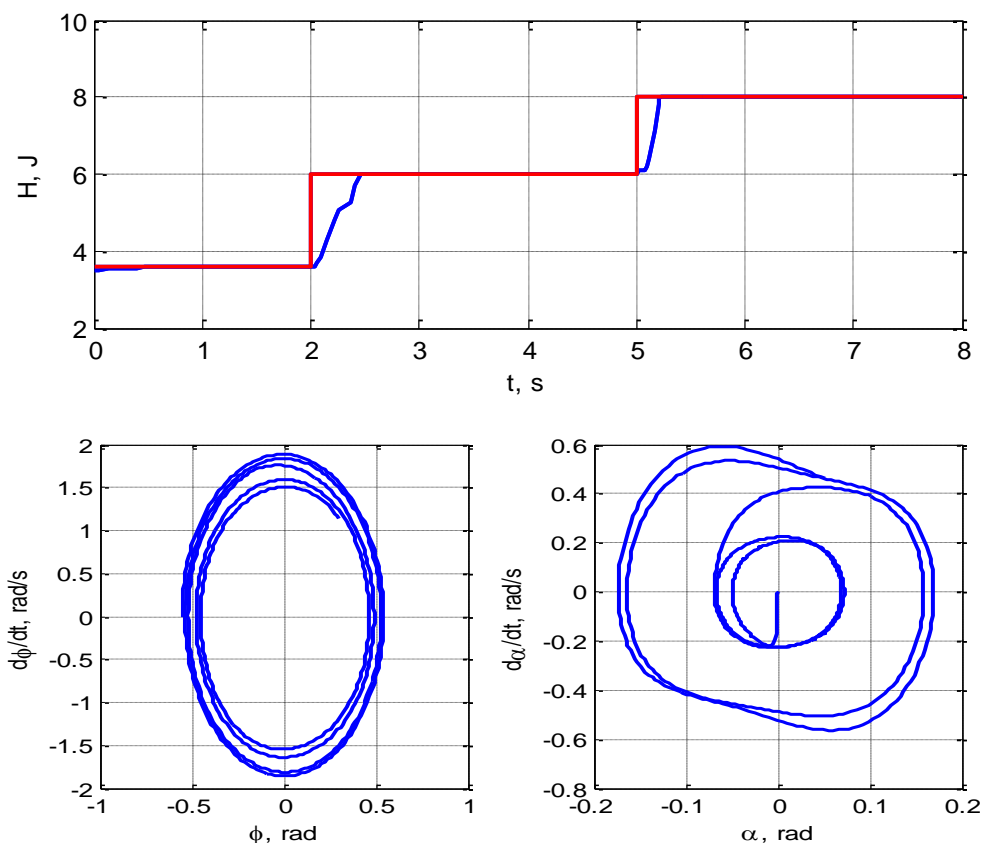


Figure 3.3 – Transients at different levels of the desired energy

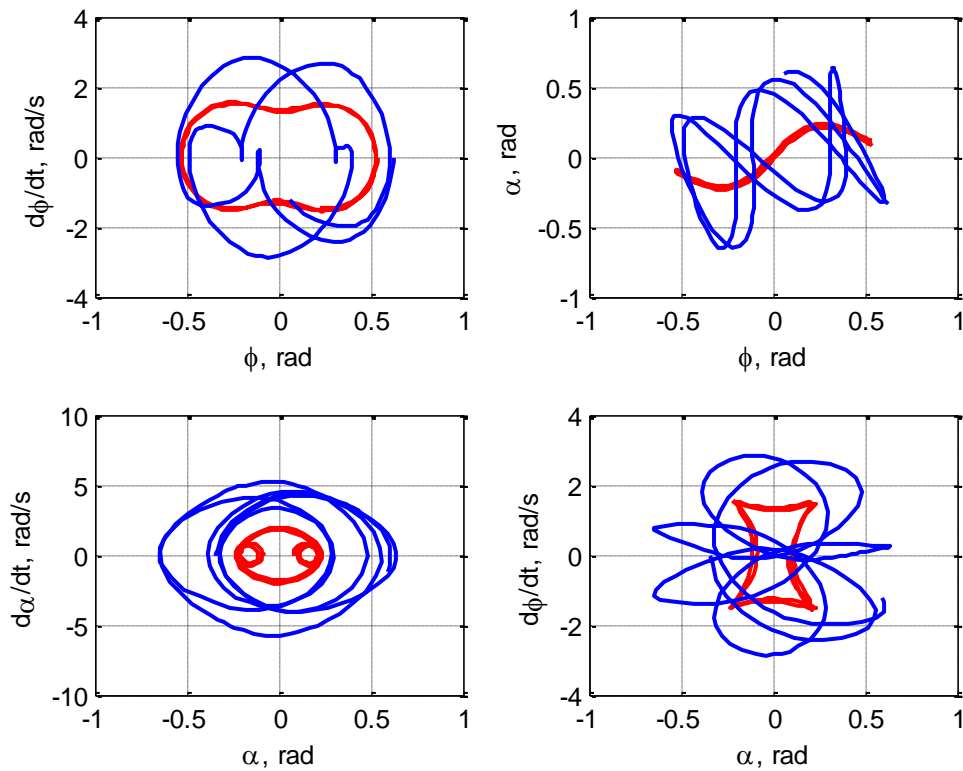


Figure 3.4 – Phase portrait of pendulum oscillations corresponding to one level of energy

Figure 3.4 shows the projections of the phase trajectory on the planes $(\varphi, \dot{\varphi})$, $(\alpha, \dot{\alpha})$, (φ, α) and $(\alpha, \dot{\varphi})$ of the double pendulum, corresponding to one level of energy and obtained at different initial conditions. The phase trajectories (s. Fig. 3.4) colored in blue were obtained with the initial conditions $\varphi = 0.05$, $\dot{\varphi} = \alpha = \dot{\alpha} = 0$. The phase trajectories in the red color were obtained with the initial conditions $\varphi = 0.08$, $\dot{\varphi} = \alpha = \dot{\alpha} = 0$.

It is necessary to point out that for the mechanism under study the same level of energy can correspond to different phase trajectories. This is explained by the fact that the differential equations of double pendulum motion have a lot of solutions which belong to the same energy level.

Unlike the variable length pendulum which was studied in the previous chapter the constant value of the total energy of the double pendulum does not define unambiguously its amplitude and oscillation frequency. Simulations shows that the pendulum when controlled by the speed gradient method has different phase trajectories in the steady- state depending on the initial conditions, in other words, it reached different periodic modes.

3.3. Periodic motion synthesis via the combination of optimal laws of swinging and damping

In papers [22], [26] it is recommended to use the method of maximization and minimization of some expression characterizing the behavior of the double pendulum to increase or decrease the amplitude of its oscillations. Let's consider this method in details. In accordance with the theorem of conservation the kinetic momentum of the system the first equation (3.3) can have the following form without torque M of the disturbing forces

$$\dot{K} = b_1 \sin \varphi + b_2 \sin(\varphi + \alpha), \quad (3.18)$$

where K is the kinetic momentum or, in other words, is the moment impulses of two link pendulum with respect to the suspension point O ,

$$K = j_1(\alpha)\dot{\varphi} + j_2(\alpha)\dot{\alpha}. \quad (3.19)$$

As expression (3.4) is always greater than zero, expression (3.19) can be rewritten as:

$$\dot{\varphi} + \frac{j_2(\alpha)}{j_1(\alpha)}\dot{\alpha} = \frac{K}{j_1(\alpha)}. \quad (3.20)$$

The left side of expression (3.20) is the derivative \dot{p} of some adjusted value

$$p = \varphi + F(\alpha). \quad (3.21)$$

To define the function $F(\alpha)$ we integrate the second member on the left side of expression (3.20).

$$F(\alpha) = \int \frac{j_2(\alpha)}{j_1(\alpha)} d\alpha = \int \frac{a_{22} + a_{12} \cos \alpha}{a_{11} + a_{22} + 2a_{12} \cos \alpha} d\alpha = \frac{\alpha}{2} - A \arctan(B \tan \frac{\alpha}{2}) \quad (3.22)$$

The constants A and B are equal

$$A = \frac{a_{11} - a_{22}}{\sqrt{(a_{11} + a_{22})^2 - 4a_{12}^2}}, \quad B = \sqrt{\frac{a_{11} + a_{22} - 2a_{12}}{a_{11} + a_{22} + 2a_{12}}}.$$

Having introduced the variable \dot{p} , expression (3.20) can be written down in the form

$$\dot{p} = \frac{K}{j_1(\alpha)}. \quad (3.23)$$

From (3.21) it follows

$$\varphi = p - F(\alpha) \quad (3.24)$$

Substituting expression (3.24) in (3.18) we obtain

$$\dot{K} = f(p, \alpha) = b_1 \sin(p - F(\alpha)) + b_2 \sin(p - F(\alpha) + \alpha). \quad (3.25)$$

Relations (3.23) and (3.25) can be considered as the equation system of the first order equations with the phase variables such as the adjusted angle p and the kinetic momentum K . For such a system the angle α can be regarded as system input.

In papers [22], [26] it is proposed to use the method of maximization and minimization of kinetic momentum for the synthesis of swinging and damping laws of the oscillations of the pendulum.

As it was mentioned above $j_1(\alpha) > 0$ for all values of the angle α , hence the value p gradually increases within the time period where $K > 0$ and this value gradually goes down if $K < 0$. Within all the time periods expressions (3.23) and (3.25) can be written as the first order equation

$$\frac{dK}{dp} = f(p, \alpha) \frac{j_1(\alpha)}{K} \quad (3.26)$$

Studying the first order equation (3.26), we can see that for the variable p in order to achieve its maximum value it is necessary and enough to have the maximally possible value within the whole period of motion in the right side of the equation. In other word, it is necessary and enough to choose such an angle α in every instant that the value of production $f(p, \alpha)j_1(\alpha)$ is maximal. According to [22] the desired law of the optimum rocking $a(p)$ depending only on the variable p can be represented as

$$a(p) = \arg \max_{|\alpha| \leq a_0} [f(p, \alpha)j_1(\alpha)] \quad (3.27)$$

Here a_0 is the maximally possible value of the interlink angle.

To achieve the optimum damping it is necessary to minimize the right side of expression (3.26)

$$a(p) = \arg \min_{|\alpha| \leq a_0} [f(p, \alpha)j_1(\alpha)] \quad (3.28)$$

It is necessary to point out that the presence of the limits a_0 allows taking into account the real constraints in a mechanical system in comparison with the speed gradient control method.

Figure 3.5 shows the plots of swinging of double pendulum with the parameters (3.17), obtained according to the algorithm (3.27). The amplitude of the pendulum oscillations in the suspension point O is increasing. The fact that in the expression $f(p, \alpha)j_1(\alpha)$, there is a term $j_1(\alpha)$ which corresponds to the inertia moment of the whole mechanism with respect to suspension point O is the evidence that this procedure allows increasing of the amplitude of

the oscillation of the whole mechanism. This means that in this case it is possible to consider the two-link pendulum as a simple pendulum with changeable location of the center of mass.

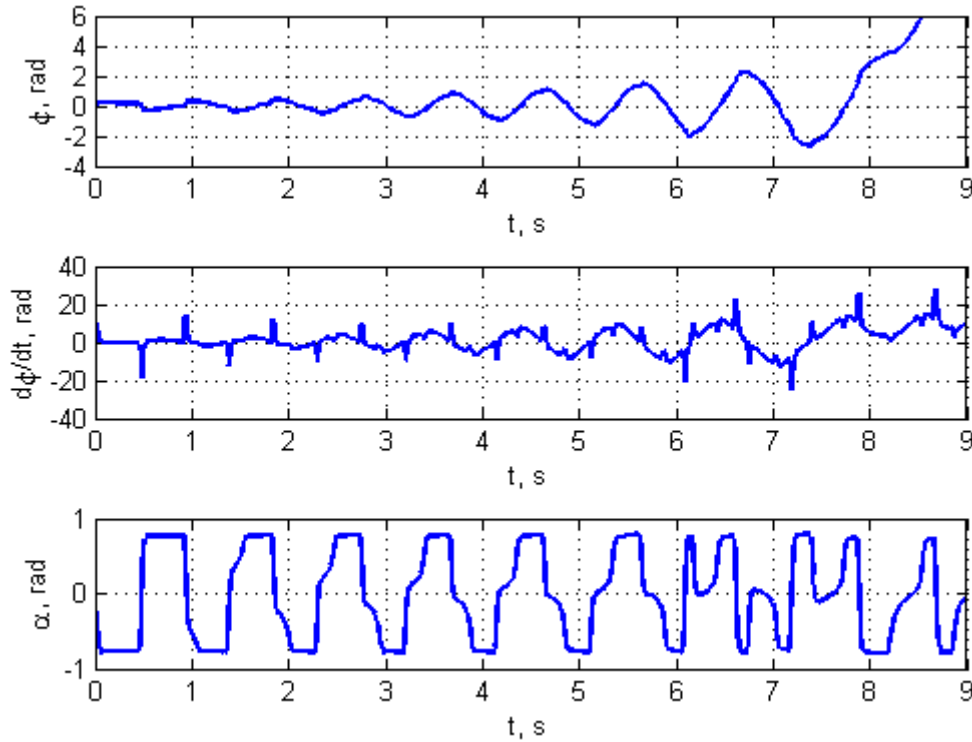


Figure 3.5 –Oscillation of the double pendulum

3.3.1. Synthesis of the control system of the oscillation amplitude of the double pendulum.

On the basis of the optimal laws of swinging and damping pendulum oscillations it is possible to formulate a control law to maintain the pre-set level of the energy of double pendulum oscillations:

$$\alpha = \begin{cases} \arg \max_{|\alpha| \leq \alpha^*} [f(p, \alpha) j_1(\alpha)], & (H_s - H) > 0 \\ 0, & (H_s - H) = 0 \\ \arg \min_{|\alpha| \leq \alpha^*} [f(p, \alpha) j_1(\alpha)], & (H_s - H) < 0 \end{cases} \quad (3.29)$$

When approaching the desired level of energy a chattering mode may arise in the system. To avoid this mode we saturate the maximum allowable values of the angle when the energy values are close to desired ones. In this case

$$\alpha^* = \begin{cases} \alpha_0, & \gamma \text{abs}(H_s - H) \geq \alpha_0 \\ \gamma \text{abs}(H_s - H), & \gamma \text{abs}(H_s - H) < \alpha_0 \end{cases} \quad (3.30)$$

The value of the parameter γ is defined in the process of modeling or experimentally.

3.3.2. Simulation results

Let us consider the mathematical model of a double pendulum (3.3) with the following parameters:

$$\begin{aligned} m_1 &= 1.8 \text{ kg}, m_2 = 2.53 \text{ kg}, l = 0.63 \text{ m}, g = -9.81 \text{ m/s}^2, \\ a_{22} &= 0,2 \text{ kg} \cdot \text{m}^2, I = 0.056 \text{ kg} \cdot \text{m}^2, r_1 = 0.315 \text{ m}, r_2 = 0.335 \text{ m}. \end{aligned} \quad (3.31)$$

The efficiency of the control law is proved in the following modes: increasing of the oscillation amplitude, damping of oscillations, increasing of the oscillation amplitude when there is an viscous friction in the suspension point O , maintaining the desired level of the energy with constant torque applied in the suspension point O .

Figure 3.6 represents the full mathematical model of the double pendulum with control system. The full model contains a dynamic model of a pendulum, a model of the torque control loop in the interlink joint, the interlink angle control loop and total energy control loop.

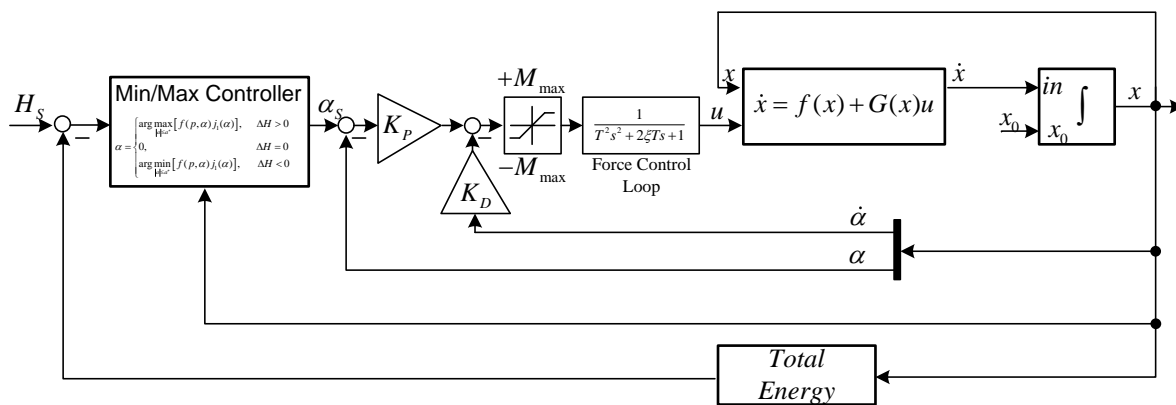


Figure 3.6 –The pendulum control system

The model of the torque control loop in the interlink joint is represented in the form of the second–order lag element with the time constant $T = 9 \text{ ms}$ and the damping coefficient $\xi = 0.707$. The maximum reached torque in the interlink joint is saturated with value $5 \text{ N} \cdot \text{m}$. The control circuit for the interlink angle is adjusted on a non-periodic process. A linear feedback with the coefficients $K = [50.5 \ 5.02]$ is used in the model. An interlink angle is saturated to the value $\alpha_{\max} = 10 \text{ deg}$.

In Figure 3.7 we can see the transients in the system while increasing the given energy level. From Figure 3.7 it is seen that the duration of the transients is 7,5 seconds when the mechanism energy increases from 0.05 J to 1 J and the system reaches the desired energy level within 8 oscillations. The transients duration is 4 seconds when the mechanism makes 5 oscillations with respect to the vertical.

Figure 3.8 shows the family of phase portraits of the double pendulum when the desired energy grows. The blue color marks the maximum cycle corresponding to the energy level 1 J. The red color shows the maximum cycle corresponding to the energy level 2 J. The fact that there are closed trajectories on the phase portrait of the double pendulum demonstrates that the oscillation process reaches its stable periodic mode.

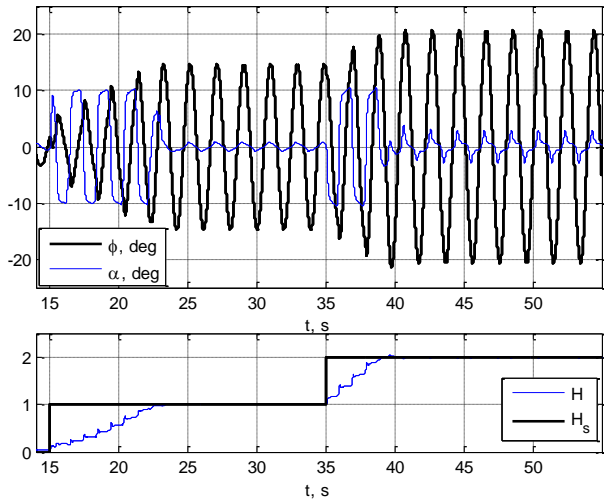


Figure 3.7 – Transients at increasing of the desired energy.

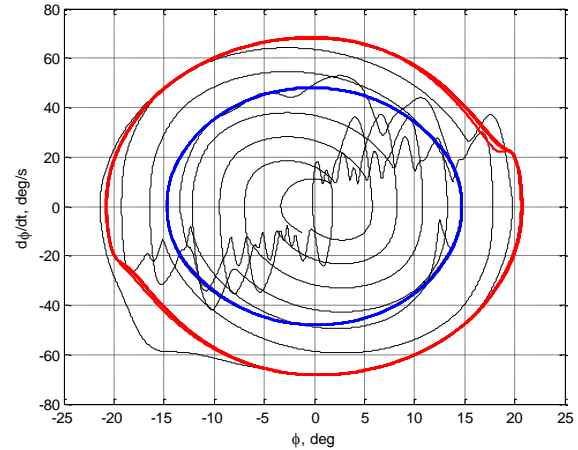


Figure 3.8 – Phase portrait in the plane $(\varphi, \dot{\varphi})$ at increasing of the desired energy.

Figure 3.9 represents the transients in the system while decreasing the desired energy level. From Figure 3.9 it is seen that the duration of the transients is 4 seconds when the mechanism energy decreases from 2 J to 1 J and the system reaches the preset energy level within 5 oscillations. The transients duration is 7,5 seconds when the mechanism energy decreases from 1 J to 0 J, the mechanism makes 8 oscillations with respect to the vertical. When the preset energy of the system is 0 J the system tends to some minimum level of energy close to 0, but in the area of narrow angles the oscillations are hardly damped out. This is caused by the fact that the control law is rather ineffective for narrow angles.

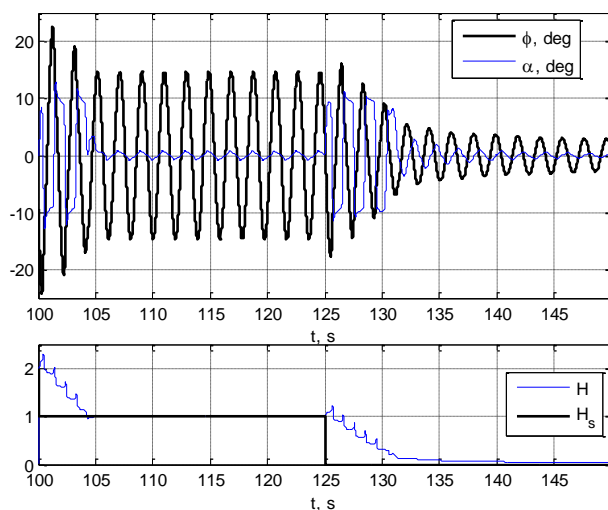


Figure 3.9 – Transients during decreasing of the desired energy.

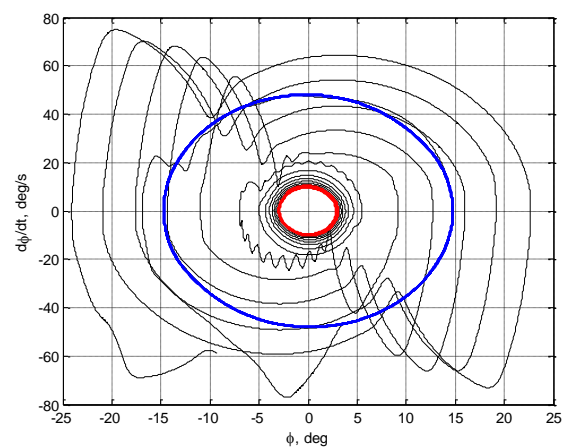


Figure 3.10 – Phase portrait during decreasing of the desired energy.

Figure 3.10 shows the phase portrait of the double pendulum during decreasing the desired energy. The blue color marks the limit cycle corresponding to the energy level 1 J. The red color shows the limit cycle corresponding to the energy level 0 J. The fact that there are closed trajectories on the phase portrait of a two link mechanism demonstrates that the oscillation process reaches its stable periodic mode.

Figure 3.11 shows the transients in the system while increasing the desired energy level at the presence of the viscous friction in the joint O . From Figure 3.11 it is seen that the duration of the transients is 9 seconds when the mechanism energy increases from 0 J to 1 J and the system reaches the preset energy level within 9 oscillations. In comparison with the experiment without the viscous friction (s. Fig. 3.7) the transients lasts 1 second longer.

Figure 3.12 represents the phase portrait of the double pendulum while increasing the desired energy. The blue color marks the maximum cycle corresponding to the initial energy level 0 J. The red color shows the maximum cycle corresponding to the energy level 1 J. Closed projections of phase trajectories of a two link mechanism are the evidence of stable periodic oscillation mode. It is necessary to note that the phase portrait in the plane $(\phi, \dot{\phi})$ (s. Fig. 3.12) is much more prolonged along the X-axis compared to the experiment without the viscous friction (s. Fig. 3.8). This may be due to the fact that the dissipation of the mechanism energy depends on the angular speed of the first link.

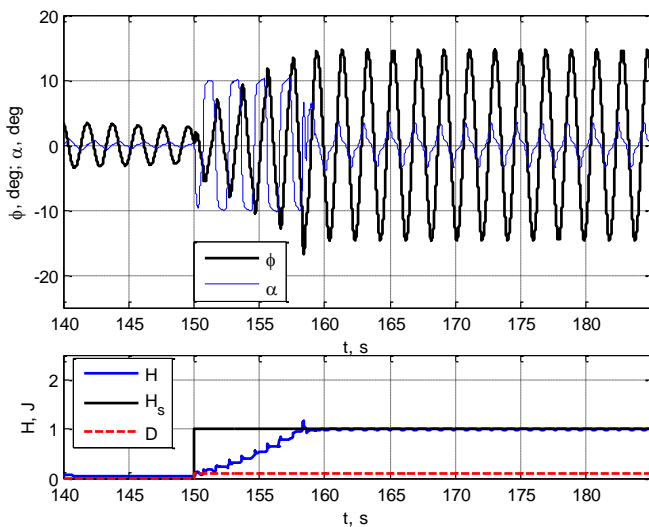


Figure 3.11 – Transients by increasing of the desired energy with the viscous friction in the suspension point.

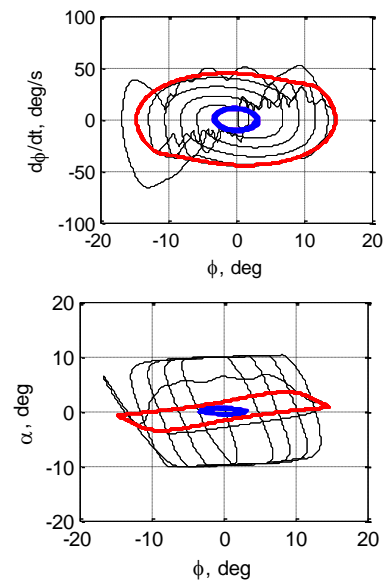


Figure 3.12 –Phase portrait of double pendulum by increasing the desired energy

In Figure 3.13 the transients in the system at increasing the viscous friction coefficient in the joint O by 10 times are given. From Figure 3.13 it is seen that the oscillation amplitude in the suspension point decreases by some degrees, and the pendulum oscillations in the interlink joint reaches the saturated value by 10 deg. The oscillation amplitude decreases as the control system is not capable to compensate the energy losses which are caused by the viscous friction coefficient increased in 10 times.

Figure 3.14 represents the phase portraits of double pendulum movement by increasing of the viscous friction coefficient in the joint O . The blue color marks the phase portraits of double pendulum corresponding to the stable periodic oscillation mode with the energy 1 J without any viscous friction. The red color marks the phase portraits of double pendulum corresponding to the stable periodic oscillation mode with the energy 1 J with some viscous friction. In the first plot, we can see a steady-state error at increased friction but it does not damper the oscillations and it only decreases their amplitude in the steady-state mode. In the phase portrait (ϕ, α) we can see the areas where the amplitude increases. Two orbits are also highlighted, before and after the friction coefficient rise. In these orbits we can see that the orbit radius decreases when the friction coefficient is higher and the system energy is lower. In the phase portrait (ϕ, α) it is clearly obvious that the interlink angle comes to the restriction 10 deg in the steady-state.

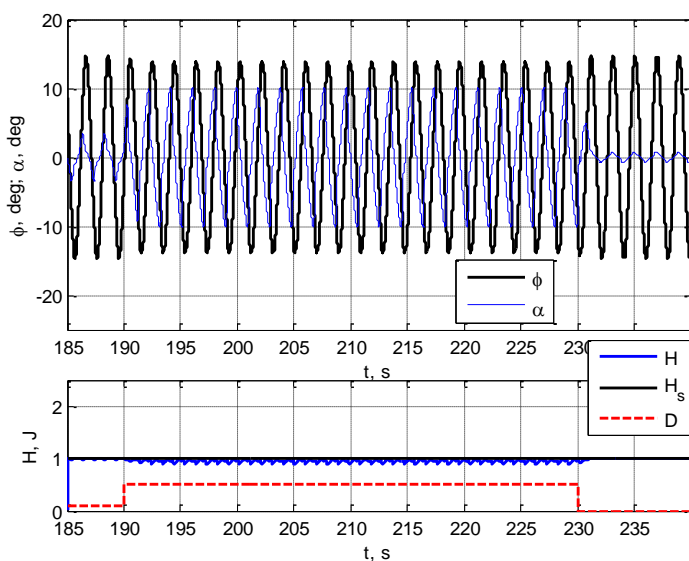


Figure 3.13 –Transients at increasing of the viscous friction coefficient in the joint O

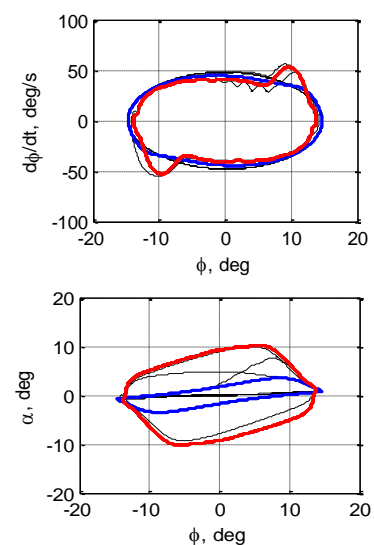


Figure 3.14 – Phase trajectories at increasing of the viscous friction coefficient in the joint O

Figure 3.15 shows the transients when there is a constantly acting torque in the suspension point O . In Figure 3.15 we can clearly see the shift of oscillation in the suspension point as regard to the vertical axis. The value of the shifting from the oscillation axis depends on the value of the applied torque in the point of the pendulum suspension. The mechanism energy varies within the desired level

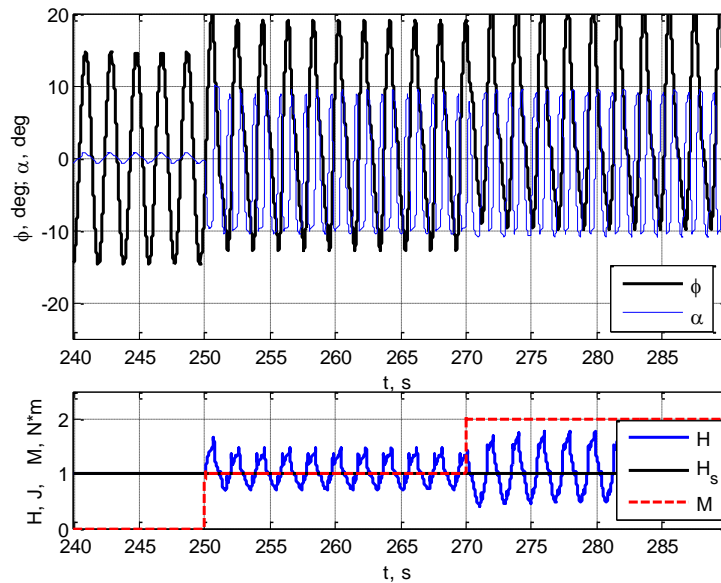


Figure 3.15 – Transients when there is a constantly acting torque in the suspension point.

3.4. Experiments

We now give the experimental results of the investigation of the double pendulum control system. The control of the experimental setup is implemented by using of Matlab xPC-Target technology (s. Fig. 3.16). On the base of xPC-Target the drives of the experimental setup are connected to the master computer by means of the industrial communication network.

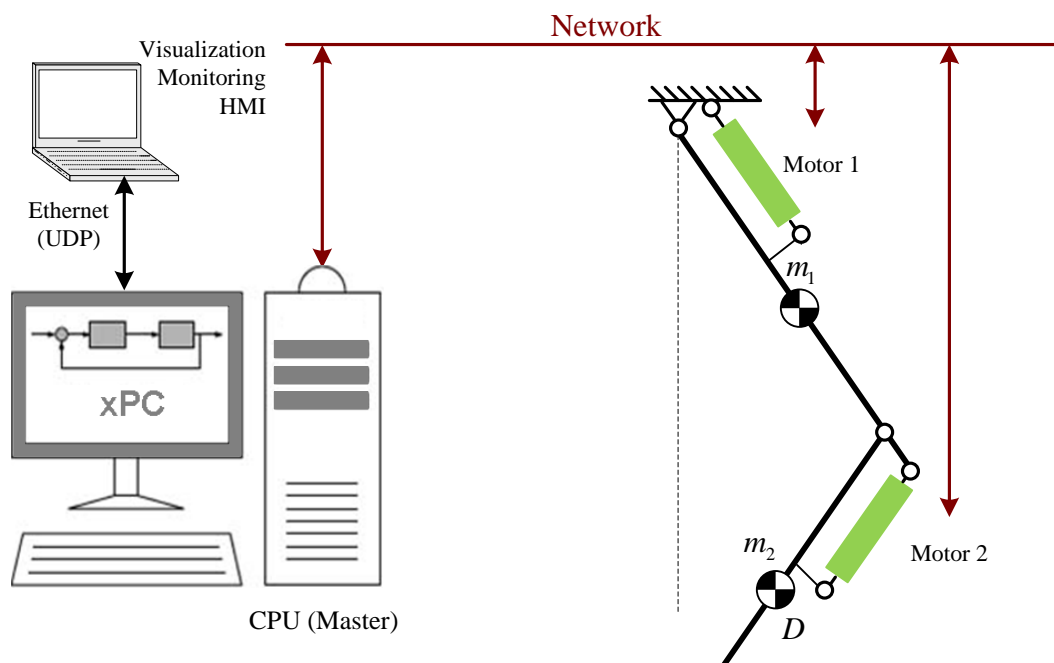


Figure 3.16 – The structure of the experimental setup

In Figure 3.17 we can see the photograph of the experimental setup. This experimental setup is assembled on the basis of the power drive, the detailed information about which is given in [38].

The pendulum consists of two links with masses m_1 and m_2 . The first mass is fixed with a bearing in the suspension point O (s. Fig. 2.16). The difference between the experimental setup and the model studied earlier lies in the unsymmetrical mass distribution. The center of mass of each link is shifted by 4 cm from its axis.

The control loop of the interlink angle is tuned exactly the same as simulation. This control loop is tuned to a non-periodic process. A linear feedback with the coefficients $K=[50.5 \ 5.02]$ is used in the model. The maximum value of the interlink angle is $\alpha_{\max} = 10 \text{ deg}$.

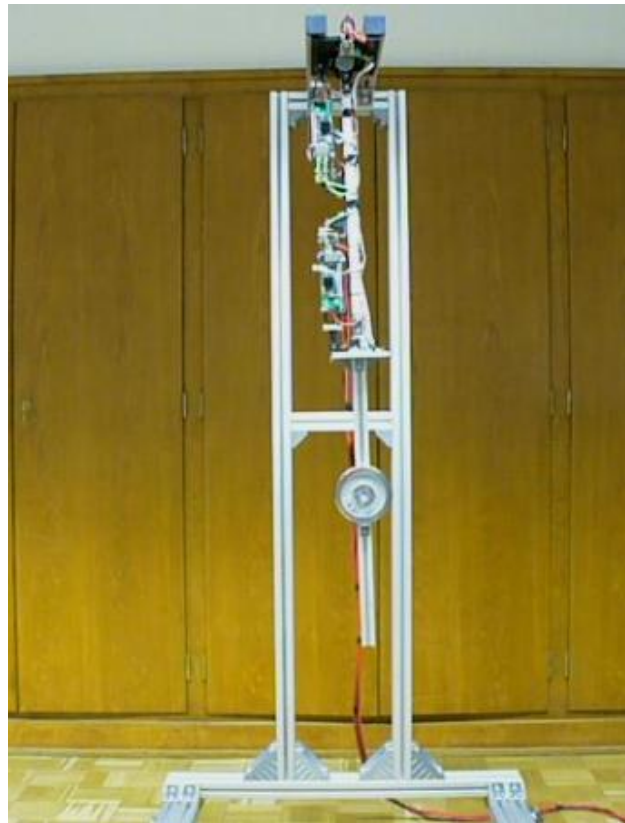


Figure 3.17 – The experimental setup of the double pendulum

The performance of the double pendulum control system on the experimental setup is tested for the following modes: oscillation amplitude increase, oscillation amplitude damping, and oscillation amplitude increase when there is the viscous friction in the suspension point O , maintaining of the predetermined level of oscillation energy in the presence of the constant torque acting in the suspension point O .

The experiment is carried out following the same conditions and the same mode as during the simulation. The parameters of both systems differ only in the shift of the center of masses from the link axes which is in the experimental setup. During the experiments, motor 1 (see Figure 3.16) produces the required torque in the suspension point.

In Figure 3.18 there are the transients in the system when increasing the desired level of energy. From Figure 3.18 it is obvious that the duration of the transients at increasing the mechanism energy from 0.05 J to 1 J is 13 seconds and the system reaches the predetermined energy level within 9 oscillations. The duration of the transients at increasing the mechanism energy from 1 J to 2 J is 7 seconds, the mechanism executing 5 oscillations with respect to the vertical.

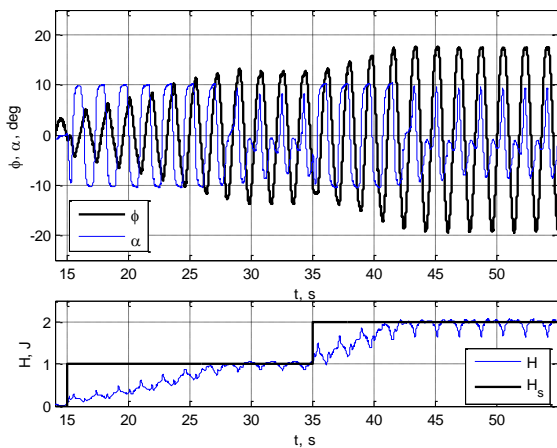


Figure 3.18 – Transients at increasing the desired energy

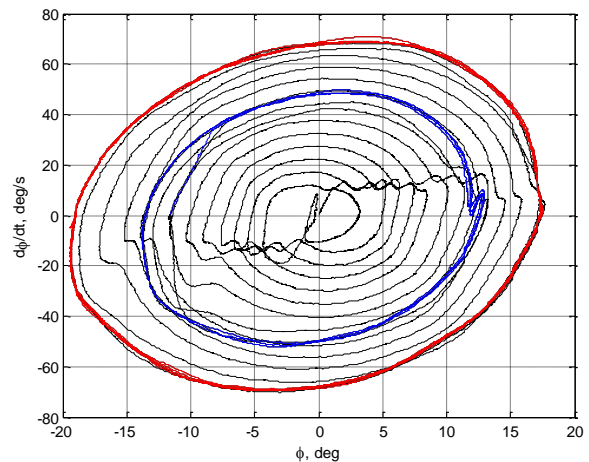


Figure 3.19 – A phase portrait at increasing the desired energy.

Figure 3.19 represents the family of phase portraits of a two link mechanism when the desired energy increases. The blue color marks the limit cycle which corresponds to the energy level 1J. The red color marks the limit cycle corresponding to the energy level 2J. The presence of the closed orbits of two link mechanism phase trajectories is the evidence that the oscillating process reaches its steady-state.

In Figure 3.20 we can see the transients in the system when the preset level of energy falls. From Figure 3.20 it is obvious that the duration of the transients at decreasing the mechanism energy from 2 J to 1 J is 7 seconds and the system reaches the predetermined energy level within 5 oscillations. The duration of the transients at decreasing the mechanism energy from 1 J to 0 J is 10 seconds, the mechanism executing 10 oscillations with respect to the vertical. When the desired energy is 0 J, the system tends to some minimum energy level close to 0, but in the area of narrow angles the oscillation amplitude is hardly damped. It is resulted from the fact that the control law is of little efficiency in this case.

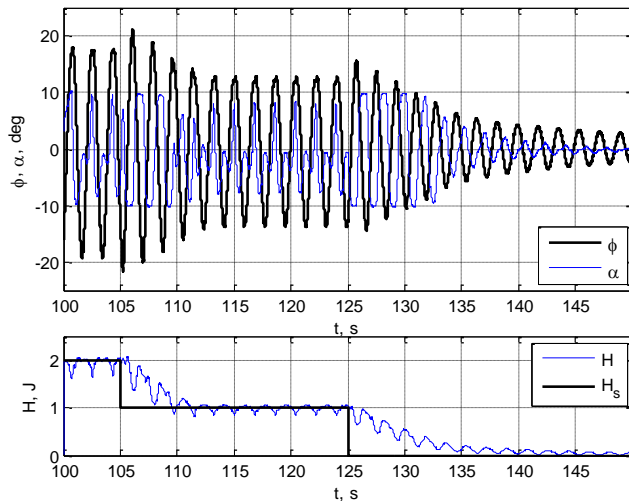


Figure 3.20 – Transients at decreasing the desired energy

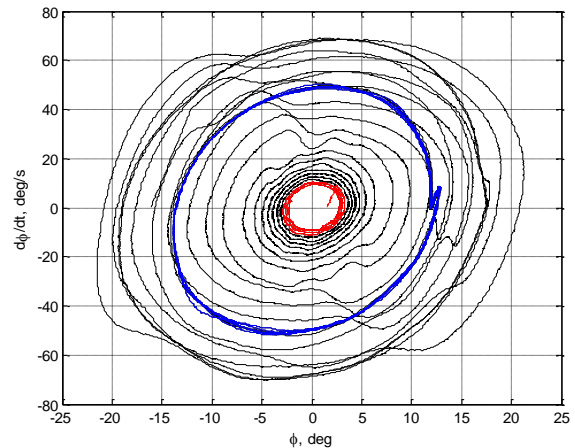


Figure 3.21 – A phase portrait at decreasing the desired energy

Figure 3.21 shows the family of phase portraits of two link mechanism at decreasing the desired energy. The blue color denotes the limit cycle which corresponds to the energy level 1J. The red color denotes the limit cycle corresponding to the energy level 0 J. The fact that there are the closed projections of two link mechanism phase trajectories says that the oscillating process reaches its steady-state period mode.

In Figure 3.22 we can see the transients in the system with the viscous friction in the joint O when the desired energy level increases. In Figure 3.22 it is evident that the transients duration at increasing the mechanism energy from 0 J to 1 J is 17 seconds and the systems comes to the desired energy level having executed 9 oscillations. In comparison with the experiment without the viscous friction (s. Fig. 3.18) the transients is 4 seconds longer.

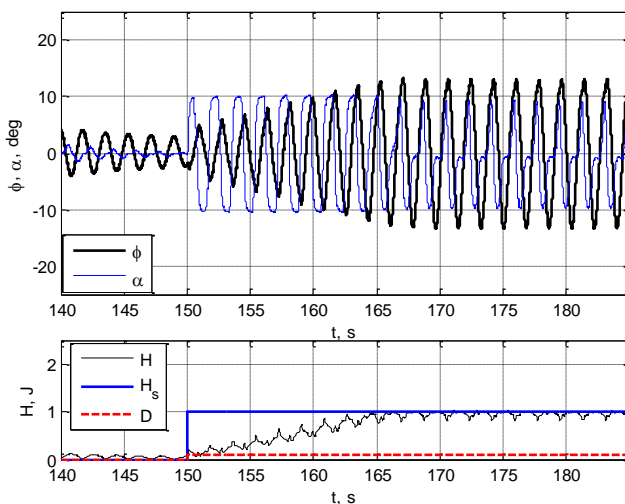


Figure 3.22 – Transients with the viscous friction

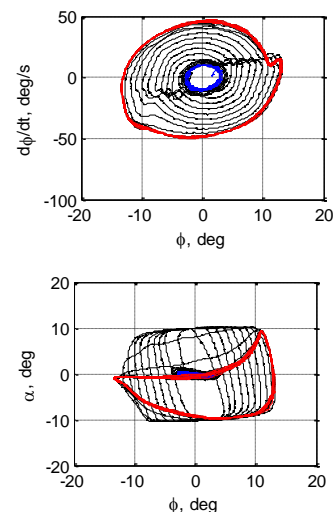


Figure 3.23 – Phase trajectories of the system with the viscous friction

Figure 3.23 shows the phase portraits of a two link mechanism by increasing of the desired energy. The blue color denotes the limit cycle corresponding to the initial energy level 0 J. The red color denotes the limit cycle corresponding to the energy level 1 J. The fact that there are the closed orbits of the phase trajectories of a two link mechanism says that the

oscillating process reaches its steady-state. It is necessary to emphasize that the phase portrait in the plane $(\varphi, \dot{\varphi})$ (see Figure 3.12) compared to the experience without any viscous friction (s. Fig. 3.8) is a lot more elongated along the X - axis. The explanation of this is that the dissipation of the mechanism energy increases as the velocity in the suspension point goes up.

Figure 3.24 shows the transients in the system while increasing the viscous friction coefficient in the joint O by 10 times. From Figure 3.24 it is seen that the oscillation amplitude in the suspension point decreases by some degrees, and in the interlink joint the pendulum oscillations reach the restriction by 10 deg. The decrease of oscillation amplitude is explained by the fact that the control system is not able to compensate the energy losses at such a value of the viscous friction.

In Figure 3.25 we can see the phase portraits of the double pendulum movement when the viscous friction coefficient in the joint O increases. The blue color marks the phase portraits of the double pendulum which correspond to the steady-state of the oscillations with the energy 1 J without any viscous friction. The red color marks the phase portraits corresponding to the steady-state of the oscillations with the energy 1 J with some viscous friction. In the first plot, we can see a steady-state error when the friction is high. In this condition the system keeps on oscillating and achieves a periodic mode. In the phase portrait (φ, α) the areas where the oscillation amplitude increases are distinctly seen. Two orbits are also highlighted, before and after the friction coefficient increase and in these orbits we can see the differences in the system behavior. In the phase portrait (φ, α) it is obviously that the interlink angle comes to the restriction 10 deg in the steady-state mode.

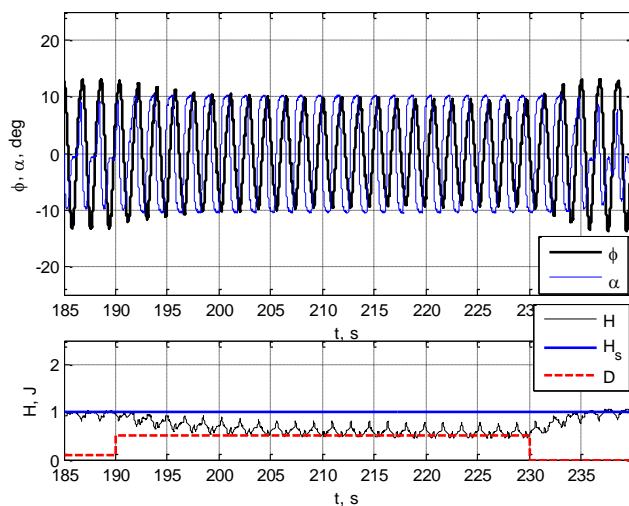


Figure 3.24 –Transients at increasing of the viscous friction coefficient in the joint O

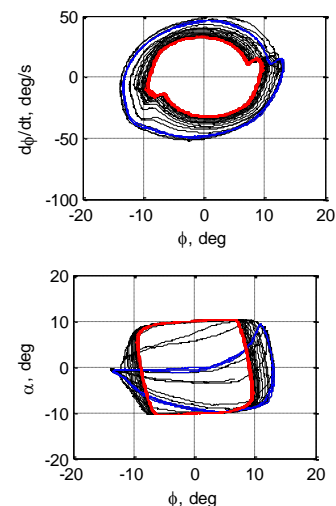


Figure 3.25 – Phase trajectories at increasing of the viscous friction coefficient in the joint O

Figure 3.26 represents the transients when there is a constant moment in the suspension point O . From Figure 3.26 it is seen that the oscillations deflect from the vertical axis. The value of the deflection depends on the value of the torque applied to the point of the pendulum suspension. The mechanism energy varies around the desired level.

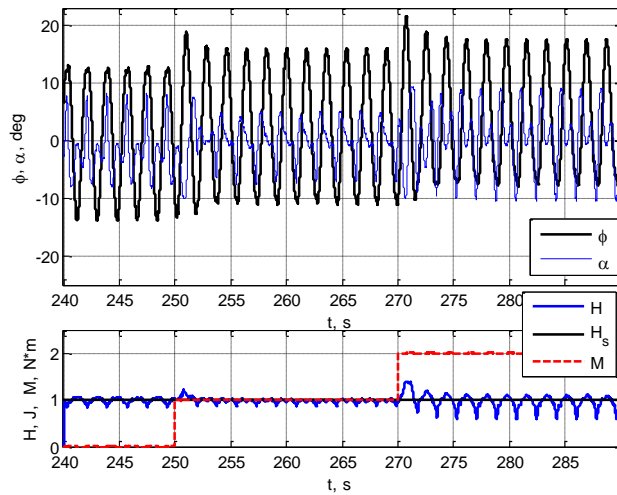


Figure 3.26 – Transients with static torque in the suspension point

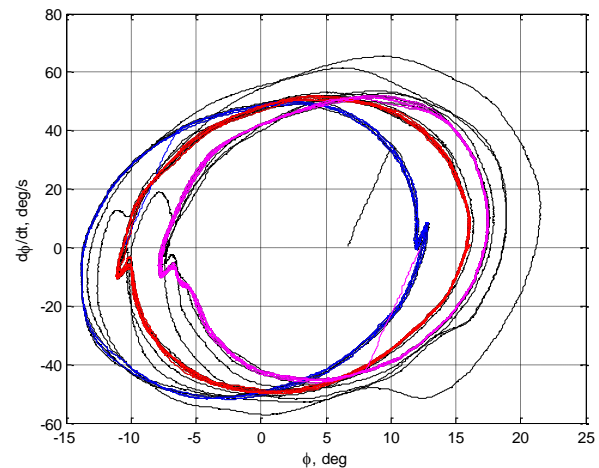


Figure 3.27 – Phase portrait with static torque in the suspension point

Figure 3.27 gives us the phase portraits when there is a static torque in the suspension point O . Three steady-state orbits are in the plot. The energy oscillates around the desired level and the oscillation center deflects from the vertical. In the phase plain $(\varphi, \dot{\varphi})$ it is seen that depending on the change of the value of a static torque in the suspension point there is a parallel trajectory transfer along x-axis. It is necessary to point that in this mode the control system operates not reaching the restrictions. The energy varies around the desired level.

The different properties of control systems performance is compared in Table 3.1.

Mode	Simulation	Experiment
Energy increase from 0 J to 1 J	Duration: 7.5 s, 8 Oscillations	Duration: 13 s, 9 Oscillations
Energy increase from 1 J to 2 J	Duration: 4 s, 5 Oscillations	Duration: 7 s, 5 Oscillations
Damping: energy decrease from 2 J to 1 J	Duration: 4 s, 5 Oscillations	Duration: 7 s, 5 Oscillations
Energy increase under the effect of the viscous friction	Duration: 9 s, 9 Oscillations	Duration: 13 s, 10 Oscillations
Viscous friction coefficient growth	Slight disagreement, the interlink angle does not reach the restriction	Slight disagreement, the interlink angle reaches the restriction
Application of a static torque in the suspension point	Deflection of the center of oscillation from the vertical axis. The energy varies around the preset level.	Deflection of the center of oscillation from the vertical axis. The energy varies around the preset level.

The main differences between the simulation and the experiment can be explained by the fact that in the mathematical model the friction forces acting in the experimental setup do not taken into account. The number of oscillations in the transients is approximately the same, but they last different time periods. This may come from the fact that in the mathematical model the shift of the centers of the link masses are not factored in. It should also be noted that during the experiments the control system works when there are various disturbances in

the suspension point, these disturbances are do not taken into account in the mathematical model.

In this chapter we consider the oscillations of the double pendulum which itself is more complicated mechanism than the variable length pendulum that was under investigation in the previous chapter. Two ways of control are used in this chapter. With the help of either of them we managed to achieve the stable periodic mode of oscillations of the double pendulum. The simulation and the experiments show the efficiency of the developed control methods.

Chapter 4. Design of the movement of a two-legged mechanism in the frontal plane

This chapter investigates movement of a planar anthropomorphic mechanism in the frontal plane. The mechanism consists of two articulated heavy parts: a body and two legs rigidly fixed to each other. We establish the equations of mechanism motion. The instantaneous double-support phase is under study and to describe it we use the equation of a perfectly inelastic impact. Two ways to control the mechanism oscillations maintenance are characterized and the simulations are carried out. At the end of the chapter, there are the experimental investigations of the control system for the oscillation maintenance.

There are two phases [10], [20] in the process of human being walking, namely, the phase of double-support motion, in other words, a double-support phase and the phase of single-support motion or the transfer phase. During the double-support motion both legs are on the surface. During the single-support motion only one of the legs, that is the supporting leg, is on the surface and the other one is in the process of transfer.

4.1. Mathematical model of single support motion

Now we consider a two link mechanism which simulates the movement of an anthropomorphic robot without feet in the frontal plane (s. Fig. 4.1)

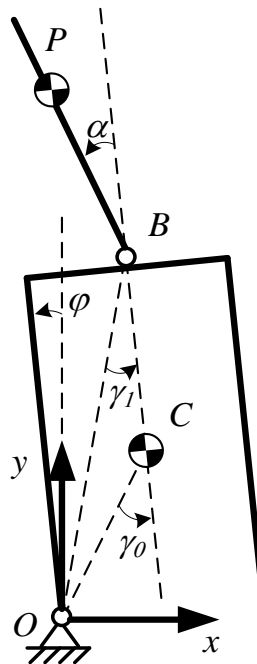


Figure 4.1– Diagram of a two link mechanism

The lower part is fixed with a joint O and is consists from three rods welded to each other: a left and right leg and a pelvis. We suppose that the legs are parallel to each other and perpendicular to the pelvis. Assume, that the lengths, masses, inertia moments of the legs and pelvis are known and it is possible to define the COM of these three parts (point C). The pelvis joint B is the connection point of the body and the pelvis and it is in the middle of the pelvis. OB and OC are the distances from the origin of coordinates to the pelvis joint B and the center of the mass C of the lower part respectively. γ_0 is the angle which is formed by the lines OC and BC . φ – is the angle of deflection of the leg from the vertical, α – is the angle of deflection of the body BP from the line BC .

The mechanism (s. Fig. 4.1) has two degrees of freedom. We choose the angles φ and α as the generalized coordinates characterizing the mechanism position. These angles and the direction of their readings are shown in Figure 4.1. We will establish the equation of two link movement using the Lagrange equations of the second order [4].

$$\frac{d}{dt} \left(\frac{\partial L}{\partial \dot{q}_i} \right) - \frac{\partial L}{\partial q_i} = Q_i \quad (i = 1, \dots, n) \quad (3.32)$$

In the equations (3.32) q_i is the generalized coordinate, Q_i is the generalized nonconservative force, $L = T - V$ is the Lagrange function, T is kinetic energy, V is potential energy of the system. For the system under investigation $n = 2$.

In order to specify the kinetic energy T of the whole mechanism we first find the kinetic energy of each link separately. To calculate the kinetic energy of each link we use the formula [4].

$$T = \frac{1}{2} [mv^2 + 2m(v \times \omega) \rho + \theta \omega^2] \quad (3.33)$$

Here v is the speed of the pole (that is arbitrary but fixed point in the link), v is the absolute value of this velocity, ω is the angular velocity of link rotation, ρ is the radius-vector of the center of mass (the origin of this vector is in the pole), m is the mass of link, θ is the link inertia moment about the pole.

The kinetic energy of the first link consisting of two legs "welded" to each other is

$$T_1 = \frac{1}{2} I \dot{\varphi}^2 \quad (3.34)$$

where I is the inertia moment of the lower part about the point O .

The kinetic energy of the second link, the body is

$$T_2 = \frac{1}{2} m_2 v_{C_2}^2 + \frac{1}{2} I_2 (\dot{\varphi} + \dot{\alpha})^2 \quad (3.35)$$

where m_2 is the body mass, v_{C_2} - is the velocity of the center of the body, I_2 is the inertia moment of the body about center of mass C_2 .

The coordinates of the joint B in the coordinate system the origin of which is at the end of the leg O around which the first link rotates, are:

$$\begin{aligned}x_B &= -OB \sin(\varphi - \gamma_1) \\y_B &= OB \cos(\varphi - \gamma_1)\end{aligned}\quad (3.36)$$

The coordinates of the center of body mass C_2 is :

$$\begin{aligned}x_{C_2} &= -OB \sin(\varphi - \gamma_1) - \rho \sin(\varphi + \alpha - \gamma_1) \\y_{C_2} &= OB \cos(\varphi - \gamma_1) + \rho \cos(\varphi + \alpha - \gamma_1)\end{aligned}\quad (3.37)$$

Here $\rho = BP$.

In order to define the kinetic energy of the second link we differentiate relation (3.37) and we receive X and Y projections of the velocity vector of the center of mass velocity of the body.

$$\begin{aligned}\dot{x}_{C_2} &= -OB \cos(\varphi - \gamma_1) \dot{\varphi} - \rho \cos(\varphi + \alpha - \gamma_1) (\dot{\varphi} + \dot{\alpha}) \\ \dot{y}_{C_2} &= -OB \sin(\varphi - \gamma_1) \dot{\varphi} - \rho \sin(\varphi + \alpha - \gamma_1) (\dot{\varphi} + \dot{\alpha})\end{aligned}\quad (3.38)$$

Using expression (3.38) we can obtain the square of the velocity vector of the center of the body mass.

$$\begin{aligned}v_{C_2}^2 &= \dot{x}_{C_2}^2 + \dot{y}_{C_2}^2 \\ &= OB^2 \dot{\varphi}^2 + \rho^2 (\dot{\varphi} + \dot{\alpha})^2 + 2OB\rho \dot{\varphi} (\dot{\varphi} + \dot{\alpha}) [\sin(\varphi - \gamma_1) \sin(\varphi + \alpha - \gamma_1) \\ &\quad + \cos(\varphi - \gamma_1) \cos(\varphi + \alpha - \gamma_1)] \\ &= OB^2 \dot{\varphi}^2 + \rho^2 (\dot{\varphi} + \dot{\alpha})^2 + 2OB\rho \dot{\varphi} (\dot{\varphi} + \dot{\alpha}) \cos \alpha\end{aligned}\quad (3.39)$$

The expression for the kinetic energy of the whole mechanism has the following form

$$T = \frac{1}{2} I \dot{\varphi}^2 + \frac{1}{2} m_2 v_{C_2}^2 + \frac{1}{2} I_2 (\dot{\varphi} + \dot{\alpha})^2 \quad (3.40)$$

here $\dot{\varphi}$ и $\dot{\alpha}$ - the angular velocities of the first part and the body.

Using expressions (3.39), (3.40) we can obtain the formula for the kinetic energy T of the whole mechanism

$$\begin{aligned}
T &= \frac{1}{2}I\dot{\varphi} + \frac{1}{2}m_2 \left[OB^2\dot{\varphi}^2 + \rho^2(\dot{\varphi} + \dot{\alpha})^2 + 2OB\rho\dot{\varphi}(\dot{\varphi} + \dot{\alpha})\cos\alpha \right] + \frac{1}{2}I_2(\dot{\varphi} + \dot{\alpha}) \\
&= \frac{1}{2}(I + m_2OB^2)\dot{\varphi}^2 + \frac{1}{2}(I_2 + m_2\rho^2)(\dot{\varphi} + \dot{\alpha})^2 + OB\rho\dot{\varphi}(\dot{\varphi} + \dot{\alpha})\cos\alpha \\
&= \frac{1}{2}(I + m_2OB^2)\dot{\varphi}^2 + \frac{1}{2}I_B(\dot{\varphi} + \dot{\alpha})^2 + OB\rho\dot{\varphi}(\dot{\varphi} + \dot{\alpha})\cos\alpha
\end{aligned} \tag{3.41}$$

Here $I_B = m_2\rho^2 + I_2$ is the inertia moment of the body about joint B, $OC \cos(\varphi - \gamma_0)$ is the ordinate of the center of mass of the first link, $OB \cos(\varphi - \gamma_1)$ is the ordinate of the joint B, $OB \cos(\varphi - \gamma_1) + \rho \cos(\varphi + \alpha - \gamma_1)$ is the ordinate of the center of mass C_2 of the body (s. Fig. 4.1).

The expression for the potential energy of the mechanism runs as follows:

$$V = m_1gOC \cos(\varphi - \gamma_0) + m_2g \left[OB \cos(\varphi - \gamma_1) + \rho \cos(\varphi + \alpha - \gamma_1) \right] \tag{3.42}$$

Here g is the gravity acceleration, m_1 and m_2 are the masses of the first and the second links respectively.

Let us introduce the following designations

$$\begin{aligned}
a_{11} &= (I + m_2OB^2), \quad a_{12} = m_2OB\rho, \quad a_{22} = I_B, \\
b_{11} &= m_1gOC, \quad b_{12} = m_2gOB, \quad b_{13} = m_2g\rho
\end{aligned} \tag{3.43}$$

and rewrite the expressions for the kinetic and potential energies

$$T = \frac{1}{2} \left[a_{11}\dot{\varphi}^2 + 2a_{12}\dot{\varphi}(\dot{\varphi} + \dot{\alpha})\cos\alpha + a_{22}(\dot{\varphi} + \dot{\alpha})^2 \right], \tag{3.44}$$

$$V = b_{11} \cos(\varphi - \gamma_0) + b_{12} \cos(\varphi - \gamma_1) + b_{13} \cos(\varphi + \alpha - \gamma_1). \tag{3.45}$$

According to (2.2) we can find the motion equations responding to two generalized coordinates φ and α .

$$\frac{d}{dt} \left(\frac{\partial L}{\partial \dot{\varphi}} \right) - \frac{\partial L}{\partial \varphi} = M_1, \quad \frac{d}{dt} \left(\frac{\partial L}{\partial \dot{\alpha}} \right) - \frac{\partial L}{\partial \alpha} = M_2 \tag{3.46}$$

Here M_1 and M_2 are torques in joints O and B .

Now we calculate the derivatives required to develop the Lagrange equations

$$\begin{aligned}
\frac{\partial L}{\partial \dot{\varphi}} &= a_{11}\dot{\varphi} + a_{12}(2\dot{\varphi} + \dot{\alpha})\cos\alpha + a_{22}(\dot{\varphi} + \dot{\alpha}), \\
\frac{\partial L}{\partial \dot{\alpha}} &= a_{12}\dot{\varphi}\cos\alpha + a_{22}(\dot{\varphi} + \dot{\alpha}), \\
\frac{\partial L}{\partial \varphi} &= b_{11}\sin(\varphi - \gamma_0) + b_{12}\sin(\varphi - \gamma_1) + b_{13}\sin(\varphi + a - \gamma_1), \\
\frac{\partial L}{\partial \alpha} &= -a_{12}\dot{\varphi}(\dot{\varphi} + \dot{\alpha})\sin\alpha + b_{13}\sin(\varphi + \alpha - \gamma_1),
\end{aligned} \tag{3.47}$$

$$\begin{aligned}
\frac{d}{dt}\left(\frac{\partial L}{\partial \dot{\varphi}}\right) &= a_{11}\ddot{\varphi} + a_{12}(2\ddot{\varphi} + \ddot{\alpha})\cos\alpha - a_{12}(2\dot{\varphi} + \dot{\alpha})\dot{\alpha}\sin\alpha + a_{22}(\ddot{\varphi} + \ddot{\alpha}), \\
\frac{d}{dt}\left(\frac{\partial L}{\partial \dot{\alpha}}\right) &= a_{12}\ddot{\varphi}\cos\alpha - a_{12}\dot{\varphi}\dot{\alpha}\sin\alpha + a_{22}(\ddot{\varphi} + \ddot{\alpha}).
\end{aligned} \tag{3.48}$$

Substituting relations (3.47), (3.48) in (3.46) gives us the equations of motion.

$$\begin{aligned}
j_1(\alpha)\ddot{\varphi} + j_2(\alpha)\ddot{\alpha} - 2a_{12}\dot{\varphi}\dot{\alpha}\sin\alpha - a_{12}\dot{\alpha}^2\sin\alpha &= \\
&= b_{11}\sin(\varphi - \gamma_0) + b_{12}\sin(\varphi - \gamma_1) + b_{13}\sin(\varphi + a - \gamma_1) + M_1
\end{aligned} \tag{3.49}$$

$$j_2(\alpha)\ddot{\varphi} + a_{22}\ddot{\alpha} + a_{12}\dot{\varphi}^2\sin\alpha = b_{13}\sin(\varphi + \alpha - \gamma_1) + M_1 \tag{3.50}$$

Here the expression $j_1(\alpha) = a_{11} + a_{22} + 2a_{12}\cos\alpha$ describes the inertia moment of the first part as for the supporting point O , $j_2(\alpha) = a_{22} + a_{12}\cos\alpha$.

Equation (3.49) can be written in the following form

$$\frac{dK}{dt} = b_{11}\sin(\varphi - \gamma_0) + b_{12}\sin(\varphi - \gamma_1) + b_{13}\sin(\varphi + a - \gamma_1). \tag{3.51}$$

Here K is the moment of momentum of a system (kinetic momentum) as for the point O

$$K = \frac{\partial L}{\partial \dot{\varphi}} = a_{11}\dot{\varphi} + a_{12}(2\dot{\varphi} + \dot{\alpha})\cos\alpha + a_{22}(\dot{\varphi} + \dot{\alpha}) = j_1(\alpha)\dot{\varphi} + j_2(\alpha)\dot{\alpha} \tag{3.52}$$

The dependence (3.51) results from the theorem about the change of the moment of momentum of the system about suspension point O .

4.2. Mathematical model of the perfectly inelastic impact for a two link mechanism

When solving the task how to organize walking of both anthropomorphic and non-anthropomorphic two-legged walking mechanisms the investigation of a double-support phase is very important. A double-support appears at the moment when one of the legs is being put on the surface. At this moment which, generally speaking, is followed by an impact, the second leg can still remain on the surface or it can already leave the surface. We will

consider the time of the double-support phase to be infinitely short, that is the double-support phase is instantaneous. Besides the change of support, in the mechanism the necessary redistribution of velocities must take place within the double-support time.

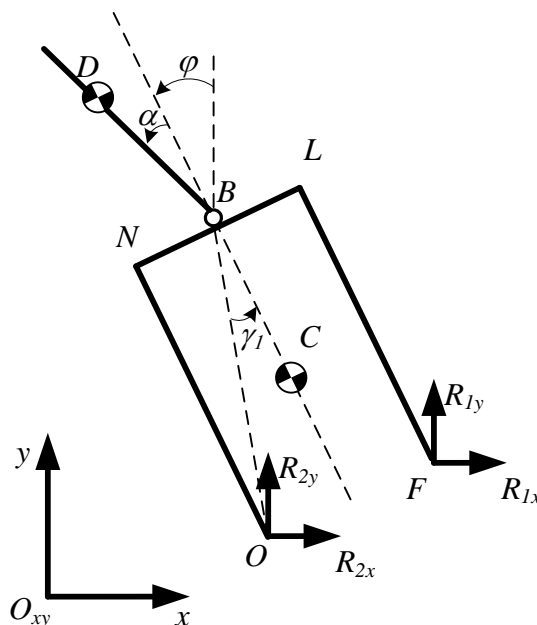


Figure 4.2 –Two link mechanism

While developing the equation of the impact it is necessary, first of all, to consider the movement of the free system (without any connections). We choose the coordinates x, y of the pelvis joint B , angles φ and α (s. Fig 4.2) to be the generalized coordinates of such a system. The expression for the kinetic energy of the described system with 4 degrees of freedom can be represented in the form

$$T = \frac{1}{2} m_1 V_C^2 + \frac{1}{2} I_1 \dot{\varphi}^2 + \frac{1}{2} m_2 V_D^2 + \frac{1}{2} I_2 (\dot{\varphi} + \dot{\alpha})^2 \quad (3.53)$$

Here I_1 is the inertia moment of the lower part consisting of two legs and a pelvis rigidly connected with each other about its mass center C , V_D is the velocity of the mass centre D of the body, I_2 is the inertia moment of the body about its mass center D .

The expressions for the coordinates and velocities of mass centers of each of the parts can be defined on the basis of the following formulas:

$$\begin{aligned} x_C &= x + BC \sin \varphi \\ y_C &= y - BC \cos \varphi \end{aligned} \quad (3.54)$$

$$\begin{aligned} \dot{x}_C &= \dot{x} + BC \cos \varphi \dot{\varphi} \\ \dot{y}_C &= \dot{y} + BC \sin \varphi \dot{\varphi} \end{aligned} \quad (3.55)$$

$$V_C^2 = \dot{x}_C^2 + \dot{y}_C^2 = \dot{x}^2 + \dot{y}^2 + 2BC\dot{\varphi}(\dot{x} \cos \varphi + \dot{y} \sin \varphi) + BC^2 \dot{\varphi}^2 \quad (3.56)$$

$$\begin{aligned}x_D &= x - BD \sin(\varphi + \alpha) = x - BD \sin \psi \\y_D &= x + BD \cos(\varphi + \alpha) = x + BD \cos \psi\end{aligned}\quad (3.57)$$

$$\begin{aligned}\dot{x}_D &= \dot{x} - BD \cos \psi \dot{\psi} \\ \dot{y}_D &= \dot{y} - BD \sin \psi \dot{\psi}\end{aligned}\quad (3.58)$$

$$V_D^2 = \dot{x}_D^2 + \dot{y}_D^2 = \dot{x}^2 + \dot{y}^2 - 2BD\dot{\psi}(\dot{x} \cos \psi + \dot{y} \sin \psi) + BD^2\dot{\psi}^2 \quad (3.59)$$

here $\psi = \varphi + \alpha$.

Substituting the relations (3.54) - (3.59) in (3.53) we can obtain the following expression for the kinetic energy of the two link mechanism with 4 DOF

$$T = \frac{1}{2} \left[(m_1 + m_2)(\dot{x}^2 + \dot{y}^2) + 2m_1 BC \dot{\varphi} (\dot{x} \cos \varphi + \dot{y} \sin \varphi) + (m_1 BC^2 + I_1) \dot{\varphi}^2 - 2m_2 BD \dot{\psi} (\dot{x} \cos \psi + \dot{y} \sin \psi) + (m_2 BD^2 + I_2) \dot{\psi}^2 \right] \quad (3.60)$$

The expression for the kinetic energy of the system can be written in the matrix form

$$T = T(z, \dot{z}) = \frac{1}{2} \dot{z}^T B(z) \dot{z} \quad (3.61)$$

Here $B(z)$ is the symmetrical matrix of the kinetic energy

$$B(z) = \begin{vmatrix} \frac{1}{2}(m_1 + m_2) & 0 & m_1 BC \cos \varphi & -m_2 BD \cos \psi \\ 0 & \frac{1}{2}(m_1 + m_2) & m_1 BC \sin \varphi & -m_2 BD \sin \psi \\ m_1 BC \cos \varphi & m_1 BC \sin \varphi & \frac{1}{2}(I_1 + m_1 BC^2) & 0 \\ -m_2 BD \cos \psi & -m_2 BD \sin \psi & 0 & \frac{1}{2}(m_2 BD^2 + I_2) \end{vmatrix} \quad (3.62)$$

$$z = \|x \quad y \quad \varphi \quad \psi\|^T \quad (3.63)$$

Elementary work δW of the forces $R_1(R_{1x}, R_{1y})$ and $R_2(R_{2x}, R_{2y})$, applied to the points F and O , respectively, is equal to

$$\begin{aligned}\delta W &= (R_{1x} + R_{2x})\delta x + (R_{1y} + R_{2y})\delta y + \\ &+ OB \left[R_{1x} \cos(\varphi + \gamma_1) + R_{1y} \sin(\varphi + \gamma_1) + R_{2x} \cos(\varphi - \gamma_1) + R_{2y} \sin(\varphi - \gamma_1) \right] \delta \varphi\end{aligned}\quad (3.64)$$

here γ_1 - is the angle between the straight lines OB and BC .

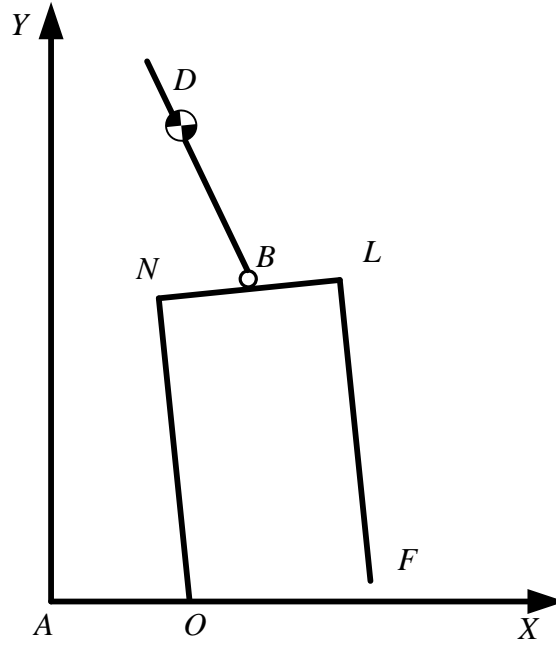


Figure 4.3 – The system of the designations when calculating the impact for the two link mechanism

Let us assume that when $t < 0$ the two link mechanism is moving in such a way that the point O is fixed, that is the leg ON when $t < 0$ remains on the horizontal surface AX . Suppose that at the instant $t = 0$ the point F of the leg LF is contacts this line (the surface) (s. Fig. 4.3). The axis AY is directed vertically. If the contact happens not with the zero velocity, then there occurs an impact at the moment of the contact. Let this impact be perfectly inelastic, that is the speed of the point F becomes zero after the impact:

$$\dot{x}_F(+0) = \dot{y}_F(+0) = 0 \quad (3.65)$$

After the collision of the link LF with the surface, the link ON may either remain on the surface or leave it. The latter is quite possible because the constraint applied to the point O is unilateral one. The double-support result does not depend on the value of the velocity of the point O before the impact, it only depends on its direction [24].

Reactions of the support (constraints) R_1 and R_2 , applied to the system at the moment of the impact $t = 0$, are impulsive actions which can be described with Dirac delta δ -functions. We denote the degrees of these actions with $E_{R_{1x}}, E_{R_{1y}}, E_{R_{2x}}, E_{R_{2y}}$

$$R_{1x} = E_{1x}\delta(t), \quad R_{2x} = E_{2x}\delta(t), \quad R_{1y} = E_{1y}\delta(t), \quad R_{2y} = E_{2y}\delta(t) \quad (3.66)$$

Except the forces R_1 and R_2 no other impulsive actions are applied to the mechanism at the impact instant. At the instant of the impact we receive the relations which correlate velocity steps with the degree of impulsive reactions.

$$\int_{-0}^{+0} B(z) \ddot{z} dt + \dots = \left\| \begin{array}{c} \int_{-0}^{+0} (R_{1x} + R_{2x}) dt \\ \int_{-0}^{+0} (R_{1y} + R_{2y}) dt \\ \int_{-0}^{+0} OB \left[\begin{array}{c} R_{1x} \cos(\varphi + \gamma_1) + R_{1y} \sin(\varphi + \gamma_1) + \\ + R_{2x} \cos(\varphi - \gamma_1) + R_{2y} \sin(\varphi - \gamma_1) \end{array} \right] dt \\ 0 \end{array} \right\| \quad (3.67)$$

Hence we obtain:

$$B(z_0) \{ \dot{z}(+0) - \dot{z}(-0) \} = \left\| \begin{array}{c} E_{1x} + E_{2x} \\ E_{1y} + E_{2y} \\ OB \left\{ \begin{array}{c} E_{1x} \cos(\varphi + \gamma_1) + E_{1y} \sin(\varphi + \gamma_1) + \\ + E_{2x} \cos(\varphi - \gamma_1) + E_{2y} \sin(\varphi - \gamma_1) \end{array} \right\} \\ 0 \end{array} \right\| \quad (3.68)$$

Here $\dot{z}(-0)$ is the vector of velocities just before the impact, $\dot{z}(+0)$ is the vector of velocities just after the impact.

According to the conditions of the impact at the instant $t=0$ the angle $\varphi=0$. The configuration of the mechanism z_0 at the impact instant does not change

$$z_0 = \|x_0 \quad y_0 \quad \varphi_0 \quad \psi_0\|^T = \|x_0 \quad h \quad 0 \quad \psi_0\|^T \quad (3.69)$$

Here x_0 is half the pelvis length.

The matrix $B(z_0)$ is

$$B(z_0) = \left\| \begin{array}{cccc} \frac{1}{2}(m_1 + m_2) & 0 & m_1 BC & -m_2 BD \cos \psi_0 \\ 0 & \frac{1}{2}(m_1 + m_2) & 0 & -m_2 BD \sin \psi_0 \\ m_1 BC & 0 & \frac{1}{2}(I_1 + m_1 BC^2) & 0 \\ -m_2 BD \cos \psi_0 & -m_2 BD \sin \psi_0 & 0 & \frac{1}{2}(m_2 BD^2 + I_2) \end{array} \right\| \quad (3.70)$$

We now substitute expressions (3.68) into equation (3.69), (3.70) and use the expressions of the velocity steps $[\dot{x}]$ and $[\dot{y}]$. We will obtain the system containing 6 algebraic equations which describe the impact.

$$\begin{cases}
\frac{1}{2}(m_1 + m_2)[\dot{x}] + m_1 BC[\dot{\phi}] - m_2 BD \cos \psi_0 [\dot{\psi}] = E_{R_{1x}} + E_{R_{2x}}, \\
\frac{1}{2}(m_1 + m_2)[\dot{y}] - m_2 BD \sin \psi_0 [\dot{\psi}] = E_{R_{1y}} + E_{R_{2y}}, \\
m_1 BC[\dot{x}] + \frac{1}{2}(I_1 + m_1 BC^2)[\dot{\phi}] = OB \left((E_{R_{1x}} + E_{R_{2x}}) \cos \gamma_1 + (E_{R_{1y}} - E_{R_{2y}}) \sin \gamma_1 \right), \\
-m_2 BD \cos \psi_0 [\dot{x}] - m_2 BD \sin \psi_0 [\dot{y}] + \frac{1}{2}(I_2 + m_2 BD^2)[\dot{\psi}] = 0, \\
[\dot{x}] = \dot{x}(+0) - \dot{x}(-0) = -[\dot{\phi}] OB \cos \gamma_1, \\
[\dot{y}] = \dot{y}(+0) - \dot{y}(-0) = -\{\dot{\phi}(+0) + \dot{\phi}(-0)\} OB \sin \gamma_1.
\end{cases} \quad (3.71)$$

Now let us suppose the leg that was on the support is leaving it. Then from the equation system (3.71) for unknown $[\dot{x}]$, $[\dot{y}]$, $\dot{\phi}(+0)$, $[\dot{\psi}]$, $E_{R_{1x}} + E_{R_{2x}}$, $E_{R_{1y}}$ (if $E_{R_{2y}} = 0$), we obtain the following solution for the velocities of the mechanism links after the impact

$$\begin{aligned}
\dot{\phi}(+0) = \dot{\phi}(-0) & \left[I_1 I_2 + BC^2 I_2 m_1 + BD^2 I_1 m_2 + \right. \\
& BC^2 BD^2 m_1 m_2 - 2BD^2 OB^2 m_2^2 \cos(2\psi) + \\
& \left. (I_2 OB^2 m_1 + I_2 OB^2 m_2 + BD^2 OB^2 m_1 m_2 - BD^2 OB^2 m_2^2) \cos(2\gamma_1) - \right. \\
& \left. 4OBm_1 BC (I_2 + BD^2 m_2) \cos(\gamma_1) \right] / \\
& \left[I_1 I_2 - BD^2 OB^2 m_2^2 + BC^2 I_2 m_1 + BD^2 I_1 m_1 + I_2 OB^2 m_1 + \right. \\
& I_2 OB^2 m_2 + BC^2 BD^2 m_1 m_2 + BD^2 OB^2 m_1 m_2 - \\
& 2BD^2 OB^2 m_2^2 \cos(2\gamma_1 - 2\psi) - \\
& \left. 4BCI_2 OBm_1 \cos(\gamma_1) - 4BD^2 BCm_1 OBm_2 \cos(\gamma_1) \right]; \quad (3.72)
\end{aligned}$$

$$\begin{aligned}
\dot{\alpha}(+0) = \dot{\alpha}(-0) & BDm_2 OB \left[(2BC^2 m_1 + OB^2 m_1 + OB^2 m_2 + 2I_1) \cos(\gamma_1 + \psi) - \right. \\
& 2(I_1 + BC^2 m_1) \cos(\gamma_1 - \psi) - (m_1 + m_2) OB^2 \cos(3\gamma_1 - \psi) + \\
& \left. 4BCm_1 OB (\cos(2\gamma_1 - \psi) - \cos(2\gamma_1 + \psi)) \right] / \\
& \left[I_1 I_2 + BD^2 I_1 (m_1 + m_2) + I_2 OB^2 (m_1 + m_2) + \right. \\
& (BC^2 m_1 + OB^2 m_1 - OB^2 m_2) BD^2 m_2 - \\
& 2BD^2 OB^2 m_2^2 \cos(2\gamma_1 - 2\psi) - 4BCm_1 OB (I_2 + BD^2 m_2) \cos(\gamma_1) \left. \right] \\
& + \dot{\alpha}(-0) + \dot{\phi}(-0) - \dot{\phi}(+0); \quad (3.73)
\end{aligned}$$

Further simulations and experimental investigations show that the leg really leaves the surface.

Figure 4.4 represents the structural diagram of the mathematical model of the two link mechanism taking into account the perfectly inelastic impact. The general mathematical model consists of the following components:

- the equations of the two link mechanism motion;
- integrator with an external reset and the input for the initial values;
- the equations of the perfectly inelastic impact for the two link model.

The impact in the mechanism takes place when the sign of the angle φ changes. In such a case the integrator (s. Fig 4.4) reinitializes the values of the velocities $\dot{\varphi}$ and $\dot{\alpha}$, which are calculated on the basis of the relations (3.72) and (3.73), and the values φ and α remain the same in the integrator.

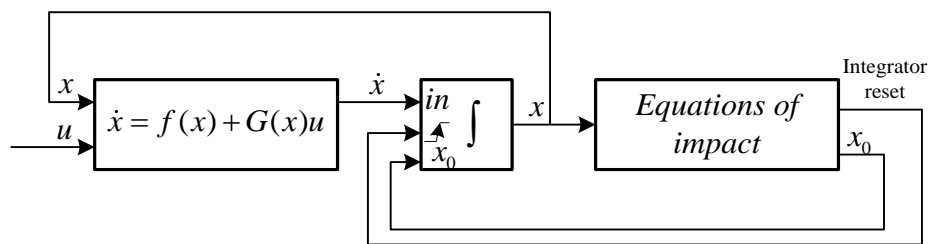


Figure 4.4 – Structural diagram of the mathematical model of the two link mechanism considering the perfectly inelastic impact

At first we will show the transients with account of the perfectly inelastic impact for the mechanism in which the body is "welded" to the pelvis, that is the angle $\alpha \equiv 0$ (the pelvis joint is blocked). These transients are given in Figure 4.5. The plots are drawn at the initial conditions $\varphi(0) = 3$ deg, $\dot{\varphi}(0) = 0$ deg/s. As the interlink joint is blocked, the values α , $\dot{\alpha}$ are equal to zero all the time.

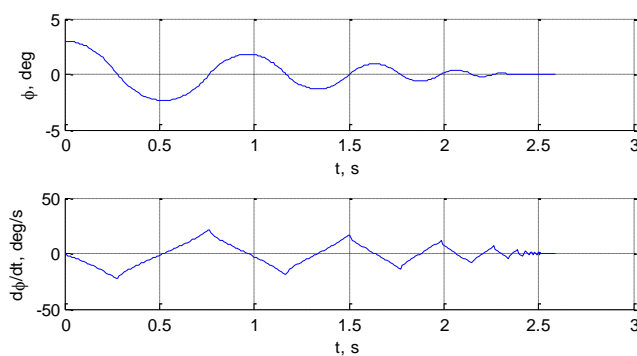


Figure 4.5 – Transients during impacts.

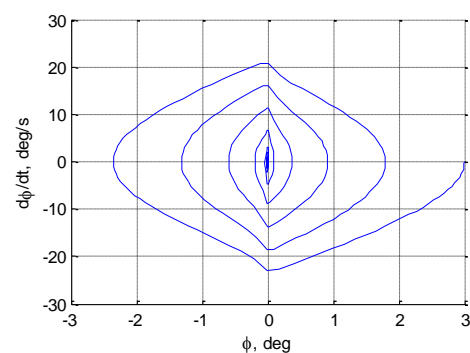


Figure 4.6 – Phase portrait $(\varphi, \dot{\varphi})$ of the motion during impacts.

As it is obvious from Figure 4.5, the oscillating process attenuates within finite amount of time, at that the oscillation frequency grows infinitely. Figure 4.6 represents the phase portrait $(\varphi, \dot{\varphi})$ of the motion. From the plot we can clearly see that after each collision with the surface the velocity $\dot{\varphi}$ decreases.

We now resume the research of a two link mechanism with two degrees of freedom φ and α . We will suppose that the control moment M_2 is applied to the pelvis joint. Figure 4.7 shows the structural diagram of the mathematical model of the two link mechanism with account of the perfectly inelastic impact and the control circuit for the interlink angle.

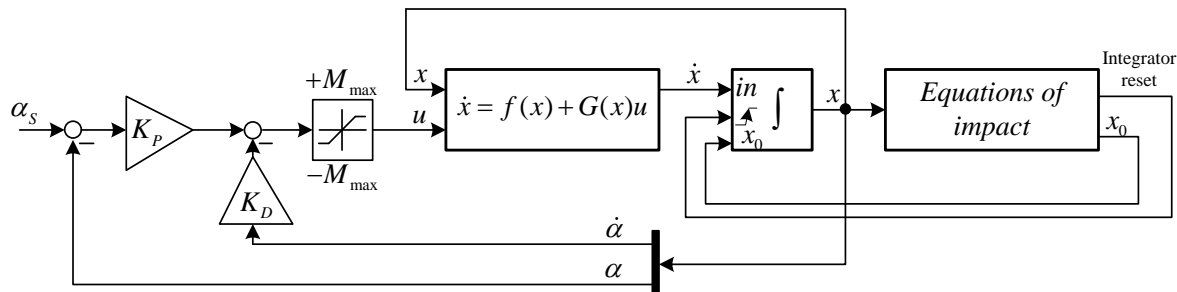


Figure 4.7 – Structural diagram of the mathematical model of the two link mechanism considering the perfectly inelastic impact.

The model of the control system (s. Fig. 4.7) consists of the following components:

- the equations of the two link mechanism motion;
- an integrator with an external reset and the input for the initial values;
- the equations of the perfectly inelastic impact for the two link model;
- a controller of the interlink joint position;
- a block constraining the control action.

The control action in the pelvis joint is developed according to the following law

$$M_2 = K_p(\alpha_s - \alpha) - K_D \cdot \dot{\alpha} \quad (3.74)$$

where K_p и K_D are the feedback (PD-Controller) coefficients (constant), α_s is the predetermined value of the angle α .

Control action constraint is implemented by the means of the following relation

$$u = \begin{cases} +M_{\max}, & \text{if } M_2 > M_{\max}; \\ M_2, & \text{if } |M_2| \leq M_{\max}; \\ -M_{\max}, & \text{if } M_2 < -M_{\max}. \end{cases} \quad (3.75)$$

Where u is the reduced moment in the pelvis joint.

In Figure 4.8 we can see the transients with account of the perfectly inelastic impact when the controller coefficients are $K_p = 200$, $K_D = 10$, initial conditions $\varphi(0) = 3$ deg, $\dot{\varphi}(0) = \alpha(0) = \dot{\alpha}(0) = 0$ and $M_{\max} = 5$ N·m. The desired value $\alpha_s = 0$. From the plot 4.8 it is evident that the oscillating process is of the convergent character.

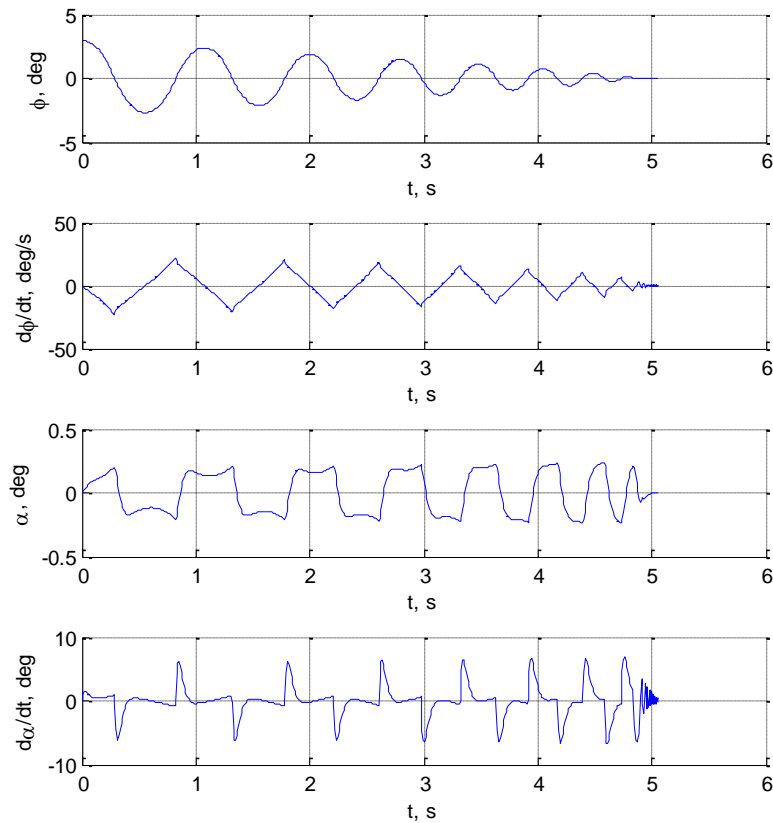


Figure 4.8 – Transients during the control of the interlink angle.

Figure 4.9 represents the phase portrait $(\varphi, \dot{\varphi})$. From the plot it is clearly seen that after each collision with the surface the velocity $\dot{\varphi}$ decreases.

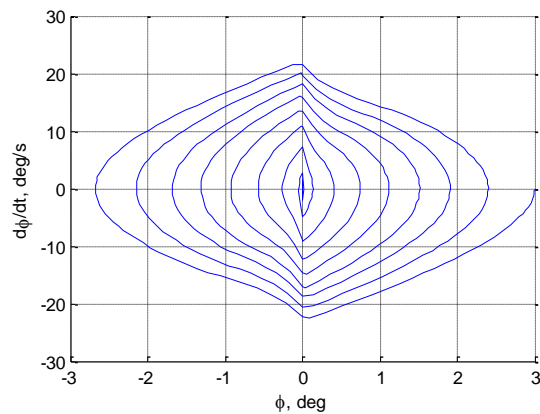


Figure 4.9 – Phase portrait $(\varphi, \dot{\varphi})$ during the control of the interlink angle.

Compared to the case when $\alpha \equiv 0$ (the pelvis joint is blocked, s. Fig. 4.6 and 4.7) the mechanism oscillations damp 2,5 times slower when the interlink joint is controlled. After each impact the body deflects towards the movement of the whole mechanism, that is the controller is not totally rigid. This leads to the fact that elastic control compensates partially the energy losses during the impact.

4.3. Synthesis of the oscillation control in the frontal plane on the basis of optimal laws of swinging and damping

In accordance with the theorem on the conservation of the kinetic momentum without the moment M of the disturbance forces the expression may be written as

$$\frac{dK}{dt} = b_{11} \sin(\varphi - \gamma_0) + b_{12} \sin(\varphi - \gamma_1) + b_{13} \sin(\varphi + a - \gamma_1), \quad (3.76)$$

here K is the kinetic momentum of the mechanism with respect to ankle joint O .

$$K = \frac{\partial L}{\partial \dot{\varphi}} = a_{11} \dot{\varphi} + a_{12} (2\dot{\varphi} + \dot{\alpha}) \cos \alpha + a_{22} (\dot{\varphi} + \dot{\alpha}) = j_1(\alpha) \dot{\varphi} + j_2(\alpha) \dot{\alpha}. \quad (3.77)$$

The expression $j_1(\alpha) = a_{11} + a_{22} + 2a_{12} \cos \alpha$ describes the inertia moment of the first body about the attachment point O and hence, $j_1(\alpha)$ is always more than zero. From the feature that $j_1(\alpha)$ is always positive the expression (3.77) may be written as (3.20).

Substituting the expression (3.24) into the relation (3.76) gives

$$\frac{dK}{dt} = b_{11} \sin(p - F(\alpha) - \gamma_0) + b_{12} \sin(p - F(\alpha) - \gamma_1) + b_{13} \sin(p - F(\alpha) + a - \gamma_1). \quad (3.78)$$

According to [22], the desired law of the optimum swinging $a(p)$, which depends only on the variable p may be represented in the form of the expression (3.27). To implement the optimum damping the desired law has the form as (3.28).

$$a(p) = \arg \min_{|\alpha| \leq \alpha_0} [f(p, \alpha) j_1(\alpha)] \quad (3.79)$$

On the basis of the optimal laws of swinging and damping the pendulum oscillations it is possible to develop the control law to maintain the desired level of the energy of two link pendulum oscillations:

$$\alpha_s = \begin{cases} \arg \max_{|\alpha| \leq \alpha^*} [f(p, \alpha) j_1(\alpha)], & (H_s - H) > 0 \\ 0, & (H_s - H) = 0 \\ \arg \min_{|\alpha| \leq \alpha^*} [f(p, \alpha) j_1(\alpha)], & (H_s - H) < 0 \end{cases} \quad (3.80)$$

To avoid the chattering mode of control action we will introduce the proportional relation of the maximum value of the interlink angle α^* on the discrepancy between the current and desired energies.

$$\alpha^* = \begin{cases} \alpha_0, & \gamma \text{ abs}(H_s - H) \geq \alpha_0 \\ \gamma \text{ abs}(H_s - H), & \gamma \text{ abs}(H_s - H) < \alpha_0 \end{cases}. \quad (3.81)$$

Expression (3.81) allows us to control indirectly the value $[f(p, \alpha)j_1(\alpha)]$, and in this way to limit the approximation gradient to the given energy level.

4.4. Simulation of the system to control oscillations in the frontal plane.

The objects under study are the mathematical model of the two link mechanism (3.49) и (3.50), the equations describing the speed steps (3.72) and (3.73) with the following parameters:

$$\begin{aligned} m_1 &= 2.2 \text{ kg}, m_2 = 3.8 \text{ kg}, BD = 0.689 \text{ m}, g = -9.81 \text{ m/s}^2, \\ a_{22} &= 0.56 \text{ kg} \cdot \text{m}^2, I = 0.32 \text{ kg} \cdot \text{m}^2, OB = 0.714 \text{ m}, OC = 0.294 \text{ m}, \\ \gamma_0 &= 23.1 \text{ deg}, \gamma_1 = 9.26 \text{ deg}, \end{aligned} \quad (3.82)$$

The efficiency of the control law is tested in the following modes: oscillation amplitude increases, oscillation decreases, oscillation amplitude increases when there is viscous friction in the suspension point O , maintenance of the given level of the oscillation energy when there is a constant moment applied in the suspension point O .

In Figure 4.10 we can see the block diagram of the full mathematical model of the two link mechanism with the control system. The full model includes the dynamic model of the two link mechanism, the model of the circuit to control the moment in the interlink joint, the model of the circuit to control the interlink angle, the model of the circuit to control the mechanism energy.

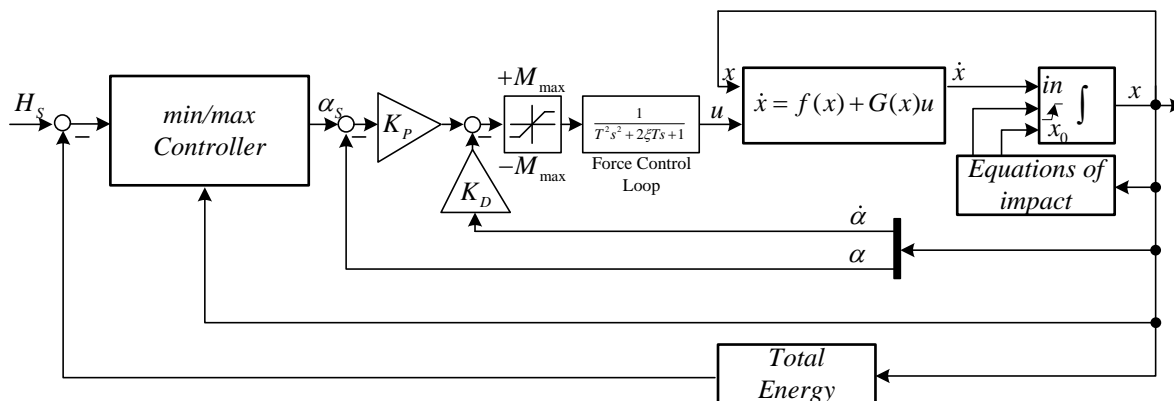


Figure 4.10 – Block diagram of the mathematical model of the control system

The model of the circuit to control the moment in the interlink joint is represented in the form of the second-order link with the time constant $T = 9 \text{ ms}$ and the damping coefficient $\xi = 0.707$, the moment is limited to the value $M_{\max} = 5 \text{ N} \cdot \text{m}$. The circuit of the interlink angle control is adjusted to a nonperiodic process. In the model the linear feedback with the coefficients $K_p = 200$, $K_D = 10$ is used. The interlink angle is limited to the value $\alpha_{\max} = 10 \text{ deg}$.

Figure 4.11 shows the transients in the system when increasing the desired energy level. From Figure 4.11 it is seen that the transients duration is 0,8 seconds when the mechanism energy rises from 0.25 J to 0.35 J and having done two oscillations the systems reaches the preset energy level. When the mechanism energy increases from 0.35 J to 0.45 J, the duration of the transients is 0,9 seconds and the mechanism does 2 oscillations with respect to the vertical axis.

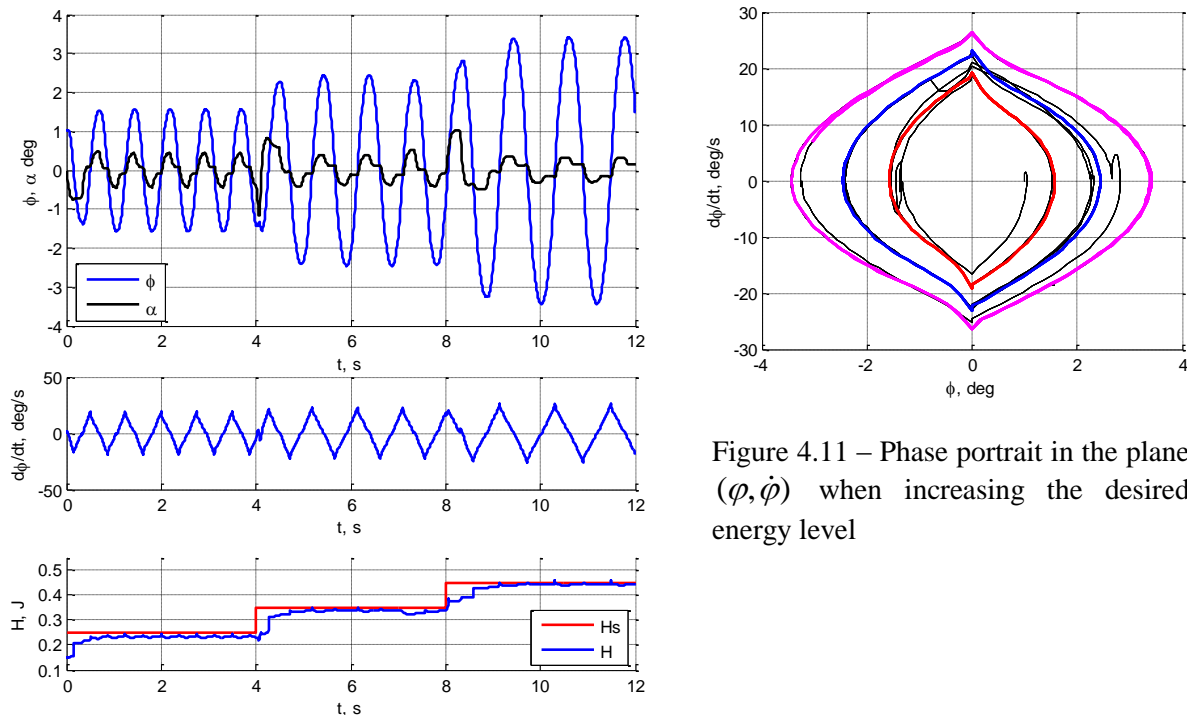


Figure 4.11 – Transients when increasing the desired energy level

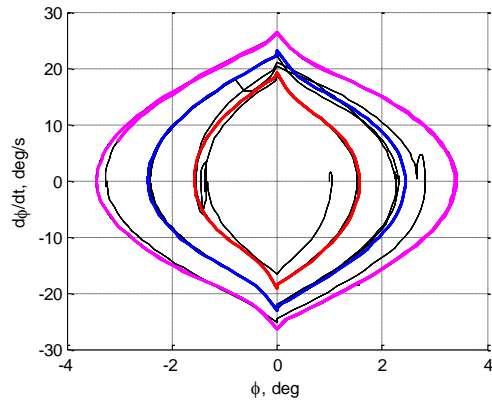


Figure 4.11 – Phase portrait in the plane $(\varphi, \dot{\varphi})$ when increasing the desired energy level

Figure 4.12 gives the phase portrait of a two link mechanism when the given energy level goes up. In Figure 4.12 there are three steady-state orbits corresponding to the different levels of the given energy. The colors denote the maximum cycles relating to the following energy levels: red corresponds to 0.25 J, blue corresponds to 0.35 J and magenta means 0.45 J. The presence of the closed phase trajectories is the evidence that the oscillating process reaches its steady-state periodic mode.

Figure 4.13 represents the transients in the system if there is the viscous friction coefficient in the ankle joint $D = 3 \text{ N} \cdot \text{m} \cdot \text{s}$. In Figure 4.13 we can see that if there is an viscous friction, the amplitude of the two link mechanism oscillations falls by 0.5 deg and the oscillation amplitude of the interlink angle α increases by two times. The decrease of the oscillation amplitude in the support joint is explained by the fact that the control system cannot compensate the energy losses at such a value of the viscous friction.

Figure 4.14 is the phase portrait of the two link mechanism at the presence of the viscous friction. The blue color shows the phase portrait when there is the viscous friction. The red color marks the phase portraits corresponding to the steady-state of oscillations without any viscous friction. In the plot depicting the energy change we can see a steady-state

error. At that the system continues oscillating with smaller amplitude and it comes to the periodic mode.

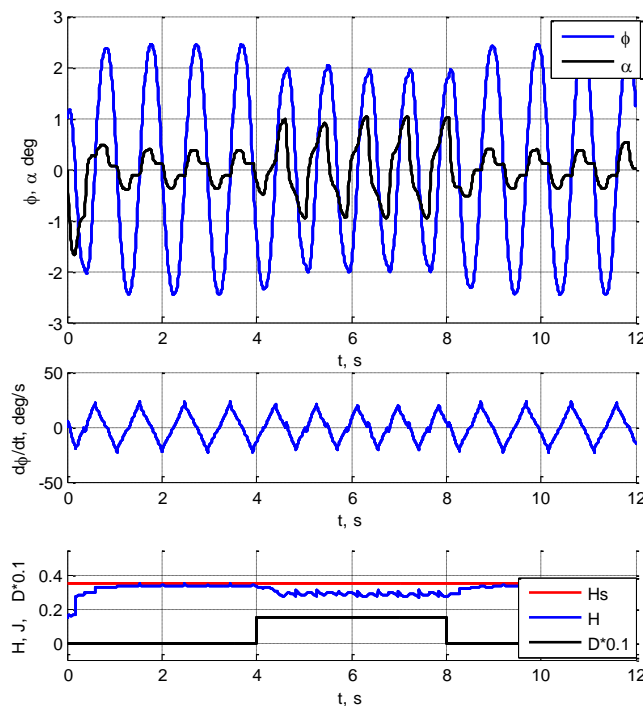


Figure 4.13 – Transients at presence of the viscous friction in the support joint

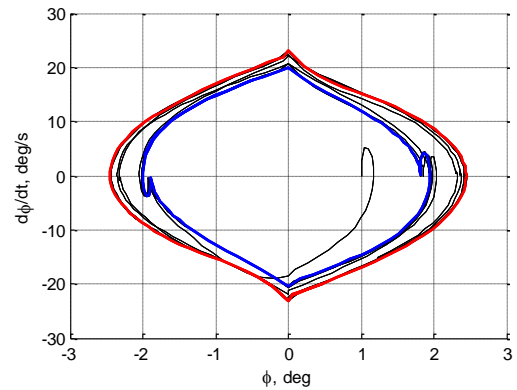


Figure 4.124 – Phase portrait at presence of the viscous friction

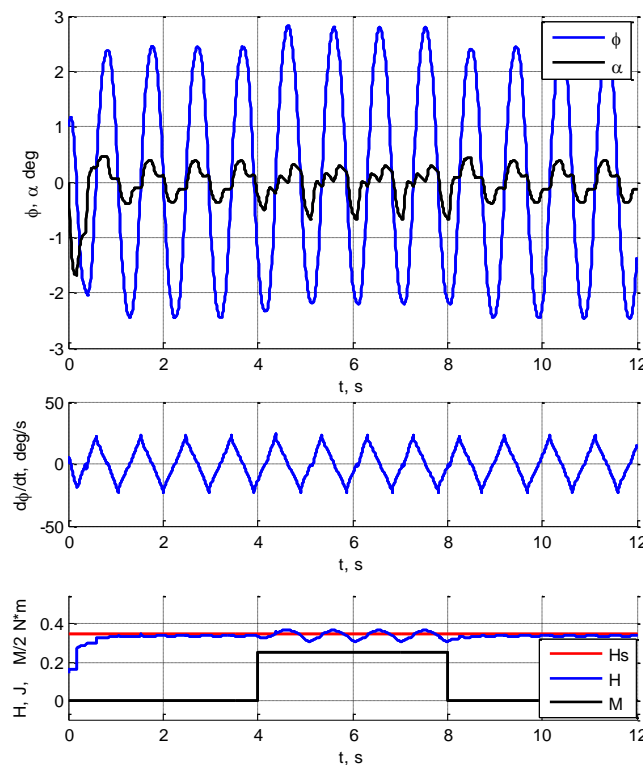


Figure 4.15 – Transients at presence of the constant moment

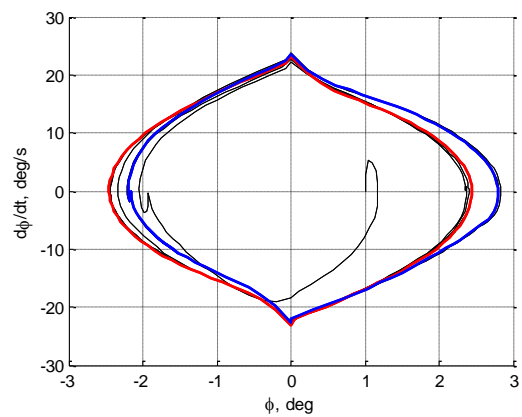


Figure 4.14 – Phase portrait at presence of the constant moment

In Figure 4.15 the transients with the constant moment in the ankle joint are given. From Figure 4.15 it is obvious that the oscillations shift away from the vertical axis. The

deviation value depends on the value of the applied moment. The energy varies around the preset level. The oscillation centre deviates from the vertical.

Figure 4.16 reflects the phase portrait with the constantly acting moment in the support point. In the plots we can clearly see two steady-state orbits. The blue color denotes the phase trajectory corresponding to the steady-state periodic mode with the viscous friction. The red color marks the phase trajectory without any disturbances.

4.5. Intuitive approach to the synthesis of the oscillation control

We now investigate the peculiarities of attenuation of the two link mechanism energy in the case when the angle in the interlink joint is controlled. From Figure 4.8 we can say that the body hits the surface it deflects to the side of falling. At that in contrast to the case with the "welded" body (s. Fig. 4.5) the mechanism oscillations damp twice as slow. This feature allows us to say that each time during the impact with the surface the mechanism has to deflect by some angle in the direction of movement in order to compensate the energy mechanism losses. On account of this feature it is possible to develop the following law controlling the angle α

$$\alpha = -\gamma(H_s - H) \cdot \text{sign}(\phi) \quad (3.83)$$

Expression (3.83) denotes that the sign of the given angle changes during the impact. Besides that the value of the given angle is proportional to the discrepancy between the current and preset values of the full energy.

Figure 4.17 shows the block diagram of the system to control the two link mechanism oscillations with the control laws (3.83). The system consists of the full energy controller, the control loop of the interlink angle and the equations of motion with the impact relation.

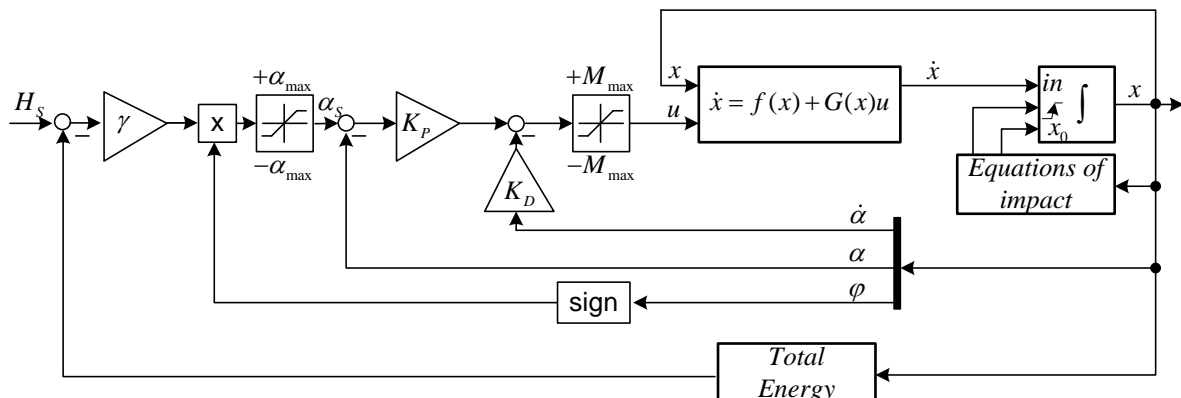


Figure 4.17 - The system to control the two link mechanism oscillations

Figure 4.18 gives the transients of the implementation of the desired value of the total mechanism energy. From the plots it is evident that the control system reaches the desired level of the energy. When the desired level of the energy changes from 0.25 J to 0.4 J the

transients time is 1 s and after 3 oscillations the mechanism reaches the steady-state oscillating mode.

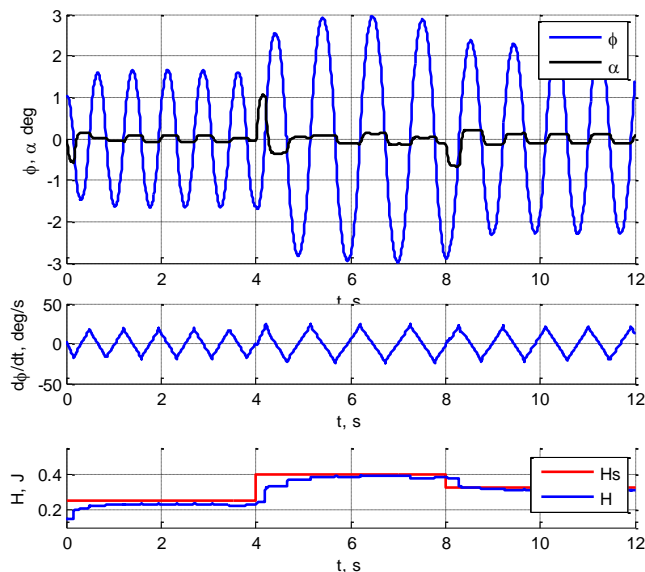


Figure 4.17 – Transients of the two link mechanism oscillations

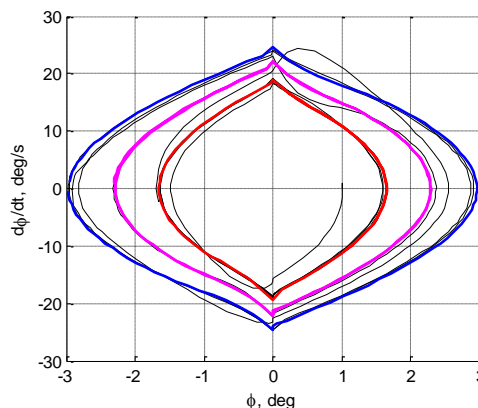


Figure 4.16 – Phase portrait of the oscillating processes

In Figure 4.19 there is a phase portrait of the oscillating processes while the energy control. In the plot we can observe three limit cycles corresponding to various levels of the full mechanism energy (red is 0.25 J, magenta is 0.32 J, blue is 0.4 J).

Figure 4.20 represents the transients with the viscous friction in the supporting joint O (the viscous friction coefficient is $D=1.5 N \cdot m \cdot s$). On the basis of the plot it is obvious that at presence of the viscous friction the energy of the mechanism decreases from the value 0.38 J to 0.3 J.

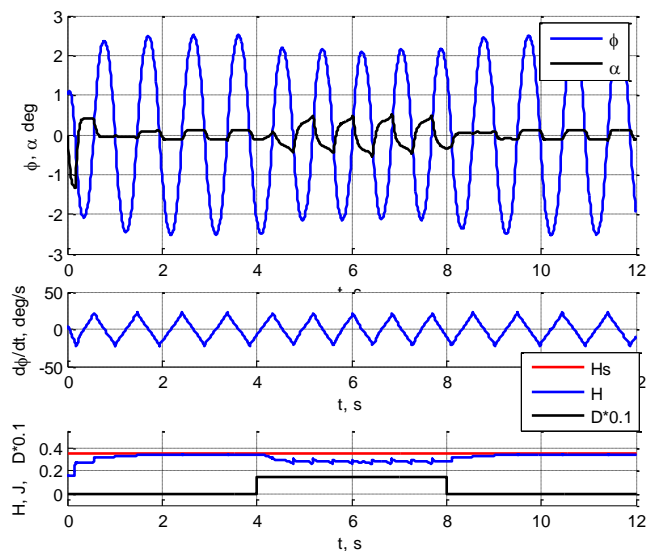


Figure 4.18 – Transients at presence of the viscous friction

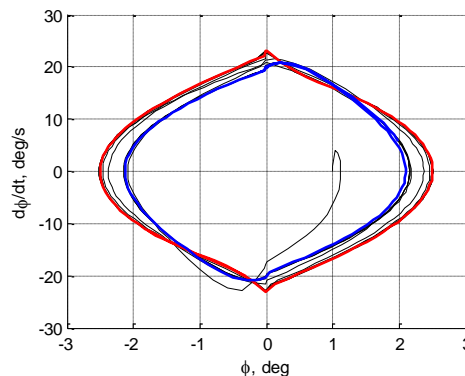


Figure 4.21 – Phase portrait at presence of the viscous friction

In Figure 4.21 we can see the phase portrait when there is the viscous friction in the supporting joint O . From the plot it is clear that the presence of the viscous friction changes the phase trajectory of the mechanism movement (blue is with the viscous friction, red is without the friction). It is necessary to note that when there is the viscous friction, the mechanism reaches the periodic oscillating process.

4.6. Experimental results

We now give the experimental results of the investigation of the control system of the two link pendulum. The control of the experimental assembly is implemented by using Matlab xPC-Target technology (s. Fig. 4.22). On the basis of xPC-Target by means of the industrial communication network the linear elastic actuator implementing the given moment in the interlink joint is connected to the Master computer.

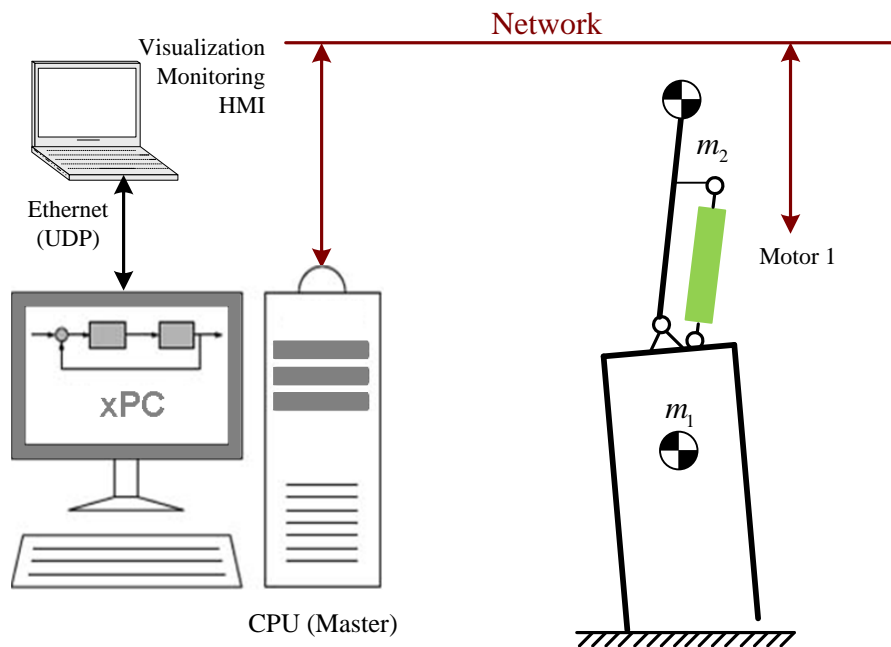


Figure 4.19 – Experimental assembly

Figure 4.23 shows the experimental assembly to investigate the operation of the control system of the periodic movement of the two legged mechanism in the frontal plane [83]. The experimental assembly is made on the base of the linear elastic actuator [38]. The two link mechanism consists of two links with masses m_1 and m_2 . The first body is the pelvis with "welded" legs. The 2nd body consists of a heavy link and the elastic actuator attached to it. The mechanism under study has the parameters (3.82). The angle α and the angular velocity $\dot{\alpha}$ are defined with the help of the absolute encoder in the interlink joint and the impulse speed sensor in the linear elastic actuator respectively. The angle φ and the angular velocity $\dot{\varphi}$ are measured by means of the gyroscope.

The control loop of the interlink angle is tuned exactly the same as during the simulation. The control loop is tuned on the nonperiodical transient. The linear feedback with

the coefficients $K_p = 200$, $K_D = 10$ is used. The interlink angle is limited by the value $\alpha_{\max} = 10$ deg. The intuitive control method is used in the experiments. The coefficient $\gamma = 0.14$



Figure 4.20 – Experimental assembly

The operation of the control system of the two link pendulum on the experimental assembly is tested for the following modes: the oscillation amplitude change, maintenance of the periodic process on the different surfaces (wood, carpet). The surfaces on which the experiment is carried out have different parameters of elasticity and damping. All the experiments are carried out with the same tuning of the control loop by the full mechanism energy.

Figure 4.24 shows the transients of the implementation of the desired level of the full energy on the wooden surface. From the plots it is seen that the sharp decrease of the full mechanism energy takes place during each impact with the surface. After each impact the control system tends to compensate full energy losses at the expense of the body movement. From the plots it is seen that the mechanism reaches the steady-state periodic mode.

. Figure 4.25 shows the transients of the implementation of the desired level of the full energy on the fabric surface. From the plots it is seen that the sharp decrease of the full mechanism energy takes place during each impact with the surface. After each impact the control system tends to compensate full energy losses at the expense of the body movement. In the plot of the energy H it is clearly seen that there is a static error while controlling by the full mechanism energy. The value of this static error can be corrected by changing the value of the coefficient γ .

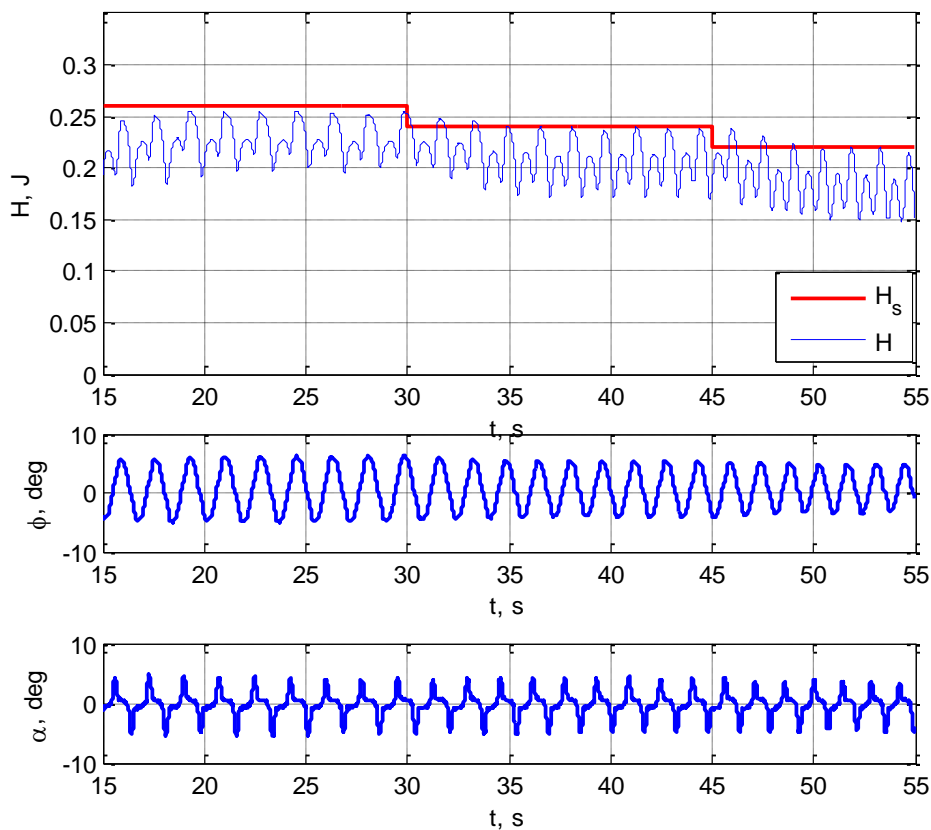


Figure 4.21 – Transients of the implementation of the energy desired level on the wooden surface

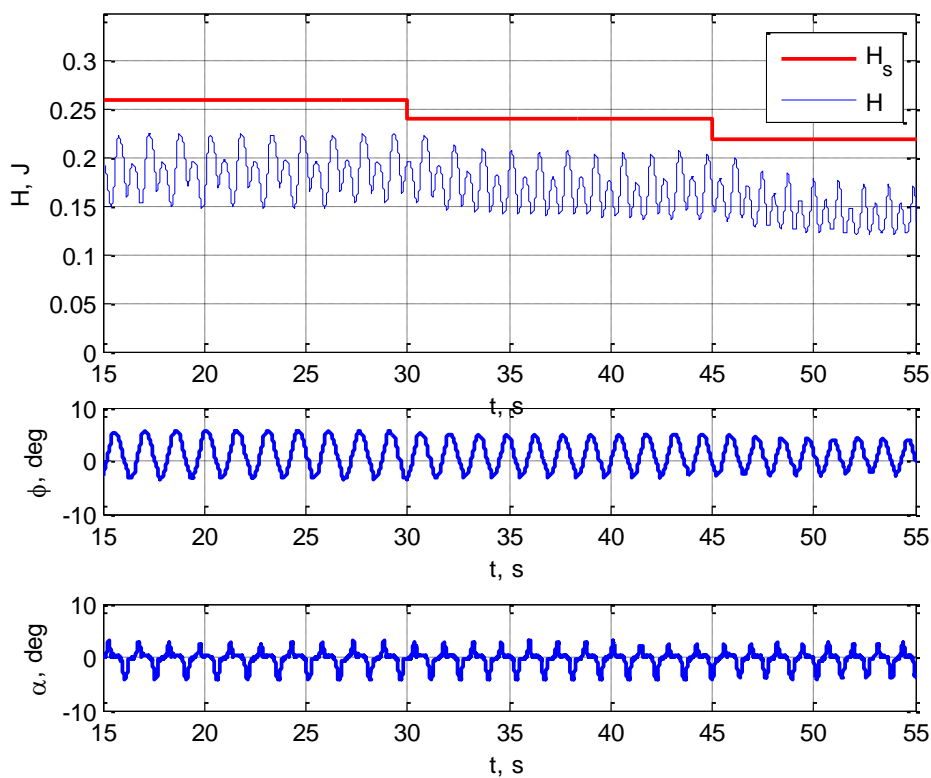


Figure 4.22 – Transients of the implementation of the energy desired level on the carpet surface.

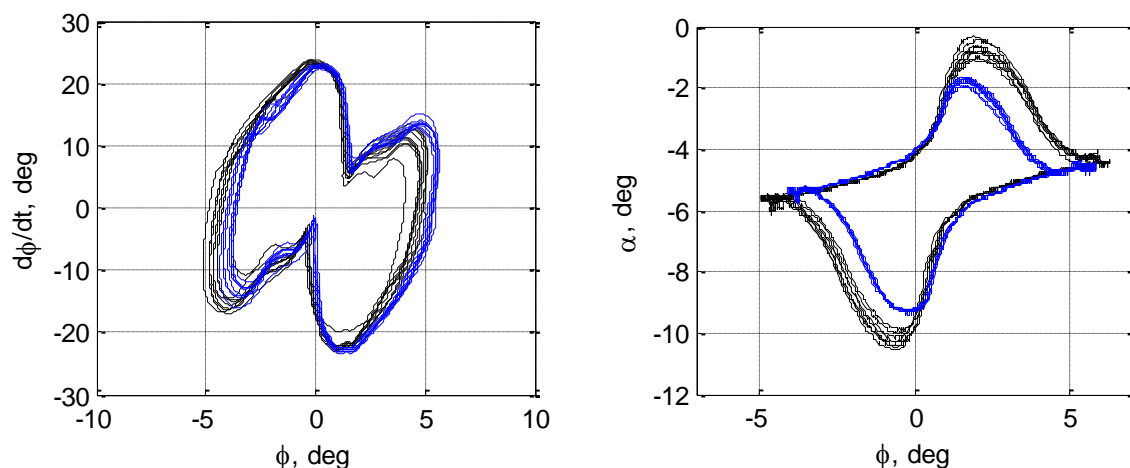


Figure 4.23 – Phase portraits of the mechanism movement on the wooden (black) and fabric (blue) surfaces.

Figure 4.26 shows the phase portraits of the mechanism movement $(\phi, \dot{\phi})$ and (ϕ, α) . In the plots we can see the steady state of the periodic mechanism movements on the wooden and carpet surfaces. From the plots it is seen that the mechanism oscillation amplitude depends on the surface properties. The oscillation amplitude is 1 degree less on the surface with bigger damping (carpet) than on the wooden surface.

In the present chapter we carry out the simulation and experimental investigations of the operation of the different control systems by maintaining the periodic motions (oscillations) of the two link pendulum which simulates the oscillations of the biped robot in the frontal plane.

The simulation and experimental investigations show that for the underactuated mechanical system under investigation it is possible to develop the periodic modes when there is the impact interaction with the supporting surface. When comparing the operation of the system to control the two link mechanism oscillations by means of simulation and experimental investigations it turns out that the surface properties influence the properties of transients and the character of the steady-state periodic mode. The simulation and experimental investigations show that the control system brings the mechanism to the stable periodic mode of oscillations on the supporting surfaces which have different properties. The developed algorithms to control the periodic motions of the two- legged mechanism in the frontal plane are used further to organize 3D walking of the biped robot.

Chapter 5. Design of dynamic walking of the biped robot ROTTO

Equation Section (Next)

In this chapter the way to synthesize walking of the two – legged locomotion mechanism is given. The walking control algorithm is developed in such a way that during locomotion the full energy of the walking mechanism is maintained to be constant. At that walking takes place in the periodic mode. The experimental investigations prove the efficiency of the developed algorithm.

5.1. Development of the dynamic model

This section deals with the methods to develop the equations of motion of complicated mechanical systems.

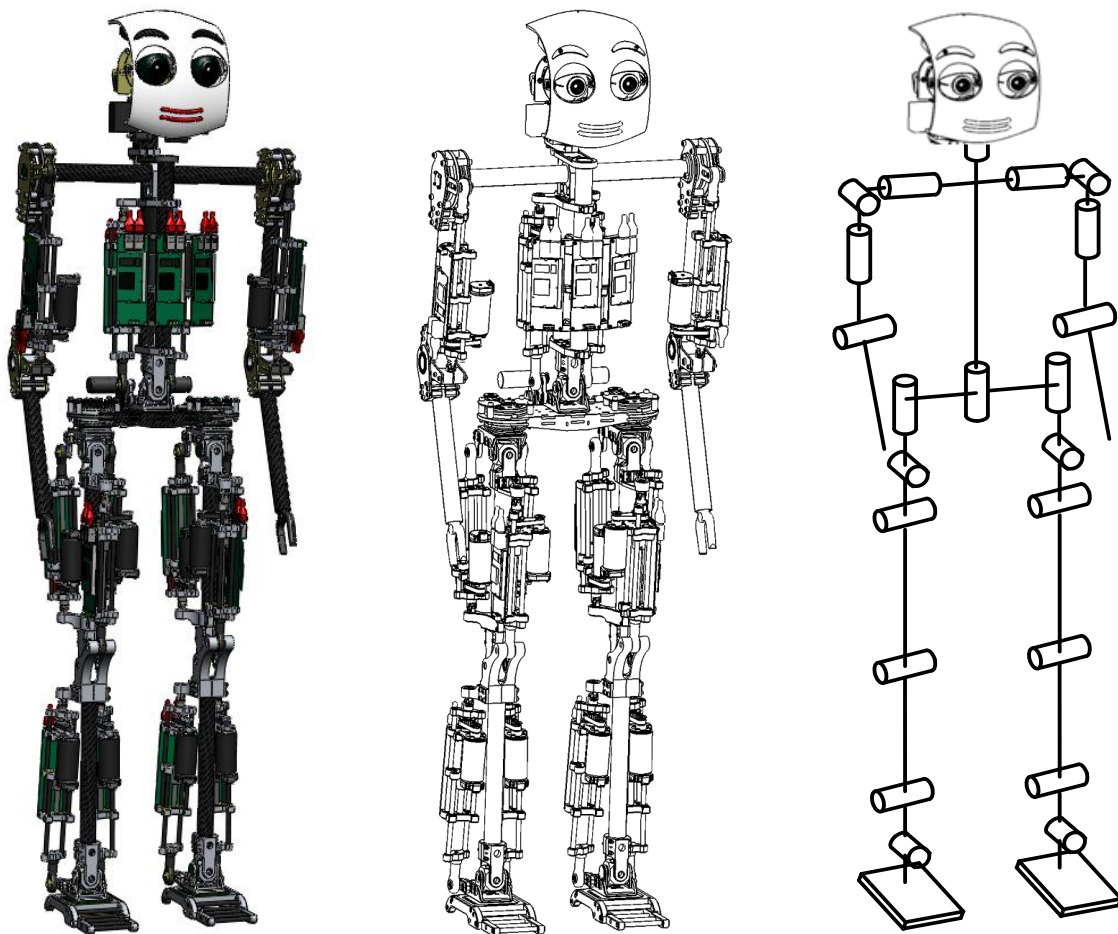


Figure 5.1 – Robot ROTTO Structure

Figure 5.1 shows the kinematics of the robot ROTTO. The robot consists of 8 heavy links and it has 30 DOF. Let us consider the methods which allow us to receive the motion equations of such a mechanism.

The dynamic of the rigid body mechanical system is described by means of the equations of motion which reflect the interrelation between the forces acting in the system and the acceleration caused by these forces. There are two types of problems, namely, forward and inverse dynamic. Forward dynamic is the calculation of the acceleration response of a given rigid-body system and inverse dynamic is the calculation of the force that must be applied to a given rigid-body system in order to produce a given acceleration response [19].

While generating the equations of motion for the mechanical system with relatively small number of DOF the methods which allow receiving the analytical description of the system dynamics are mainly used. The motion equations of such systems are visible and during the simulation they do not require big computational cost. Very often there is no point in generating the equations of motion for the mechanical systems with relatively big number of DOF in an analytical form. This is explained by the fact that the equations of motion become lengthy and boundless. For the system with big number of DOF the recursive algorithms are used. Depending on the type of dynamic presentation different methods are used (s. Fig. 5.2).

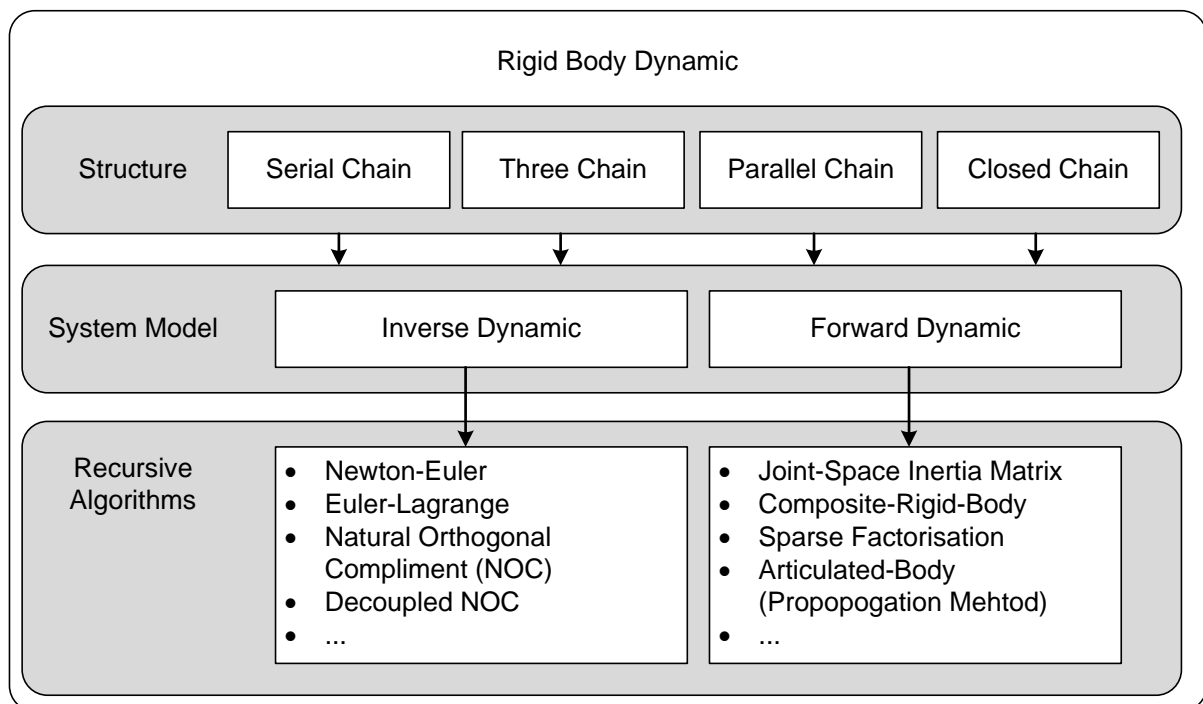


Figure 5.2 – Rigid Body Dynamic

The robot ROTTO has a tree-like kinematics structure. That is why to develop the motion equations for this robot we use the recursive Newton-Euler algorithm.

Inverse Dynamic – Recursive-Newton Euler Algorithm

Inverse dynamic for a chain or a tree- like kinematic structure of a mechanism according to the method of the recursive Newton Euler algorithm is calculated in three steps [19]:

1. Calculate the velocity and acceleration of each body in the tree.
2. Calculate the forces required to produce these accelerations.
3. Calculate the forces transmitted across the joints from the forces acting on the bodies.

Step 1: Let us calculate the velocity v_i and acceleration a_i of i -body. The velocity of i -body in the kinematics chain can be defined recursively as the sum of the velocity of the previous ($i-1$) body and the velocity across the i -joint

$$v_i = v_{i-1} + S_i \dot{q}_i \quad (v_0=0) \quad (4.1)$$

Here S_i is the transformation matrix of the body coordinates from the local system into the global one.

The expressions for the accelerations of the system are received when differentiating expressions (4.1) and have the following form

$$a_i = a_{i-1} + S_i \ddot{q}_i + \dot{S}_i \dot{q}_i \quad (a_0=0) \quad (4.2)$$

Here \dot{S}_i is Jacobian received when we differentiate the transformation matrix of the body coordinates.

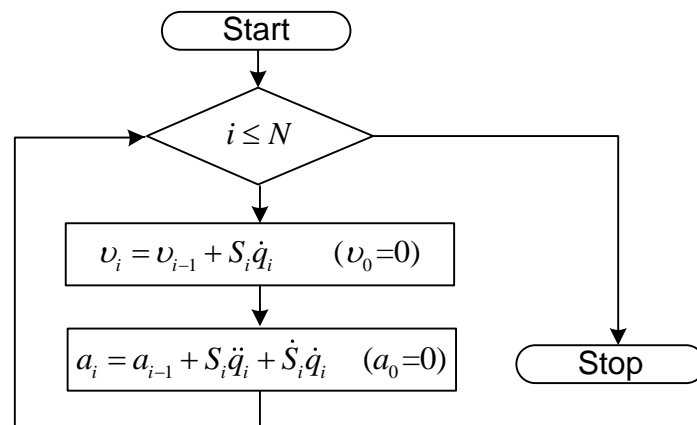


Figure 5.3 – Iteration algorithm of calculation of the velocities and accelerations of the mechanism links.

The calculations of the velocities and accelerations for all the bodies are performed iteratively with $i=1, \dots, N$, where N is the number of the bodies. Having calculated the velocities and accelerations it is possible to pass on to the calculation of the forces acting on the links.

Step 2: The overall equivalent torque f_i^B acting on the i -body is connected with the acceleration of the i -body by the following expression

$$f_i^B = (I_i + ml^2)a_i + v_i \times I_i v_i \quad (4.3)$$

Here I_i - is the body inertia about center of the body mass. Assume that f_i is the equivalent torque acting from the parent body ($i-1$) on the i -body across the i -joint and assume that f_i^x is any external force acting on the i -body, f_j, f_k, f_l are the forces acting on the children bodies (s. Fig. 5.4).

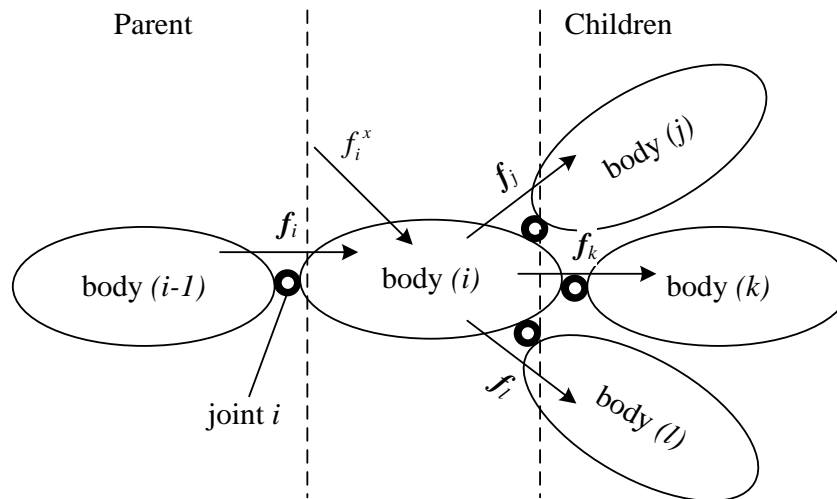


Figure 5.4 – Kinematic diagram of the mechanical system.

Step 3: The force f_i acting on the i -body is calculated from the expression

$$f_i = f_i^B - f_i^x + \sum (f_j + f_k + f_l + \dots) \quad (4.4)$$

Generalized torques are calculated from the following formula

$$\tau_i = S_i^T f_i \quad (4.5)$$

As a result of the algorithm implementation it is possible to receive the equation of the mechanism motion in the inertial coordinate system. These motion equations can also be written in the coordinate system of the mechanism links.

There are the methods of the motion equation development in the form of forward dynamic. The description of these methods can be found in the papers [77], [94], [19].

At present there are a great number of software packages which allow developing the equations of motion for free structure mechanical systems. MATLAB [52] and Dymola [15].

can be referred to the software packages of this type. The mathematical model of the robot ROTTO is made in both applications. The equations given in [34] are used for simulation of the contact processing.

In the laboratory RobotsLab the concept HIL/SIL simulation was developed which allows us to reduce essentially the time for the development and implementation of the algorithms to control the robots. This concept is described in the article [17] .

5.2. Synthesis of the robot movement on the basis of ballistic trajectories

As it has already been noticed in the first chapter there are a lot of methods to organize walking of two-legged locomotion mechanisms. Simple trial- and - error methods as well as complicated methods based on the criteria of the minimum energy consumption, ZMP, FRI, CMP and others are used to solve this problem. The stability criterion ZMP which indicates whether the given movement leads to overturning or not is the method commonly used to synthesize the movement trajectories. The control of walking on the basis of the criterion ZMP with the application of the linear inverted pendulum model (LIPM) is the example of such a method. The application of the model LIPM leads to considerable simplification of the robot joint motions. When observing the criterion ZMP the robot locomotion in some “stable” zone. In spite of the fact that such an algorithm of generating the robot motion trajectories is one of the most successful for the time being and it is used in the majority of robots (Asimo, HRP and others) the robot gait does not look natural when this algorithm is used. The application of the dynamic properties of the mechanism is greatly limited because of the considerable simplification of the robot dynamic model.

The obvious requirement for the modern methods of the trajectory generation is the application of the dynamic peculiarities of the mechanism when developing the anthropomorphic walking. Within the frames of the given work the method of the trajectory synthesis is developed. The basis of this method is the free mechanism movement. In other words the method is based on the so-called ballistic trajectories.

This chapter deals with the method of synthesis of the ballistic trajectories for the anthropomorphic robot. To simplify the task a five - link model of the mechanism is investigated and the family of ballistic trajectories is obtained. The procedure how to obtain the trajectories of the 12 - link mechanism with 14 DOF is considered further in the work.

5.2.1. Basic of ballistic trajectories

The investigations in the sphere of human walking biomechanics [3], [24], [88], [92] show that during walking the muscles of a human being are active only for some, relatively short, periods of time. In the periods between the muscle activities human motions are similar to ballistic ones. In these periods the parts of a human body move along the free (natural) trajectories using own dynamics and practically without usage of any additional energy. As a result of such movement the kinetic energy of the links is transformed into the potential one and then again into kinetic. In papers [46], [94] the assumption is made that such movement

is close to energy – efficient and energy-optimal one. For the first time the problem of ballistic movement synthesis was considered in the papers of A. M. Formalskiy in 1975 [20]. Then it was considered in the papers of Mochon [62], McGeer [54], [55], McMahon [57]. The investigations of these authors show that ballistic trajectories have a great similarity to the trajectories of human being movement in a single-support phase.

We consider the five-link mechanism without any feet (s. Fig. 5.5) as an example of the ballistic trajectory synthesis.

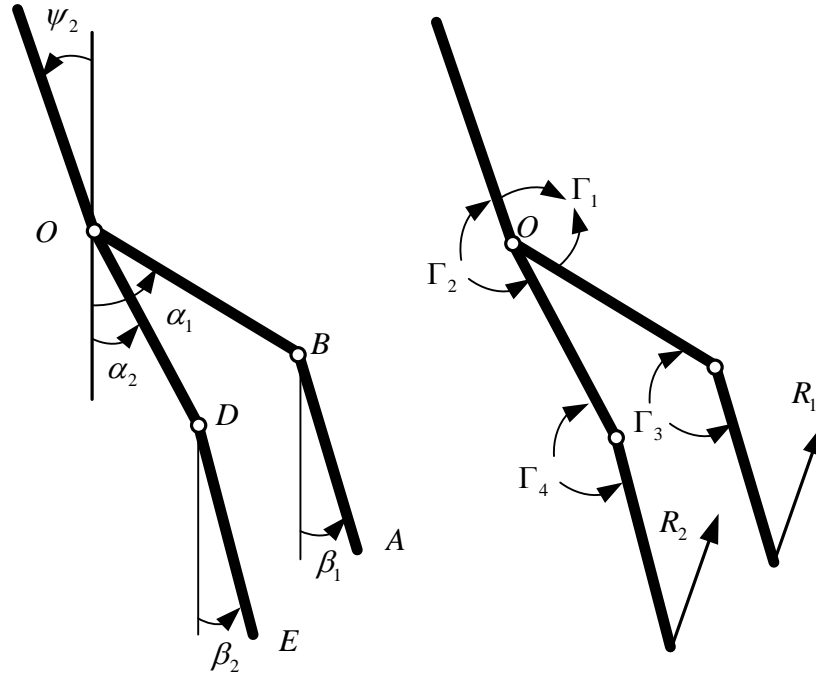


Figure. 5.5 – Scheme of the 5-link biped

The equations of motion for the five-link mechanism can be obtained on the basis of the recursive method Newton-Euler [77] or developed analitically. In accordance with [2], [3], [21], [24] the equation for the five-link mechanism can be presented in the matrix form

$$H(q)\ddot{q} + gL\|\sin q_i\| + M(q)\|\dot{q}_i^2\| = \Gamma \quad (4.6)$$

Here $H(q)$ is the matrix of the kinetic energy, L is the diagonal matrix of the potential energy, g is the gravity acceleration, $M(q)$ is the skew-symmetric matrix,

$$q = \|q_i\| = \begin{Bmatrix} \psi \\ \alpha_1 \\ \alpha_2 \\ \beta_1 \\ \beta_2 \end{Bmatrix}, \quad \|\sin q_i\| = \begin{Bmatrix} \sin \psi \\ \sin \alpha_1 \\ \sin \alpha_2 \\ \sin \beta_1 \\ \sin \beta_2 \end{Bmatrix}, \quad \|\dot{q}_i^2\| = \begin{Bmatrix} \dot{\psi}^2 \\ \dot{\alpha}_1^2 \\ \dot{\alpha}_2^2 \\ \dot{\beta}_1^2 \\ \dot{\beta}_2^2 \end{Bmatrix}, \quad \Gamma = \begin{Bmatrix} \Gamma_1 \\ \Gamma_2 \\ \Gamma_3 \\ \Gamma_4 \end{Bmatrix} \quad (4.7)$$

Ballistic motions represent the solutions of differential equations (4.6) if $\Gamma = 0$. Assume that in equations (4.6) $\Gamma = 0$, they become as follows

$$H(q)\ddot{q} + gL\|\sin q_i\| + M(q)\|\dot{q}_i^2\| = 0 \quad (4.8)$$

The problem of obtaining the ballistic trajectories can be formulated in the following way: it is necessary to find such a vector of the initial velocities $\dot{q}(0)$ of the mechanism links which make the mechanism move from the given state $q(0)$ into the given state $q(T)$ for the given time T (s. Fig. 5.6).

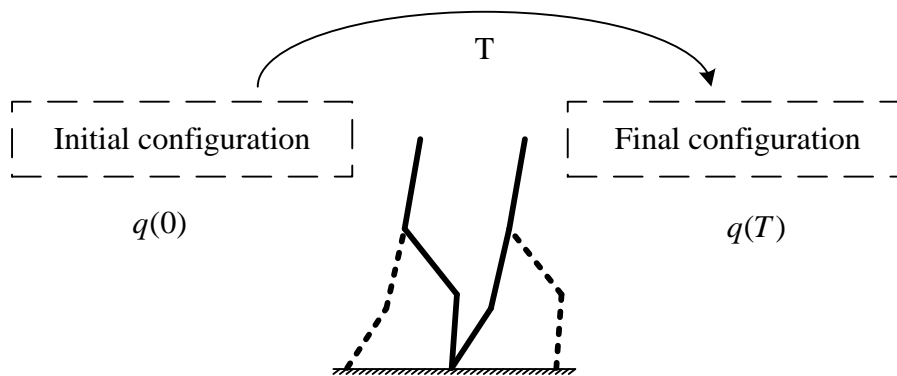


Figure 5.6 – Boundary configurations of the biped in the swing phase

The configurations $q(0)$ and $q(T)$ exactly coincide but the legs are swapped. Thus, the problem to design the ballistic trajectories is reduced to the boundary value problem, from mathematical point of view. This boundary value problem can be solved by means of the shooting method, Newton method and other ways.

In this paper the key to the boundary value problem solution is the minimization method Levenberg-Marquardt [45], [63] of goal function E (s. Fig. 5.6). This objective function describes the disparity between the desired configuration at the instant T and the configuration obtained during the iteration at the instant T . To integrate the differential equations the adaptive integration methods Runge-Kutte of the 4-th and the 5-th order are used.

The goal function E (s. Fig. 5.7) depends on N - variables (the number of DOF). The function values become lower and tend to the global minimum [94] in the process of minimization (iterative process).

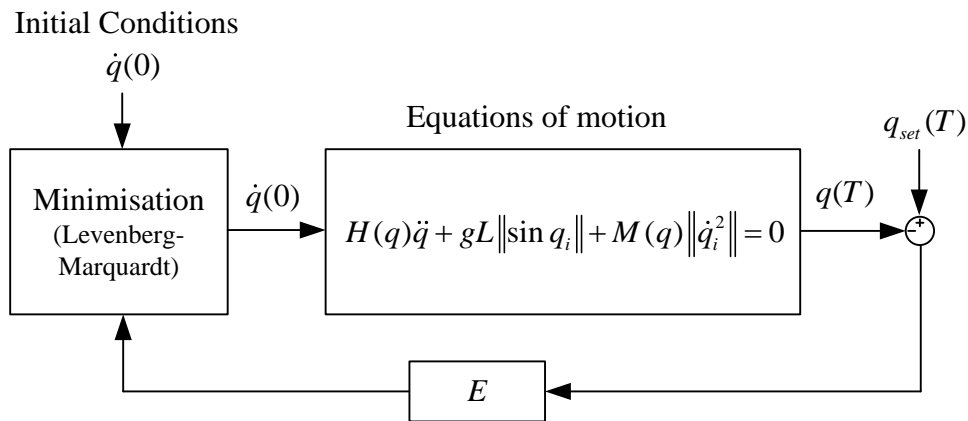


Figure 5.7 – Minimization algorithm

Mathematical simulation shows that the solution of the boundary value problem is sensitive to the change in the initial conditions and the duration of the step T , which is the consequence of the instability of the trivial solution of system (4.8). If choice of initial approximation $\dot{q}(0)$ is unsuccessfully, then the iteration of the boundary value problem solution converges slowly which is explained by the essential nonlinearity of the equation of motion. The boundary value problem for the linearized problem is solved analytically. Under some conditions it has only one solution for the linearized equations .

Let us consider the solutions obtained for the model with the following parameters: link masses are $m_{OD} = m_{DE} = m_{OB} = m_{BA} = 1.5 \text{ kg}$, $m_{OC} = 6 \text{ kg}$, the centers of masses of all the links which are considered to be homogenous are in the middle of the rods OD , DE , OB , BA , OC and the inertia moments are calculated $J = \frac{1}{12} ml^2$, where l is the length of the rod. The lengths of the rods are $l_{OD} = l_{DE} = l_{OB} = l_{BA} = 0.25 \text{ m}$, $l_{OC} = 0.3 \text{ m}$.

Figure 5.8 shows the ballistic trajectories and the motion sequences of the mechanism movement. These trajectories are obtained as the result of the boundary value problem solutions for the following conditions:

$$T = 0.5 \text{ s}, q(0) = [0; -12; 12; -12; 12]^T \text{ deg}, q(T) = [0; 12; -12; 12; -12]^T \text{ deg}.$$

Below there are three boundary value problem solutions which were obtained:

1. $\dot{q}(0) = [2.5141; 0.4460; -4.3407; 1.2731; -2.9552] \text{ rad/s}$ - - symmetric step
2. $\dot{q}(0) = [2.4080; 0.4835; -4.1299; -1.7022; 5.6827] \text{ rad/s}$ - knee forward step
3. $\dot{q}(0) = [2.5729; 0.7076; -5.0528; 4.4603; -10.5426] \text{ rad/s}$ - knee backward step

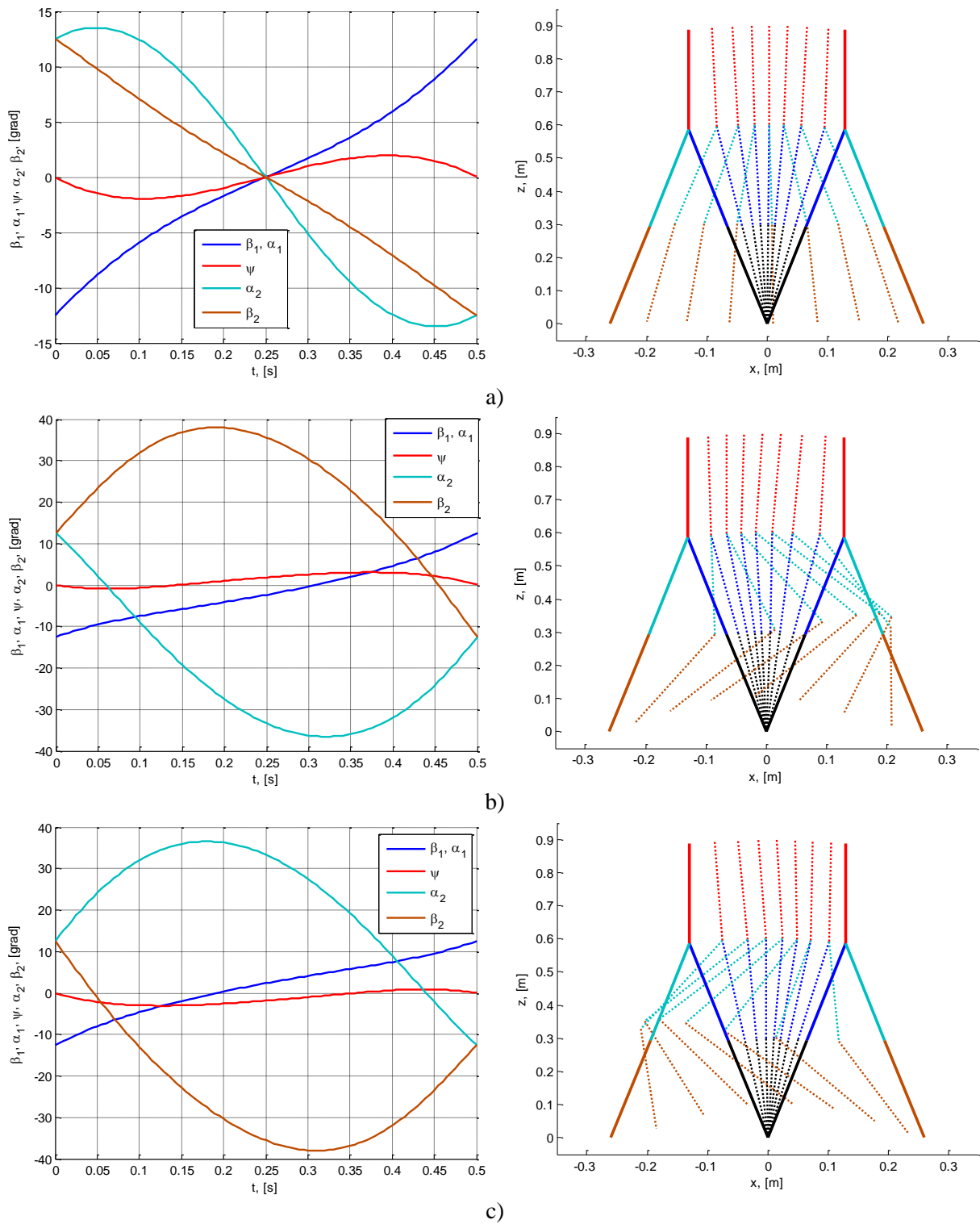


Figure 5.8 – Ballistic trajectories and the motion sequences
a) symmetric step, b) knee forward step,
c) knee backward step

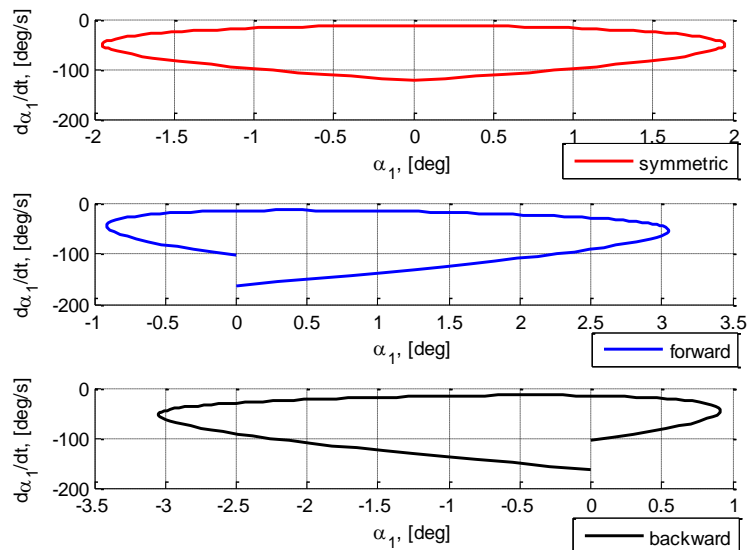


Figure 5.9 – Dependence of the velocity value on the interlink angle value for the five-link mechanism.

Figure 5.9 represents the graphs in the plane, velocity $\dot{\alpha}_1$ values and the values of the interlink angle α_1 . Red, blue and black colors mark the dependences obtained for the symmetric step (branch), knee forward step and knee backward step respectively. From the plots we can see that only in the symmetric step there is no velocity jump while changing the supporting leg.

5.2.2. Three-Dimensional Ballistic Walking of the Biped Model with many degrees of freedom

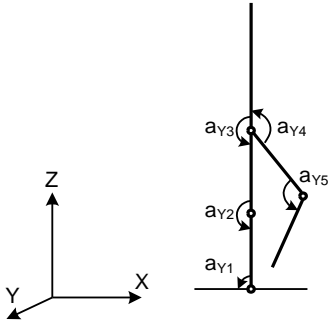
This section provides an example of finding a ballistic trajectory for the mechanical 14 DOF anthropomorphic robot models using a method of gradually increasing number of degrees of freedom in the model of robot. All studies were made with the help of software package Matlab SimMechanics [52] and based on ideas about the works of ballistic motion under A.M. Formalskiy [21].

The starting point for building a complex multi-body mechanical model of the biped mechanism is a simple model of the planar five link robot. An initial mechanical structure is a five body mechanism with two legs with the knee joint and the torso. For such system the first and the last configuration are chosen, such as on the Fig. 1, and the initial angular velocities are selected equal to zero.

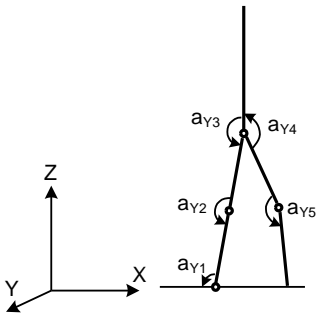
As a result, the system comes to a symmetrical solution. Symmetrical solution is not desired, because it is not similar to human walking. For acquisition non symmetrical solution to define the initial velocity of the knee joint swing leg must be much more different from symmetrical solution (1 rad/s replace by 10 rad/s). The result should be a solution to meet the two paired equation of the ballistic motion (s. Step 1)

Below the procedure of obtaining 3D ballistic trajectories [94] is given in simplified form.

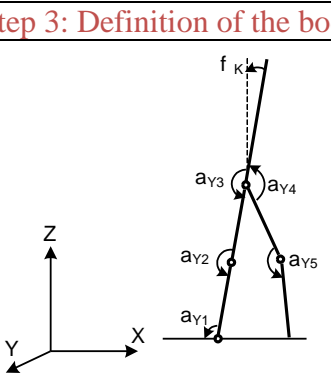
Step 1: Definition of direction and velocity

	5 DOF ZX-Plane	Definition of solution with the right motion of the knee. Optimization of the step height relative to the step length
---	-------------------	---

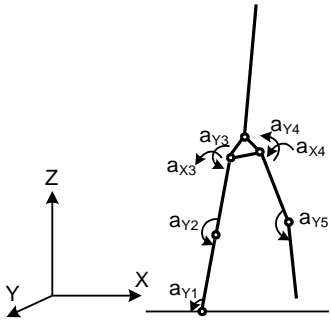
Step 2: Generation of the gait step in 2D

	5 DOF ZX-Plane	Optimization of the step length. Desired length of the step can be obtained using the stepwise increasing of it
--	-------------------	---

Step 3: Definition of the body bending

	5 DOF ZX-Plane	Desired body bending can be obtained using the stepwise increasing of it
---	-------------------	--

Step 4: Modification of the gait step in 3D

	5 DOF +2 DOF X-Axis in pelvis 3D-Step	Generation of the 3D motion using the addition of DOF in the pelvis.
---	---	--

Step 5: Addition of the second DOF in the pelvis		
	<p>7 DOF +2 DOF Z-Axis in pelvis 3D-Step</p>	<p>Adding of the second (vertical) DOF in the pelvis and generation of 3D Step.</p>

Step 6: Addition of the DOF in the body		
	<p>9 DOF +1 DOF Z-Axis in body 3D-Step</p>	<p>Addition of the DOF in the body for the potential compensation of the rotatory moment.</p>

Step 7: Addition of the two shoulder joints		
	<p>10 DOF +4 DOF XY-Axis in hands 3D-Step</p>	<p>Adding two arms and generation of the 3D step.</p>

Having done all the steps enumerated above it is possible to obtain 3D ballistic motion of the anthropomorphic mechanism with 14 DOF (s. Fig. 5.10). The parameters of the mathematical model of the mechanism correspond to the parameters of the robot ROTTO. The parameters of the mechanism are in the appendixes [94].

From the sequence of motion configurations of 3D ballistic robot motion (s. Fig. 5.10) it is seen that in the process of a step the robot oscillates his pelvis with respect to the vertical and at the shoulders also performs oscillations with respect to the vertical, but in the opposite direction. Such type of locomotion is similar to human walking.

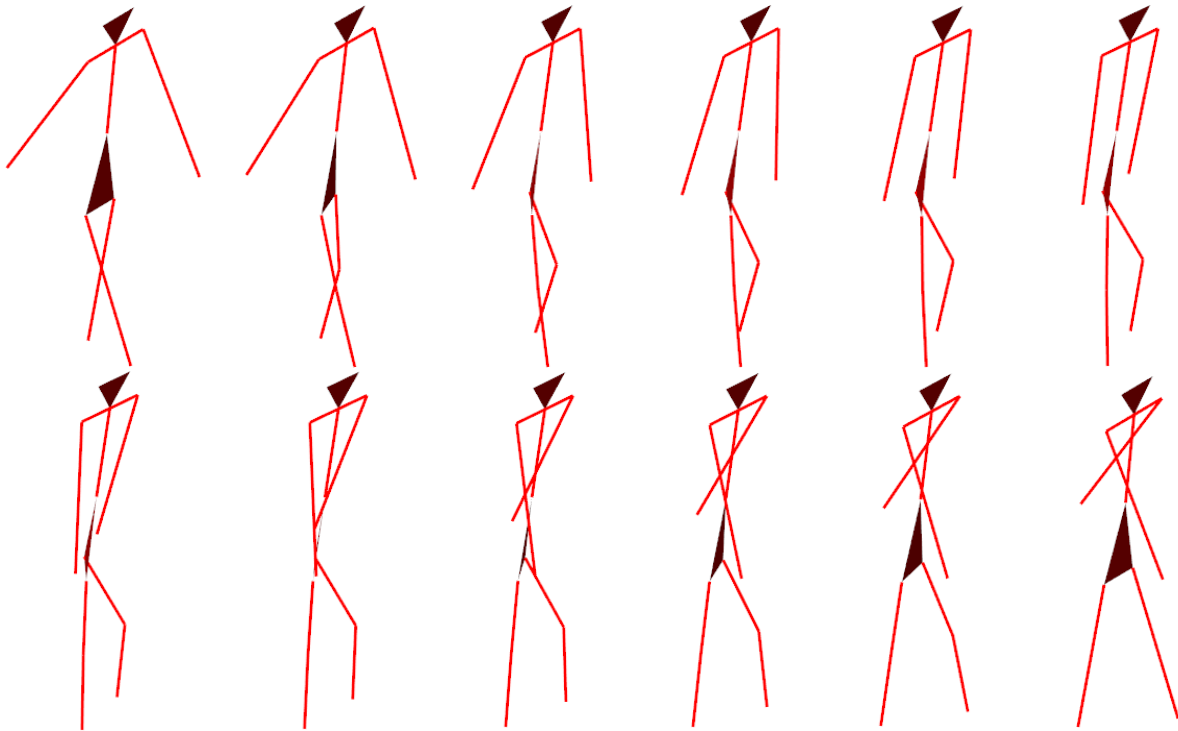


Figure 5.10 – Synthesis of the 3D step

From Figure 5.11 can be seen that while making a step the projection CoM of the whole mechanism on the supporting surface is not under the foot during the single-support phase. Thus, according to the definition given in the first chapter it is possible to consider this type of walking as dynamic one.

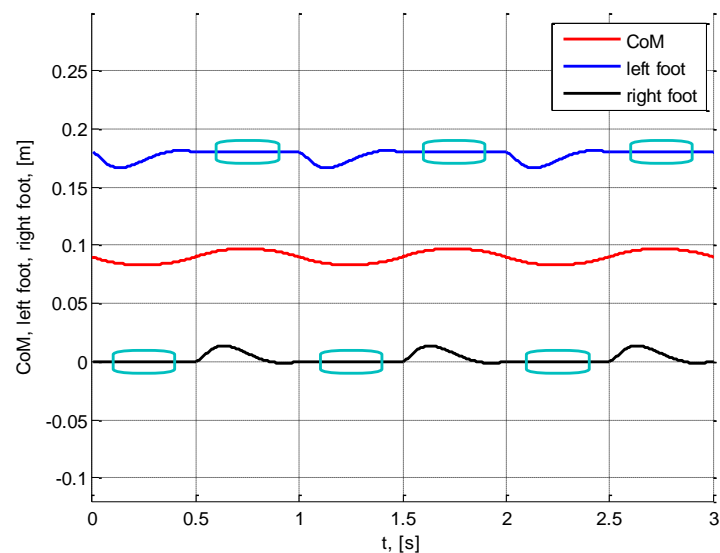


Figure 5.11 – Motion projection COM

It is necessary to point out that the obtained 3D ballistic motion is similar to the human step. It can be explained by the fact that the ballistic motion is free, that there are no control moments in the mechanism joints during movement. Free movement is apparently characteristic for human walking

5.2.3. Ballistic Motion of Two Link Model

This chapter has the materials from the article published in [84]

Obtaining of virtual constraints [78] for linked leg movements (interlink angle and the angle of the support leg against surface) is based on the ballistic method to construct free motion of a mechanism without friction in joints. The mathematical model of a 2D two-mass mechanism (s. Fig. 5.12 a) is considered. It can be described using the Lagrange equations of 2nd order. Its linearized model is:

$$\begin{aligned} [b_1 + 2b_2(a_2 + cg_{2y})]\ddot{\varphi} + [b_3 + b_2(a_2 + cg_{2y})]\ddot{\alpha} - \\ - m_2 g((a_2 + cg_{2y})(\varphi + \alpha) + a_1 \varphi) - m_1 g(a_1 + cg_{1y})\varphi = 0 \\ [b_3 + b_2(a_2 + cg_{2y})]\ddot{\varphi} + b_3 \ddot{\alpha} - m_2 g(a_2 + cg_{2y})(\varphi + \alpha) = 0 \end{aligned} \quad (4.9)$$

where a_1 and a_2 - lengths of links, m_1 and m_2 - masses of links, I_1 and I_2 - moments of inertia of links about the centers of mass. Centers of mass of links OB and BD are located at the distances cg_{1y} , cg_{2y} from the points B and D , $b_2 = m_2 a_1$, $b_3 = I_2 + m_2(a_2 + cg_{2y})^2$, $b_1 = I_1 + I_2 + m_1(a_1 + cg_{1y})^2 + m_2((a_2 + cg_{2y})^2 + a_1^2)$.

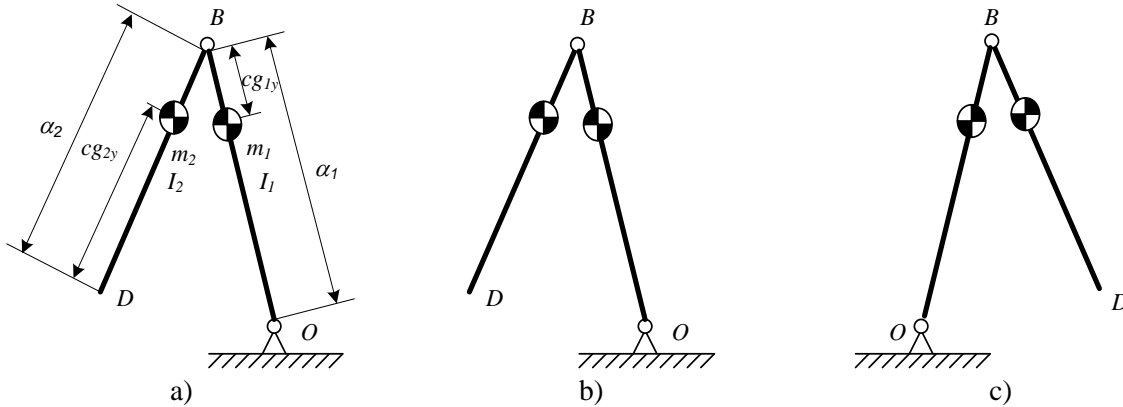


Figure 5.12 – Two-mass mechanism, its initial and final position

Equation (4.9) can be transformed into matrix form:

$$B\ddot{z} + Az = 0 \quad (4.10)$$

An analytical solution of the system of differential equations can be obtained using the transition matrix R to convert equations to a normal form, by the method proposed in [24]

$$\ddot{x}_1 + w_1^2 x_1 = 0, \quad \ddot{x}_2 - w_2^2 x_2 = 0. \quad (4.11)$$

where w_i^2 - the roots of (4.10). Analytical solution of the equations (4.11) is:

$$\begin{aligned} x_1 &= [x_1(T) \sin w_1 t + x_1(0) \sin w_1(T-t)] / \sin w_1 T \\ x_2 &= [x_2(T) \operatorname{sh} w_2 t + x_2(0) \operatorname{sh} w_2(T-t)] / \operatorname{sh} w_2 T \end{aligned} \quad (4.12)$$

Here $x(0) = R^{-1}[\varphi(0) \quad a(0)]^T$ and $x(T) = R^{-1}[\varphi(T) \quad a(T)]^T$ - vectors of initial and final conditions for system (4.11). The boundary value problem for the unknown velocities $\dot{\varphi}(0)$, $\dot{\varphi}(T)$ and

step time T is to solve using equations (4.12). The boundary conditions, which are shown on Fig. 5.12 b) (initial position) and Fig. 5.12 c) (final one), can be presented as:

$$\begin{aligned} x(0) &= R^{-1}[\varphi(0) \quad a(0)]^T, & \dot{x}(0) &= R^{-1}[\dot{\varphi}(0) \quad \dot{a}(0)]^T, \\ x(T) &= R^{-1}[\varphi(T) \quad a(T)]^T, & \dot{x}(T) &= R^{-1}[\dot{\varphi}(T) \quad \dot{a}(T)]^T. \end{aligned} \quad (4.13)$$

The obtained trajectories should be realizable. The velocity in the interlink joint must be equal to zero up to the impact moment in order to “freeze” the mechanism. Blocking of joint B (s. Fig. 2) during the impact is important for entering and leaving the contact at a given configuration. According to [24] for the symmetric boundary value problem boundary conditions are:

$$\begin{aligned} x(0) &= R^{-1}[\varphi(0) \quad a(0)]^T, & \dot{x}(0) &= R^{-1}[\dot{\varphi}(0) \quad 0]^T, \\ x(T) &= R^{-1}[-\varphi(0) \quad -a(0)]^T, & \dot{x}(T) &= R^{-1}[\dot{\varphi}(0) \quad 0]^T. \end{aligned} \quad (4.14)$$

The resulting equations $\alpha = f(\varphi)$, and the total energy as function of the step length are shown in Figure 5.13.

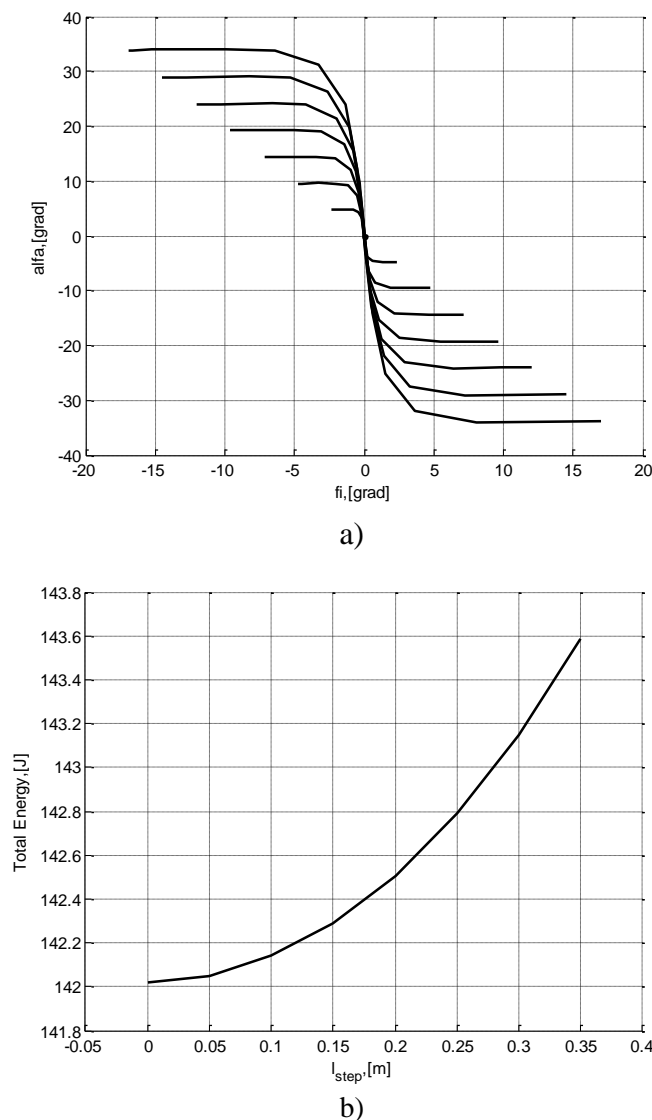


Figure 5.13 – Resulting equations and the total energy as function of the step length

It should be noted that the obtained solutions for this task have the following properties: for every step length, the time of the step is constant, the dependence of $\alpha = f(\varphi)$ is scalable (s. Fig.5.13 a), depending on step length. At the same time to maintain a constant step time, system must have more initial energy for longer steps, as it can be seen in Fig.5.13 b).

5.3. Walking control in sagittal plane

This chapter has the materials from the article published in [84]

To solve the walking control problem a 5-mass mechanism with attached ground reaction is considered (s. Fig. 5.14 a)).

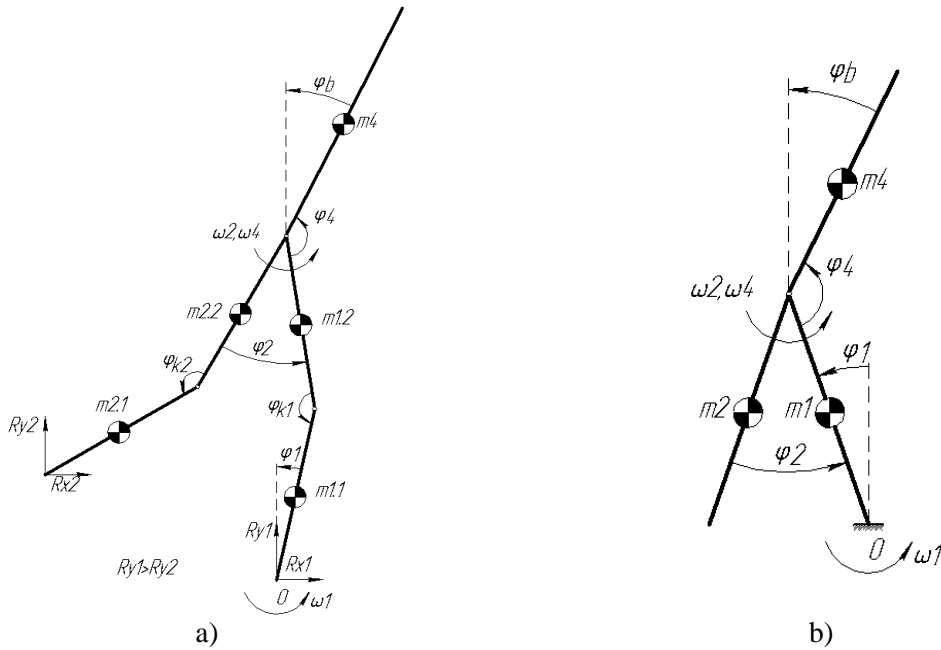


Figure 5.14- Anthropomorphic mechanism, the sagittal plane.

Angles are denoted as φ_1 – angle of support leg respect to the vertical, φ_2 – interlink angle, φ_4 – body position respect to support leg, φ_b – angle of the body respect to vertical, φ_{k1} – angle of the knee joint of support leg, φ_{k2} – angle of the second knee joint.

The original mechanical system, which is described as a system of first order non-linear differential equations in matrix form, has the state vector \mathbf{x} and input vector \mathbf{u} :

$$\begin{aligned} \mathbf{x}^T &= [\varphi_1 \ \varphi_2 \ \varphi_4 \ \varphi_{k1} \ \varphi_{k2} \ \omega_1 \ \omega_2 \ \omega_4 \ \omega_{k1} \ \omega_{k2} \ x_0 \ y_0 \ \dot{x}_0 \ \dot{y}_0], \\ \mathbf{u} &= [M_1 \ M_2 \ M_4 \ M_{k1} \ M_{k2} \ R_{x1} \ R_{x2} \ R_{y1} \ R_{y2}] \end{aligned} \quad (4.15)$$

where M_i – torque at the i -th joint; R_{x1}, R_{y1} – forces acting on a body in the fulcrum; R_{x2}, R_{y2} – forces acting on a body at the end of the second leg; x_0, y_0 – global coordinates of the fulcrum O .

Contact processing is implemented according to [34]. Due to the position control loops, realized in all joints except the supporting one, as well as the presence of internal links

in the system, the vectors of inputs and considered states can be rewritten as: $\mathbf{x}^T = [\varphi_1 \varphi_2 \varphi_4 \varphi_{k1} \varphi_{k2} \omega_1 \omega_2 \omega_4 \omega_{k1} \omega_{k2}]$ $\mathbf{u} = [\varphi_{2s} \varphi_{4s} \varphi_{k1s} \varphi_{k2s}]$. The system under control is artificially introduced as feedback system (expression for interlink angle as a function of the support leg supplemented with adjustments related to the function of the knee). Final expressions are

$$\begin{bmatrix} \varphi_{k1s} \\ \varphi_{k2s} \end{bmatrix} = fk(\varphi_2, \omega_1) = \begin{cases} \pi & \\ \pi - \varphi_{k \max}, & \omega_1 \cdot \varphi_2 \leq 0 \\ \pi - \varphi_{k \max} \frac{\varphi_{2 \max} - |\varphi_2|}{\varphi_{2 \max}}, & \omega_1 \cdot \varphi_2 > 0 \end{cases}. \quad (4.16)$$

$$\varphi_{2s} = \begin{cases} f_{sri}(\varphi_1) + \frac{1.1}{2}(\pi - \varphi_{k2s}), & \text{forward} \\ f_{sri}(\varphi_1) + \frac{0.9}{2}(\pi - \varphi_{k2s}), & \text{backward} \end{cases} = f_{sr}(\varphi_1, \text{Direction}, \varphi_{k2s}) \quad (4.17)$$

Where f_{rsi} – virtual constraint for step control. Introducing such feedback, the system is obtained with the following state and input vectors: $\mathbf{x}^T = [\varphi_1 \varphi_2 \varphi_4 \omega_1 \omega_2 \omega_4]$ $\mathbf{u} = [\varphi_{4s}]$.

The system can be reduced to the mechanism presented in Fig. 5.14 b). For this mechanism the total energy is calculated as $H = V + T$, intuitive control is built, that implements the increment (falling) of energy of the system over the period of oscillations (a step) through inclination of the body with respect to the vertical. The setpoint of the angle of the body with respect to the support leg is:

$$\varphi_{4s} = \pi + \frac{\varphi_2}{2} - \Delta\varphi_{4s} \quad (4.18)$$

Such a setpoint means, that for $\Delta\varphi_{4s} = 0$, both legs deviate from the body at the same angle. Symmetric lifting, moving of leg and placing of leg on a surface will cause a symmetric oscillation of the body with respect to the vertical. Setting any other $\Delta\varphi_{4s}$ will lead to asymmetric oscillations of the body, with a forward or backward inclination of the body. Analogously to the method of the energy increment for an one-mass parametric pendulum (the change of the radius vector of the COM [50]), the influence of an increment of the total energy of the oscillation per period on the input $\Delta\varphi_{4s}$ is approximately obtained as:

$$\frac{\partial H}{\partial u} \equiv \Delta\varphi_{4 \max} \text{sign}(\omega_1) \quad (4.19)$$

The angle $\Delta\varphi_{4s}$ is calculated proportionally to the error of the energy, thus avoiding switching mode. This leads to a controller form [26], [22], similar to the method of speed-gradient:

$$\Delta\varphi_{4s} = u = -\gamma(H - H_s) \frac{\partial H}{\partial u} = -\gamma(T + V - H_s) \cdot \Delta\varphi_{4 \max} \text{sign}(\omega_1) \quad (4.20)$$

The resulting block diagram of control system is shown in Figure 5.15

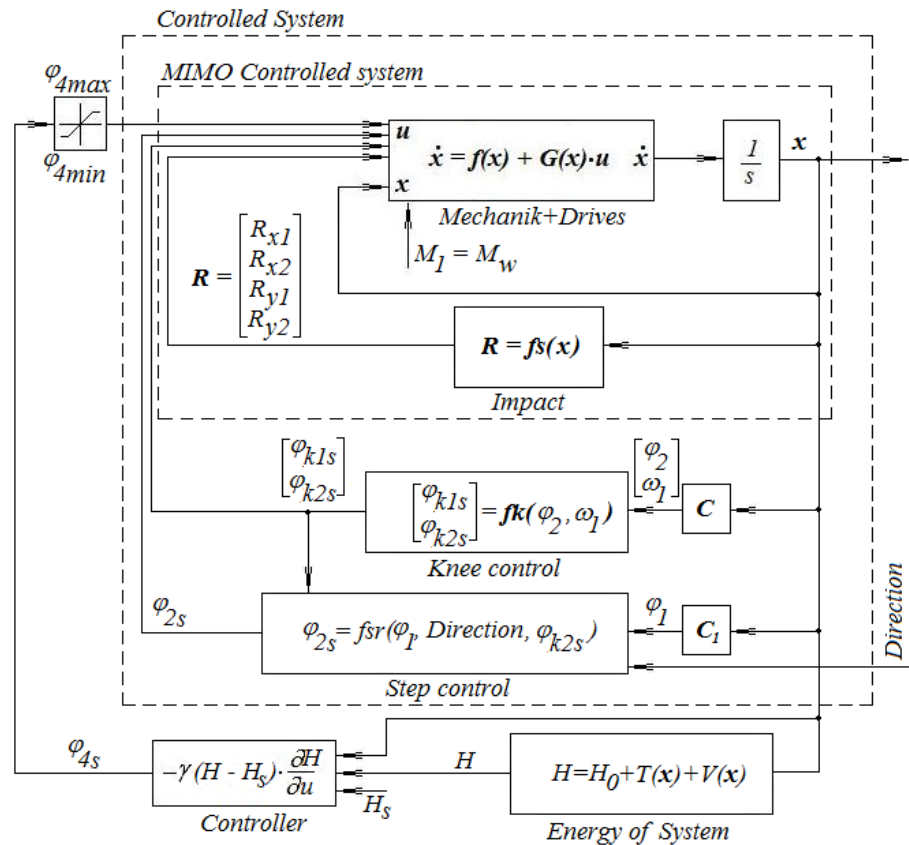


Fig. 5.15 - Resulting block diagram of control system

Simulation Results:

The parameters of mechanism (Fig. 4a) are: masses of links $m_{1,1} = m_{1,2} = m_{2,1} = m_{2,2} = 2.2$ kg, $m_4 = 12$ kg; moments of inertia of links respect to centers of mass $J_{1,1} = J_{1,2} = J_{2,1} = J_{2,2} = 0.02$ kg·m², $J_4 = 0.001$ kg·m²; lengths of links $a_{1,1} = a_{1,2} = a_{2,1} = a_{2,2} = 0.35$ m, $a_4 = 0.5$ m; centers of mass of links CG1, CG2 and CG4 are located at a center of link. Simulation results are shown in Fig.5.16 a), phase diagrams in the steady-state behavior are shown in Fig. 5.16 b)

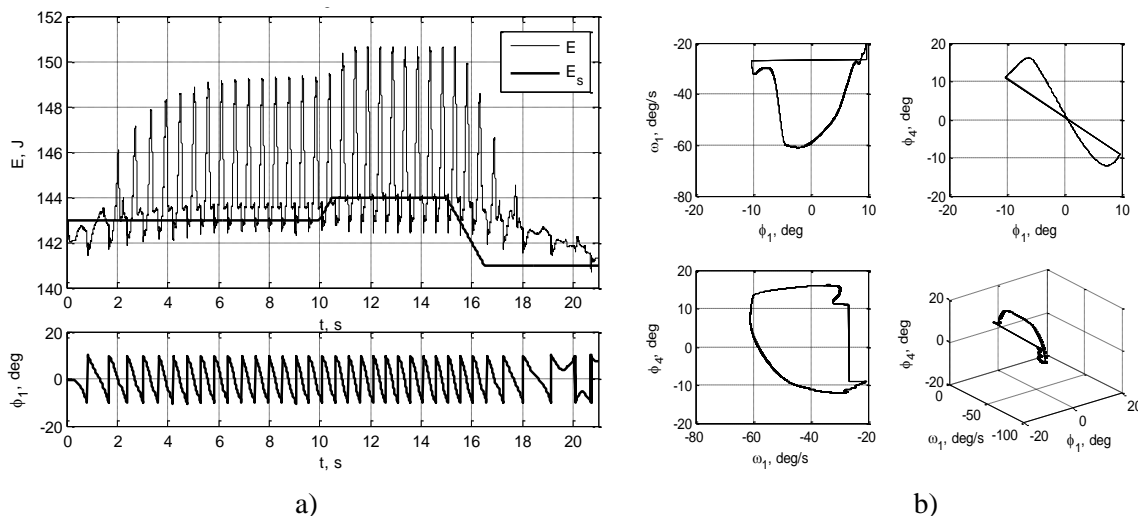


Fig. 5.16 – a) Transients while walking forward, b) phase diagrams in the steady-state behavior 12-15s

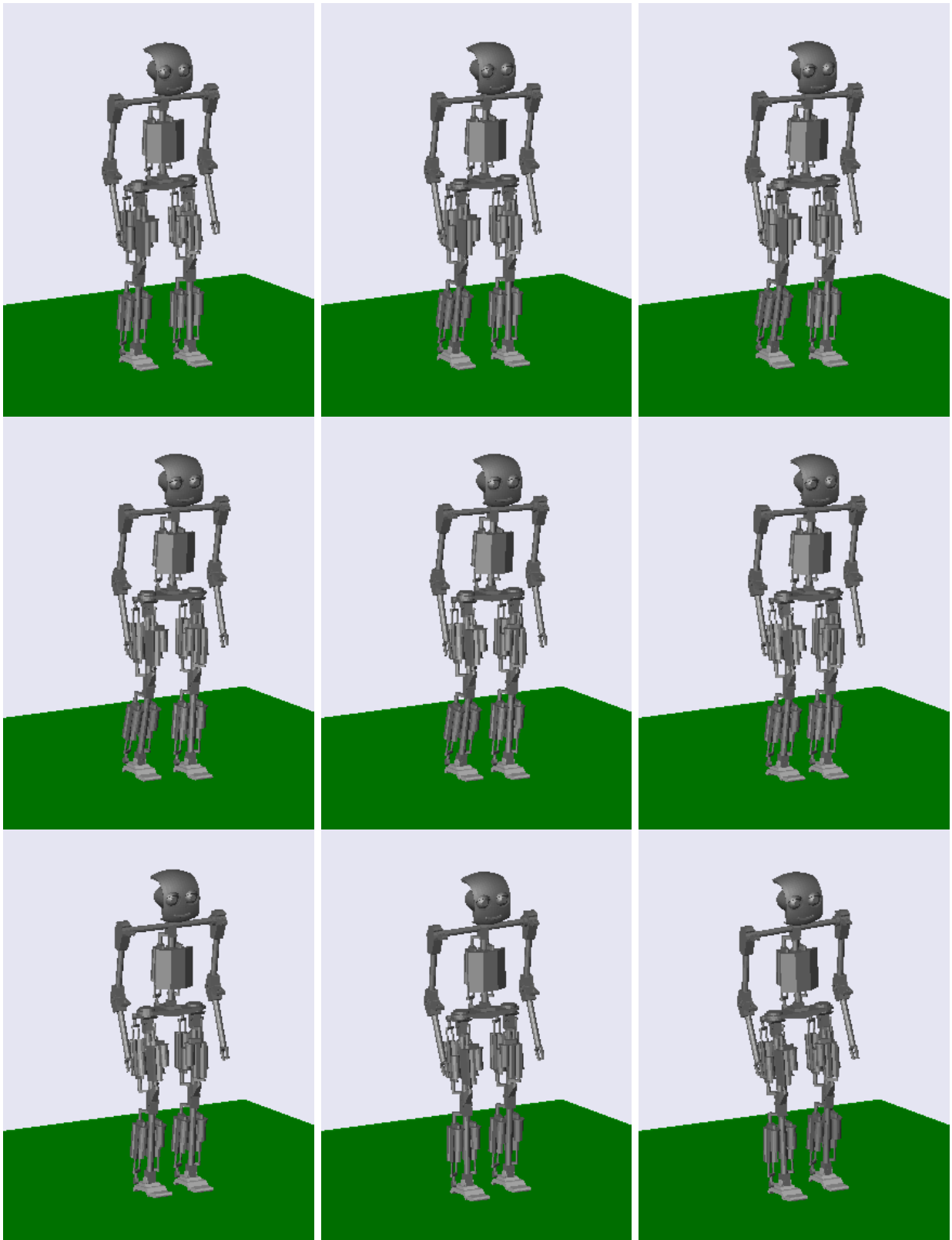


Fig. 5.17 – Simulation of 3D walking

Figure 5.17 represents the motion sequence of 3D walking. From the Figure it is seen that when walking the robot performs oscillations in the frontal plane. The video of simulation can be found here [74]

Plots were obtained by walking forward with constant step length of $\phi_{2\max} = 20^\circ$. Mechanism starts to move from a vertical position slowly gaining energy, coming up to the periodic mode. Step time is 0.54 seconds (1.85 Hz step frequency, by step length of 0.24m velocity is 0.45 m / s = 1.6km / h). System is noticeably faster gaining energy after increase of set point. This can be explained by increase of energy during the period - the mechanism makes more steps over the same time with increasing frequency. After increase of the energy level step time becomes 0.49s (frequency of step is 2.04 Hz, for step length 0.24m velocity is 0.49 m / s = 1.75km / h). When the energy level set point is less than required to perform step, mechanism reduces the speed and at the 19th second starts to make steps on the spot. From the phase trajectory (Fig 6a) can be concluded that the system works in a stable oscillation regime in the period between 12 and 15 sec.

5.4. 3D walking synthesis. Experimental investigations

Experimental investigations of the operation of the control algorithm for dynamic walking were carried out on the robot ROTTO. Some information about the robot parameters, set of sensors, power sensors, communication and control system can be found in the published papers [39], [40], [85], [64].

The control of the robot ROTTO is implemented with the application of Matlab xPC-Target technology (s. Fig. 5.18). On the basis of xPC-Target by means of the industrial communication network several robot drives are connected to the master computer. The drives implement the given moments in the joints or monitor the given trajectories.

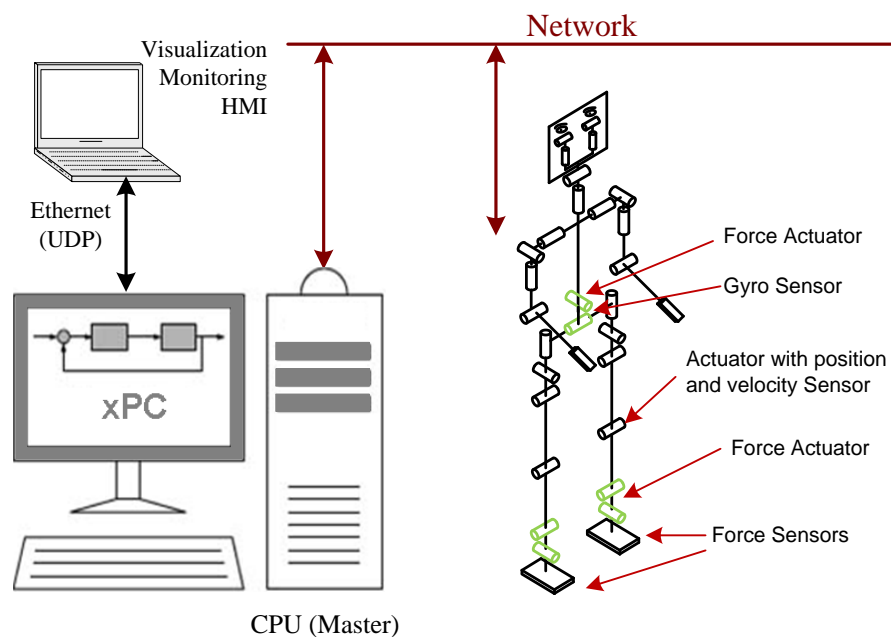


Figure 5.18 – The experimental assembly

Position sensor and an angular velocity sensor are in each joint of the robot. 3-axis gyroscope and 3-axis accelerometer are placed in the pelvis, 6-component force sensor is in the robot feet (s. Fig. 5.18).

5.4.1. Swinging in frontal plane

This section of the work deals with the experimental investigations of the robot swinging in frontal plane. The control algorithm with the help of which the oscillations were obtained is described in Chapter 4.

Figure 5.19 shows the plots of the given (red), current (blue) и average (black) values of the full mechanism energy. From the plot it is clearly seen that at the moment of impact the sharp decrease of the full mechanism energy is observed. Having made approximately two oscillations the mechanism reaches the given value.

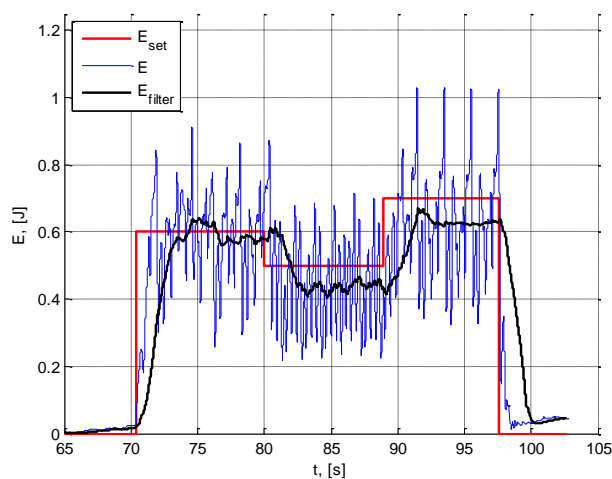


Figure 5.19 – Energy oscillations with the different desired levels

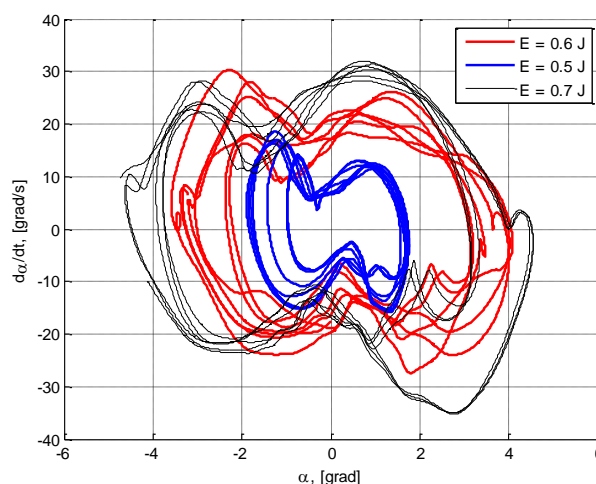


Figure 5.20 – Phase portraits

Figure 5.20 shows the phase portraits in the plane at different values of the given energy and the angle of deflection of the support leg from the vertical. From the plots it is seen that the large amplitude of oscillations correspond to the high level of energy. The experiments show that the periodic cycle is stable.

Figure 5.21 shows the sequence of configurations of on robot in frontal plane. The robot oscillations in frontal plane were registered with the help of the video camera. It is possible to watch the video films on the site RobotsLab [74].

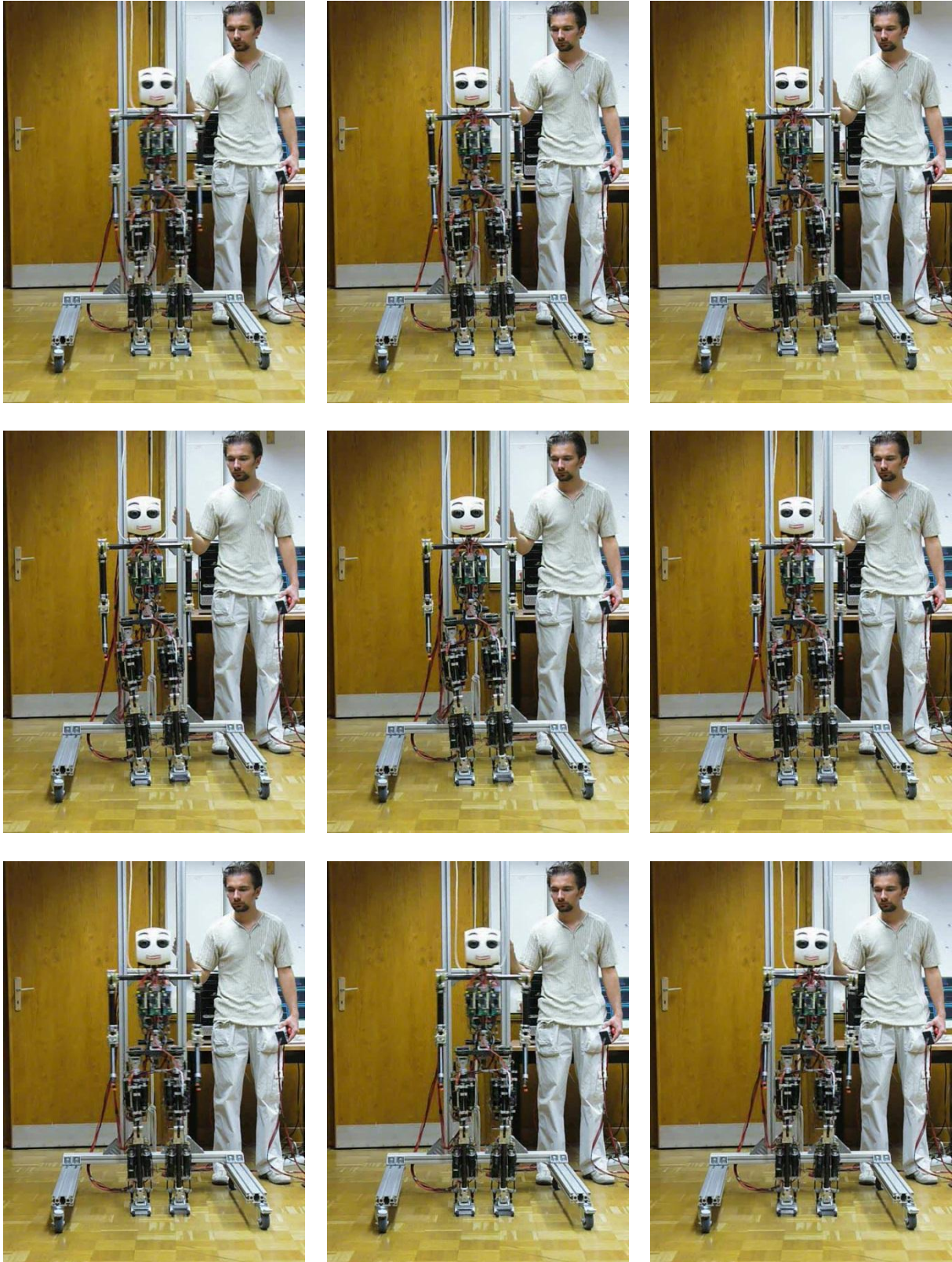


Figure 5.21 – Robot motion sequence with oscillation control in frontal plane

5.4.2. 3D Walking on the horizontal surface

This section of the work deals with the experimental investigations of 3D robot walking on the flat surface by swinging in frontal plane and with the help of the algorithm of the energy maintenance in sagittal plane (s. section 5.3 of the given paper) .

The main idea of the algorithm of 3D walking development is the synchronization of oscillations in sagittal and frontal planes. The frontal plane is the main and determining one. The value of the interlink angle in the sagittal plane $\alpha_{sagittal} = f(\varphi_{frontal}, \varphi_{Sagittal}, \dot{\varphi}_{Sagittal})$ is the function of the value of the current deflection from the vertical of the supporting leg (4.12) in the sagittal plane $\varphi_{sagittal}$ and the current position of the robot in the frontal plane $[\varphi_{frontal}, \dot{\varphi}_{frontal}]$. This function is used as the program trajectory and it is calculated as

$$\alpha_{sagittal} = r \cdot f(\varphi_{sagittal}) \quad (4.21)$$

Here r is the coefficient which is proportional to the current energy of oscillations in the frontal plane and it is calculated using the formula

$$r = k_1 \varphi_{frontal}^2 + k_2 \dot{\varphi}_{frontal}^2 \quad (4.22)$$

The coefficients k_1 and k_2 are tuned experimentally in such a way that in the walking steady-state the value r is constant. In case of big disturbances acting on the robot the value r is filtered with the low-frequency filter with the time constant corresponding to the time of step.

Figure 5.22 shows the motion sequence of one step of the robot. The length step is 9 cm. From the Figure it is seen that the robot is moving its leg during the deviation in the frontal plane. At that the moving leg rises by 3 cm over the surface. The leg bends in the knee by 7 grad. The supporting leg deflection from the vertical by 3 grad. The maximum forward walking velocity of the robot which was reached during the experiments was 0,5 km/h. The robot walking was registered with the help of the video camera. It is possible to watch the video films on the site RobotsLab [74].

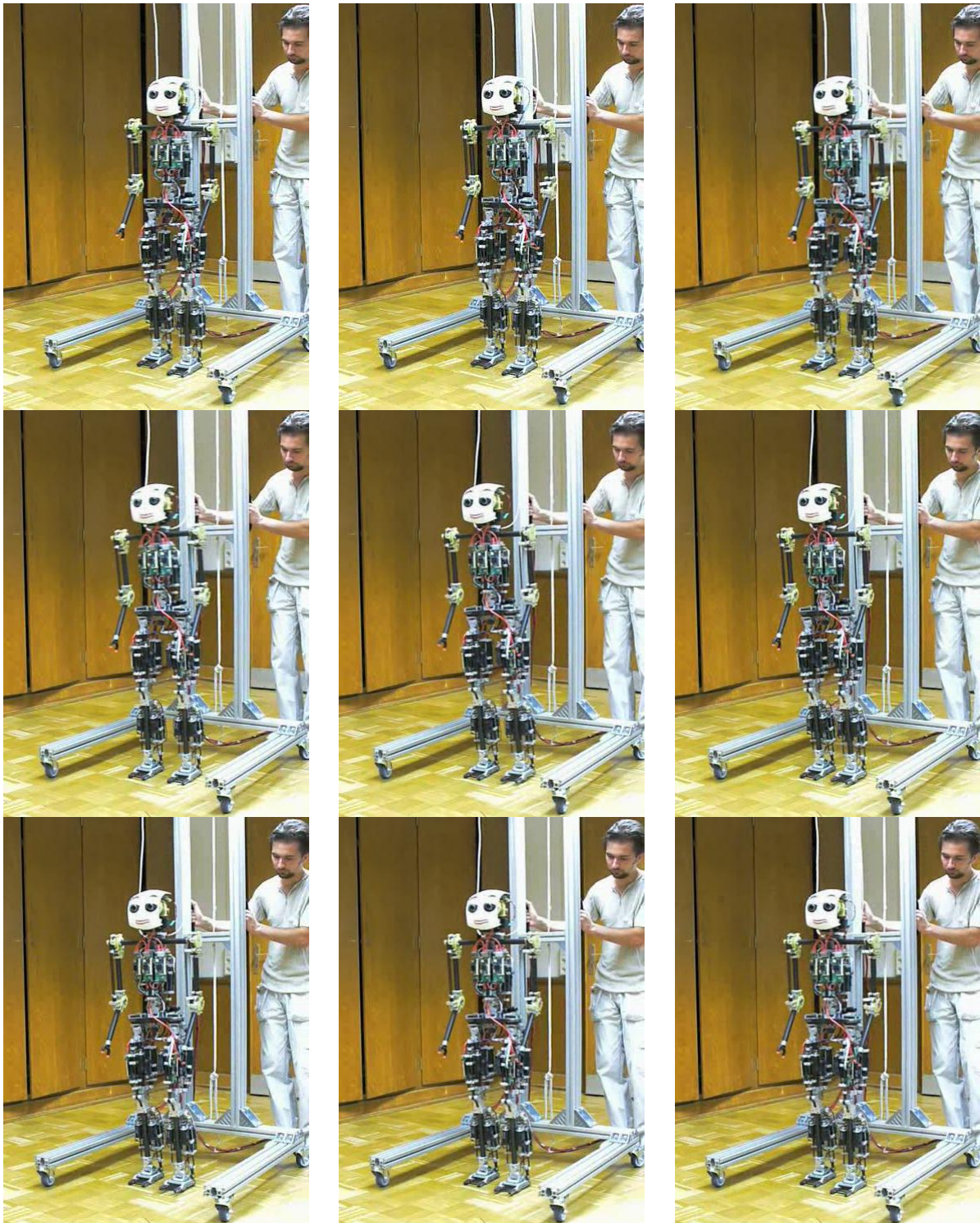


Fig. 5.22 – sequence of configurations 3D walking of the robot when maintaining oscillation energy

Figure 5.23 represents the plots of the total given (red), current (blue) and average (black) energy of the robot. Figure 5.23 shows the phase portrait of the oscillation in the frontal plane. Figure 5.23 shows the plot of robot forward velocity changes in the sagittal plane. Figure 5.26 represents the plot of the interlink angle (between the hips) changes in the sagittal plane. Figure 5.27 shows the plot of the support reaction changes.

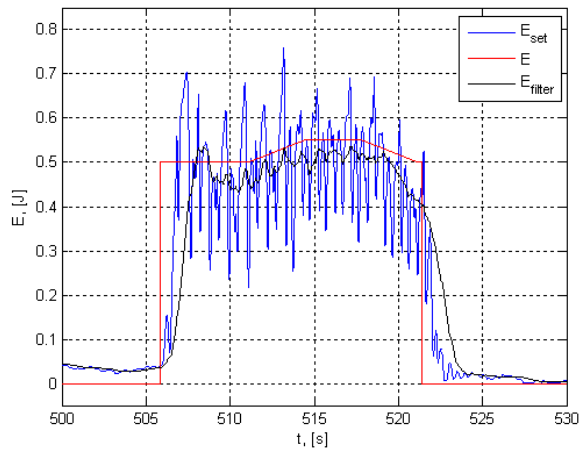


Fig. 5.23 – Robot total energy

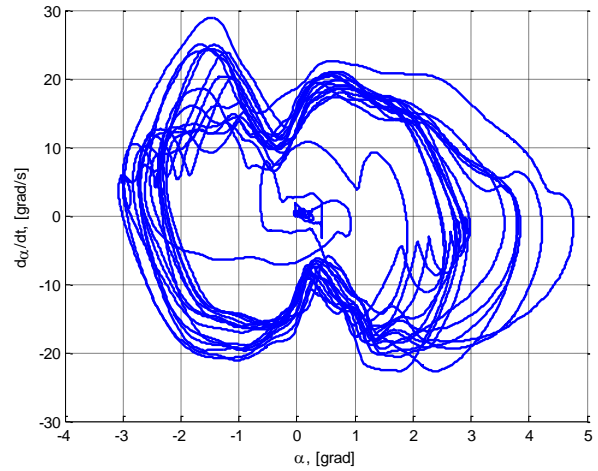


Fig. 5.24 – Phase portrait of the oscillation in the frontal plane

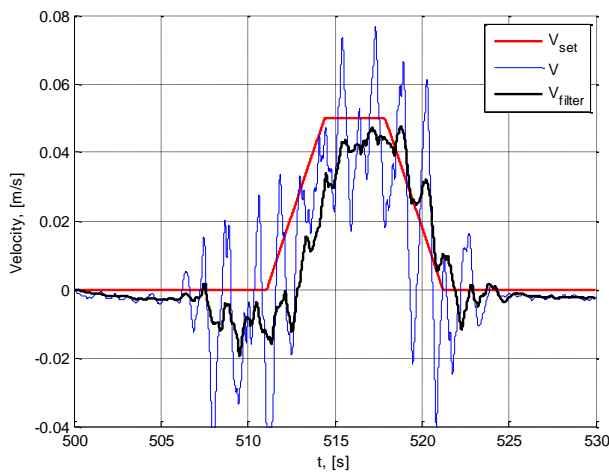


Fig. 5.25 – Robot forward velocity in the sagittal plane

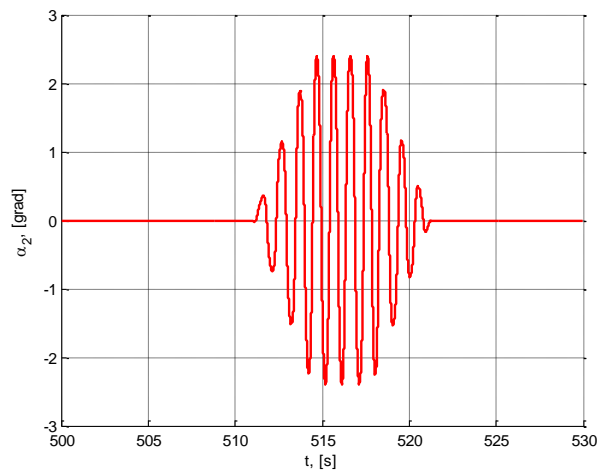


Fig. 5.26 – The value of the interlink angle in the sagittal plane

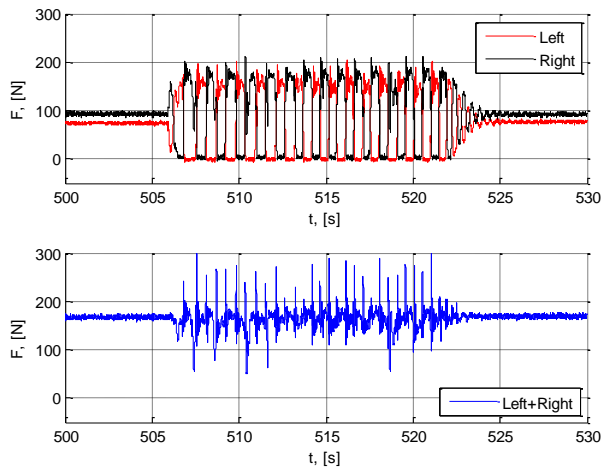


Fig. 5.27 – Vertical components of the support reactions.

From the plots represented here it is seen that the robot oscillates periodically in the frontal plane. The system of oscillation energy maintenance compensates the energy losses which occur during the impact of the moving leg against the support surface. If the given value of the total energy and the coefficient r increase smoothly, the robot increases smoothly its forward velocity in the sagittal plane.

This chapter deals with the simulation of the control algorithm by maintaining movement (oscillations) of the five-link mechanism. Simulation and the experiments showed that for the mechanical system under study it is possible to develop the periodic mode when there is impact interaction with the support surface. Simulation and the experiments show that the control system brings the mechanism to the stable periodic mode of oscillations in the frontal plane and maintains stable dynamic 3D walking.

Conclusion

The consideration of the problem of dynamic walking design from the point of view of the periodic movement development allowed us to look differently at the problem of step cycle formation, balance maintenance, external disturbances compensation. This also allowed us to concentrate on maintenance of the system orbital stability and, as a consequence, of periodic walking design.

At first the work deals with the comparatively simple control object, that is the variable length pendulum. The control type was developed at which the amplitude of the pendulum oscillations increases. Then the control law was designed at which the amplitude of the pendulum oscillations decreases. Combining these control laws we managed to develop the control law at which the given amplitude of oscillations is maintained. In this control law the feedback from the deviation of the current energy value from the given value was used.

Then we considered oscillations of the double pendulum which is more complex mechanism than a simple variable length pendulum. During the control design two methods were used. Using each of them we managed to develop a stable periodic mode of double pendulum oscillations. Simulation and experiments showed the efficiency of the developed control algorithms.

The following stage of work was the design of the control algorithm by maintaining the periodic movement (oscillations) of the two-link mechanism, namely, a model of the biped walking robot in the frontal plane. Simulations and experiments showed that for this underactuated mechanical system it was possible to design the periodic modes when there is impact interaction with support surface. When analyzing the control system operation by simulations and the experiments it turned out that the surface properties influence the properties of transients and the character of steady-state periodic mode. The developed algorithms to control the periodic motion of a two-legged mechanism in the frontal plane allowed us to pass on to the synthesis of biped robot movement in the sagittal plane.

In the concluding part of the work we developed the methods of design the ballistic trajectories for relatively simple, planar models, as well as for multilink 3D models of an anthropomorphic robot. On the basis of these methods the trajectories of the movement of the biped in the sagittal plane were obtained. In the work we carried out the simulation of the control system operation by maintaining the periodic movement (oscillations) of a five-link mechanism. Basing on the conception of the synchronization of the motions in the frontal and sagittal planes the simple algorithm of design of 3D walking of the biped robot ROTTO was developed. Simulations and experiments showed that the control system brings the mechanism to the stable periodic mode and maintains the stable dynamic 3D walking.

The further direction in the development of the ideas of this thesis may be the improvement of the algorithm to control walking on the basis of the principle of the energy

maintenance. This approach may enable to decrease the load on the control system by maintaining the oscillations and to decouple the motions in the sagittal and frontal planes.

Zusammenfassung

Die Synthese des dynamischen Gehens eines anthropomorphen Roboters auf der Basis von periodischen Bewegungen bietet neue Möglichkeiten für die Entwicklung von Schrittzyklen, die Gleichgewichtserhaltung und Kompensation von Störeinflüssen für das zweibeinige Gehen. Dieses Verfahren garantiert orbitale Stabilität und lässt sich auf das dynamische Gehen übertragen.

In dieser Arbeit wurde zuerst ein Pendel mit variabler Länge als ein vereinfachtes System betrachtet. Zu Beginn wurde ein System untersucht, bei dem die Schwingungsamplitude zunimmt. Anschließend erfolgte die Betrachtung eines Systems mit abnehmender Schwingungsamplitude. Durch Kombination beider Algorithmen wurde ein Regelungssystem entworfen, bei dem die Schwingungsamplitude gleich bleibt. Hierbei wird die Gesamtenergie des Systems auf einem konstanten Niveau gehalten.

Es wurde ein Zwei-Massen-Pendel, das eine komplexere Struktur darstellt, betrachtet. Für dieses System wurden zwei Regelungssysteme nach unterschiedlichen Verfahren entworfen. Beide Regelungssysteme garantieren die Einhaltung von stabilen Schwingungen des Zwei-Massen-Pendels bei unterschiedlichen Störereinflüssen. Die Funktionsfähigkeit dieser Methoden wurde durch numerische Untersuchungen und Experimente nachgewiesen.

Die nachfolgenden Betrachtungen behandeln die Entwicklung eines Regelungssystems für die periodischen Bewegungen (Schwingungen) eines vereinfachten Modells des zweibeinigen Roboters. Dieses Modell bestand aus zwei Gelenken und beschränkte sich auf die frontale Bewegung des Laufroboters. Numerische und experimentelle Untersuchungen haben die Stabilität der Regelungssysteme bei sprunghaftigen Störereinflüssen (Kontakt des Fußes mit unterschiedlichem Untergrund beim Auftreten) nachgewiesen. Es wurde gezeigt, dass Oberflächeneigenschaften des Untergrunds Einfluss auf die Übergangsprozesse und auf die Art des stationären periodischen Betriebs haben.

Im letzten Kapitel der Arbeit wurde die Entwicklung einer Methode zum Entwurf von ballistischen Trajektorien sowohl für das vereinfachte 2D als auch für das mehrgliedrige 3D-Modell des anthropomorphen Roboters betrachtet. Mit Hilfe der entwickelten Methoden wurden die Bewegungstrajektorien für Beine und Körper in der Sagittalebene bestimmt. Hierfür wurden numerische Untersuchungen des Regelungssystems für die periodischen Bewegungen (Schwingungen) des 5 DOF Systems in der sagittalen Ebene durchgeführt. Auf der Basis des Konzept der Synchronisierung der Bewegungstrajektorien in der frontalen und sagittalen Ebene wurden einfache Algorithmen für die Synthese des dynamischen Gehens des Roboters ROTTO entwickelt. Die Phasendiagramme der Regelgrößen stellen Grenzyklen (limit cycles) dar und weisen die Effizienz der entwickelten Algorithmen nach.

Zukünftige Arbeiten sollten sich auf die Erweiterung und Weiterentwicklung von Algorithmen des dynamischen Gehens auf der Basis der Schwingungsregelung konzentrieren. Die vorgeschlagenen Konzepte sind in der Lage, das Steuerungssystem zu entlasten und die Bewegungen in der sagittalen und frontalen Ebene zu entkoppeln.

References

- [1] **Aldebaran Robotics** Robot NAO <http://www.aldebaran-robotics.com>.
- [2] **Aoustin Y. and Formal'skii A. M.** On optimal swinging of the biped arms. Intelligent Robots and Systems. Piscatawy, N.J, IROS 2008.
- [3] **Aoustin Y., Formal'sky A.M., Lavrovsky E.** Ballistic run of an anthropomorphic biped CLAWAR. pp. 399-406 2002
- [4] **Appel P.E.** Teoreticheskaya Mechanica. Tom 1,2. (Rus.) Moskow: Fizmatlit, 1960.
- [5] **Bogdanov V.A., Gurfinkel V.S.** Biomehanika lokomocij cheloveka. Fiziologija dvizhenija. (Rus.) L., 1976.
- [6] **Boston Dynamics** Robot PETHMAN. http://www.bostondynamics.com/robot_petman.html.
- [7] **Butkovskiy A. G.** Phase Portrait of Control Dynamical Systems. Kluwer 1991.
- [8] **Chandana P.** Morphology and Computation. Proceedings of the International Conference on the Simulation of Adaptive Behaviour. 2004.
- [9] **Chernyy G.** Walking Robots. Kvant. Vol. 3. Moskow 2009.
- [10] **Chevallereau C., Abba G., Aoustin Y., Plestan F., Westervelt E., Canudas-de-Wit C., Grizzle J.** RABBIT: A testbed for advanced control theory. IEEE Control Systems Magazine. 2003. Vol. 23, no. 5, pp. 57–79.
- [11] **Collins S. H., Wisse M., Ruina A., Tedrake R.** Efficient bipedal robots based on passive-dynamic Walkers Science Magazine, 2005. Vol. 307, pp. 1082-1085.
- [12] **Collins S. H., Wisse M. and Ruina A.** A 3-D Passive Dynamic Walking Robot with Two Legs and Knees. International Journal of Robotics Research, 2001. Vol. 20, pp. 607–615.
- [13] **Cornell robots** Passive Walker. - <http://ruina.tam.cornell.edu/research/topics/robots/index.php>.
- [14] **D.V. Efimov** Robust and adaptive control of nonlinear oscillatons (Rus.) St. Petersburg : Nauka, 2005.
- [15] **Dassault Systemes AB, Lund, Sweden** Dymola. - <http://www.3ds.com/products/catia/portfolio/dymola>.
- [16] **Delft Biorobotics** Delft Biorobotics Laboratory. <http://home.tudelft.nl/en/>.
- [17] **Dzhantimirov S., Palis F., Schmucker U., Telesh A., Zavgorodniy Y.** HIL/SIL by development of six-legged robot SLAIR2. Advances in climbing and walking robots, 2007. Singapore [u.a.]: World Scientific, pp. 652-661.

- [18] **Erbatur K., Koca Ö, Taşkıran E, Yılmaz M., Seven U.** ZMP Based Reference Generation for Biped Walking Robots. World Academy of Science, Engineering and Technology 58. 2009.
- [19] **Featherstone. R.** Rigid Body Dynamics Algorithms. New York: Springer, 2008.
- [20] **Formal'skii A. M** Motion of anthropomorphic mechanism via impulsive control. (Rus.) Moscow: Institute of Mechanics Lomonosov Moscow State Univ Rep. No. 1731 ,Part I, pp. 56, 1975.
- [21] **Formal'skii A. M.** Ballistic Walking Design via Impulsive Control. Journal of aerospace engineering, 2010.
- [22] **Formal'skii A.M.** Global Stabilization of a Double Inverted Pendulum with Control at the Hinge between the Links, Mechanics of Solids, 2008. Vol. 43, No. 5, pp. 687–697.
- [23] **Formal'sky A.M.** Ballistic Locomotion of a Biped. Control of Two Biped Machines Human and Machine Locomotion, pp. 191-230. Wien, New York: Springer, 1997.
- [24] **Formal'sky A.M.** Peremeshenie antropomorfnyh mehanismov. (Rus.) Moskow: Nauka, 1982.
- [25] **Formalskii A.M.** Controllability and Stability of Systems with Restricted Control Resources. (Rus.) Moscow: Nauka, 1974.
- [26] **Formalskii A.M.** On the Design of Optimal Feedback Control for Systems of Second Order . Applied Mathematics , 2010. - Vol. 1, pp. 301-306.
- [27] **Fradkov A.L.** Cybernetical Physics: From Control of Chaos to Quantum Control . Heidelberg-New York : Springer, 2007.
- [28] **Gaßmann B., Scholl, K.-U., Berns, K.** Behavior Control of LAURON III for Walking in Unstructured Terrain CLAWAR, 2001. Karlsruhe, Germany.
- [29] **Goswami A.** Postural Stability of Biped Robots and the Foot-Rotation Indicator (FRI) Point. The International Journal of Robotics Research. 1999. Vol. 18, No. 6, 523-533.
- [30] **Goodwin G. C., Graebe S.F., Salgado M. E.** Control System Design : P.ce H.11, 2000.
- [31] **Grischin A.A., Formalsky A.M., Lensky A.V., Zhitomirsky S.V.** Dynamic Walking of a Vehicle With Two Telescopic Legs Controlled by Two Drive International Journal of Robotic Research. 994. Vol. 13, No. 2.
- [32] **Hirai K., Hirose, M., Haikawa, Y., Takenaka, T.** The Development of Honda Humanoid Robot. Conference on Robotics and Automation, 1998.
- [33] **Honda Corp.** Robot ASIMO. <http://asimo.honda.com>.
- [34] **Juhasz T., Konyev M., Rusin V., Schmucker U.** Contact processing in the simulation of CLAWAR Advances in climbing and walking robots . 2007. Singapore [u.a.] : World Scientific, pp. 583-590.
- [35] **Kajita S., Morisawa M., Harada K., Kaneko K., Kanehiro F., Fujiwara K. Hirukawa H.** Biped Walking Pattern Generator allowing Auxiliary

- ZMP Control International Conference on Intelligent Robots and Systems, 2006.
- [36] **Kajita S., Tani, K.** Experimental study of biped dynamic walking Control Systems Magazine. 1996. Vol.16, Nr.1 pp.13-19.
- [37] **Kameta K., Kanamiya Y.** Walking Control around Singularity Using a Spherical Inverted Pendulum Humanoid Robots, 7th IEEE-RAS International Conference, 2007.
- [38] **Konyev M., Palis F., Zavgorodniy Y., Melnikov A., Rudskiy A., Telesh. A.** "Walking Robot "ANTON": Design, Simulation, Experiments" CLAWAR, 2008.
- [39] **Konyev M., Palis F., Zavgorodniy Y., Melnykov A., Rudskyy A., Telesh A., Schmucker U.** Low-level control system of a new biped robot "ROTTO" Mobile robotics, 2010. New Jersey: World Scientific, pp.559-566.
- [40] **Konyev M., Palis F., Zavgorodniy Y., Melnykov A., Rudskyy A., Telesh A., Schmucker U.** Presentation of a view biped robot "ROTTO" Mobile robotics, 2010. New Jersey : World Scientific, pp. 551-558.
- [41] **Korea Advanced Institute of Science and Technology** Robot KHR-3. - <http://www.hubolab.com>.
- [42] **Kuo A.** Choosing your steps carefully: Trade-offs between economy and versatility in dynamic walking bipedal robots IEEE Robotics and Automation Magazine. 2007. Vol. 14, no. 2, pp. 18–29.
- [43] **Kuo A.D, Donelan J.M and Ruina A.** Energetic Consequences of Walking Like an Inverted Pendulum: Step-to-Step Transitions. Exercise and Sport Sciences Reviews, 2005. Vol. 33, Nr. 2 .
- [44] **Leonov G.A., Ponomarenko D.V.** Criterion of orbital stability of the dynamical systems. Moskow: Izvestia Visshih Uchebnihih Sovedenij (rus), 1993.
- [45] **Levenberg K.** A Method for the Solution of Certain Non-Linear Problems in Least Squares. The Quarterly of Applied Mathematics. 1944. Vol.2, pp. 164–168.
- [46] **Linde R. Q.** Actively controlled ballistic walking Proc. IASTED Int. Conf. Robotics & Applications. 2000. pp.135-142.
- [47] **Löffler K., Gienger, M., Pfeiffer F.** Controller Design for a Biped Jogging Robot Proceedings of the 6th IFAC Symposium on Robot Control (SYROCO), 2000.
- [48] **Löffler K., Gienger, M., Pfeiffer F.** Dynamic Control of a Biped Walking Robot Journal of Applied Mathematics and Mechanics, 1999.
- [49] **Lurie A.I.** Analytical Mechanics, Berlin : Springer, 2002.
- [50] **Magnus. K** Schwingungen. Wiesbaden: Vieweg + Teubner, 2008.
- [51] **Massachusetts Institute of Technology** Robot Flamigo. - http://www.ai.mit.edu/projects/leglab/robots/Spring_Flamigo/Spring_Flamigo.html.
- [52] **MathWorks** MATLAB. <http://www.mathworks.com>.

- [53] **McGeer T.** Dynamics and control of bipedal locomotion *Journal of Theoretical Biology*, 1993. Vol.166 (3), pp. 277-314.
- [54] **McGeer T.** Passive bipedal running *Technical Rep. No. CSS-IS TR 89-02*, 1989. Centre for Systems Science.
- [55] **McGeer T.** Passive dynamic walking, *International Journal of Robotics Research*,1990 Vol. 9, No., 2, pp. 62-82.
- [56] **McGeer T.** Passive walking with knees *IEEE Robotics & Automation Conference*, 1990. Cincinnati, OH, pp. 1640-1645.
- [57] **McMahon T. A.** Mechanics of locomotion *International Journal of Robotic Research*, 1984. Vol. 3 (2), pp. 4–28.
- [58] **Melnykov A., Konyev M., Palis F., Schmucker, U., RobotsLab** Linear Elastic Actuator of the Biped Robot “ROTTTO” *Emerging Trends in Mobile Robotics, Proceedings of the 13th International Conference on CLAWAR 2010*. Nagoya Institute of Technology, Japan.
- [59] **Menga G., Ghirardi M., Confermato R., Pegueroles J.** Design of sensorized feet for a kid-sized biped robot *ISAAC Project*. 2011. Politecnico di Torino.
- [60] **Mettin U.** Applications of the Virtual Holonomic Constraints Approach. Analysis of Human Motor Patterns and Passive Walking Gaits *Umeå University: Ph.D Thesis*, 2008.
- [61] **MIT Humanoid Robotics Group**
<http://www.ai.mit.edu/projects/humanoid-robotics-group/>
- [62] **Mochon S.** A mathematical model of human walking, *Lectures on mathematics in life sciences*, Vol. 14, American Mathematical Society, Providence, R.I, 1981 .
- [63] **Nocedal J. and Wright S.** *Numerical Optimization*. 2nd Edition . N.Y.: Springer, 2006.
- [64] **Palis F. Zavgorodniy Y., Konyev M., Telesh A., Melnykov A., Rudskyy A.** Lynejnyj pryvod dlja antropomorfnoho rodota ROTTO (Rus.) *Vestnik Nacional'nogo Technicheskogo Universiteta "ChPI"*. Char'kov , 2008. Vol. 30.
- [65] **Pfeiffer F. and Inoue H.** *Walking: technology and biology: Philos Transact A Math Phys Eng Sci.*, 2007.
- [66] **Pratt J. and Paluska J.** *Bipedal Walking Robots in Biomimetic Robotics [Book]*. - Brezeal, C. and Yoseph Bar-Cohen, Ed., SPIE Press, 2003.
- [67] **Pratt J., Chew C.M., Torres A., Dilworth P., Pratt G.** Virtual Model Control: An Intuitive Approach for Bipedal Locomotion. *International Journal of Robotics Research*, 2001. Vol. 20(2), pp.129-143.
- [68] **Pratt J., Krupp B., Morse C.** Series elastic actuators for high fidelity force control. *Industrial Robot Journal*, 2002. Vol. 29, No. 3, pp. 234-241.
- [69] **Pratt J., Tedrake R.** Velocity-Based Stability Margins for Fast Bipedal Walking, Presented at the First Ruperto Carola Symposium in the International Science Forum of the University of Heidelberg entitled "Fast Motions in Biomechanics and Robots, Heidelberg, 2005.

- [70] **Pratt J.** Virtual Model Control of a Biped Walking Robot Massachusetts: M.Eng. Thesis, Department of Electrical Engineering and Computer Science, Massachusetts Institute of Technology, 1995.
- [71] **Pratt J., Dilworth, P., Pratt, G** Virtual Model Control of a Bipedal Walking Robot. Proceedings of the IEEE International Conference on Robotics and Automations (ICRA '97) . 1997.
- [72] **Pratt J., Pratt, G.** Exploiting Natural Dynamics in the Control of a 3D Bipedal Walking Simulation. Proceedings of the International Conference on Climbing and Walking Robots (CLAWAR). 1999.
- [73] **Raibert M. H.** Legged Robots That Balance . Cambridge: MIT Press, 1986.
- [74] **RobotsLab Team** Robot ROTTO, Anton. 2011.
http://www.ovgu.de/ieat/robotslab/rotto_videos.php.
- [75] **Sardain P. and Bessonnet G.** Forces acting on a biped robot. Center of pressure-zero moment point. Systems, Man and Cybernetics, Part A: Systems and Humans, IEEE Transactions on. Vol. 5 2004
- [76] **Scheint M., Sobotka M., Buss M.** Virtual holonomic constraint approach for planar bipedal walking robots extended to double support Joint 48th IEEE Conference on Decision and Control and 28th Chinese Control Conference Shanghai, P.R. China. 2009.
- [77] **Schilling R.J.** Fundamentals of Robotics: Analysis and Control : Simon & Schuster Trade, 1996.
- [78] **Shiriaev A., Perram J. and Canudas-de Wit C.** Constructive tool for orbital stabilization of underactuated nonlinear systems: Virtual constraints approach IEEE Trans. Automat. Cont. 2005. Vol. 50, no. 8, pp. 1164–1176.
- [79] **Sony Corp.** Robot QRIO. - http://www.aibo-kennel.com/QRIO/QRIO_Main.htm.
- [80] **Stern J.T., Demes B., Kerrigan D.C.** Modeling human walking as an inverted pendulum of varying length Cambridge Studies in Biological and Evolutionary Anthropology. 2004.
- [81] **Sultanov I. A.** Studying the Control Processes Obeying Equations with Underdefinite Parameters Automation and Remote Control. 1980. No. 10, pp. 30-41.
- [82] **Takanishi A., Ishida, M., Yamazaki, Y. and Kato, I.** The realization of dynamic walking by the biped walking robot WL-10RD Proc. of the Int. Conference on Advanced Robotics . 1985. - pp. 459-466.
- [83] **Telesh A., Palis F., Rudskyy A., Melnykov A., Dynn timer T., Konyev M., Schmucker U.** Energy control of periodical oscillations of biped robot in the frontal plane . Field Robots. CLAWAR. 2011.
- [84] **Telesh A., Palis F., Rudskyy A., Melnykov A., Dynn timer T., Konyev M., Schmucker U.** Limit cycles walking of biped robot based on total energy control and virtual constraints. Field Robotics. 2011. Singapore [u.a.] : World Scientific, pp. 579-586.

- [85] **Tsepkovskiy Y., Telesh A.** Adaptyvnyj nejro fazzy reholjator skorosty dlja dvyhatelja postojannoho toka na baze FPGA. (Rus.) Vestnik Nacional'nogo Techniceskogo Universiteta "ChPI". 2008.
- [86] **TU München** Robot Johnnie. <http://www.amm.mw.tum.de>.
- [87] **Tucker V. A.** The energetic cost of moving about American Scientist . - 1975. - Vol. 63 (4), pp. 413–419.
- [88] **Vitenson A.S** Gesetzmäßigkeiten des normalen und pathologischen menschlichen Ganges . Moskow : Zerkalo, 2001.
- [89] **Vukobratović M., Borovac B.** Zero-moment point -Thirty five years of its life International Journal of Humanoid Robotics . 2004. Vol. 1, No. 1, pp. 157-173.
- [90] **Vukobratovic M., Juricic D.** Contribution to the synthesis of biped gait IEEE Trans. Biomedical Eng. 1969. Vol. 16(1).
- [91] **Westervelt E., Grizzle J., Chevallereau C., Choi J., Morris B.** Feedback Control of Dynamic Bipedal Robot Locomotion: CRC Press, Taylor and Francis Group, 2007.
- [92] **Winter D. A.** Muscle mechanics Biomechanics and Motor Control of Human Movement. 1990. ch.7, pp.165–189.
- [93] **Xiao J., Zhang S., Xiao J., Xi N.** Motion mode control in double inverted pendulum system . Advanced Intelligent Mechatronics. 2005. Proceedings, IEEE/ASME.
- [94] **Zavgorodniy Y.** Konstruktion und Steuerung von Schreitrobotern mit ballistischem Laufverhalten. Ph. D. Thesis. Magdeburg: OvGU, 2009.